APPLICATION OF KAOLIN-BASED SYNTHESIZED ZEOLITE MEMBRANE SYSTEMS IN WATER DESALINATION

By

Usman Mohammed Aliyu

A thesis submitted in fulfilment of the academic requirements for the degree of

DOCTOR OF ENGINEERING: CHEMICAL ENGINEERING

Department of Chemical Engineering,

Faculty of Engineering and the Built Environment

Durban University of Technology

Supervisors:

Prof. Yusuf Makarfi Isa

Co-supervisor:

Prof. Sudesh Rathilal

May 2021

DEDICATION

This work is dedicated to my late father Malam Ali Maikanwa Disina (*gone but not forgotten his handwork*) and to my mother Hajiya Khadijat (Tatu).

DECLARATION

I, Usman Mohammed Aliyu declare that:

i. Except where otherwise noted, the study stated in this thesis is my original work

ii. This thesis has not been submitted for any degree or review at any other institution

iii. This thesis does not contain other person's data, pictures, graphs, or other information unless specifically acknowledged as being the source from other persons.

iv. Other people's writing is not used in this thesis unless it is expressly accepted as a source from other scholars. When other written sources are cited, then:

a) Their sentences have been rewritten, but the basic knowledge credited to them has been mentioned;

b) Where their actual words have been used, their writing has been surrounded by quotation marks and referenced.

v. Where I have reproduced a publication of which I am an author, co-author, or editor, I have specified which portion of the publication was written entirely by myself and have thoroughly referenced those publications.

vi. This dissertation does not include text, diagrams, or tables copied and pasted from the internet unless the source is expressly mentioned, and described in the thesis and reference parts.

Signature Date 09th May, 2021…….

Usman Mohammed Aliyu (Candidate)

As the student supervisor, I give my approval for this study to be submitted:

Signature……. Date……

Prof. Yusuf Makarfi Isa (Supervisor)

As the student Co-supervisor, I give my approval for this study to be submitted.

Signature ……. Date…….

Prof. Sudesh Rathilal (Co-supervisor)

ACKNOWLEDGMENT

First, I'd like to express my heartfelt gratitude and thanks to Allah for rewarding me with progress in my academic career as well as good health, perseverance, power and patient to reach my ambition despite all the challenges posed by 2020.

I would also like to thank Prof. Yusuf Makarfi Isa, my capable boss whom I am indebted for his unlimited time, technical and financial support, and generosity in guiding, critical and objective criticism throughout my study. I do appreciate his encouragement and support in my ‘’down face’’ time! It will be an enjoyable memory the time I worked with him.

I would like to express my gratitude to my co-supervisor, Prof. Sudesh Rathilal, for his invaluable assistance, guidance, and support during the study. I would never forget him.

I would like to express my gratitude to my wife (Aneesah) for her invaluable assistance and motivation during my studies, as well as for motivating me to get underway. I would also like to thank my mother (Tatu), late father (Malam Ali), and daughter Hafsat Usman for their moral support, affection, and motivation. I would like to thank my wife to be (Umaina Hamidu) for the support, encouragement, push and love during this study. I am indebted to you all.

I would like to express my heartfelt gratitude to Sherif Ishola Mustapha for his help and many thoughts, good advice, and discussions about this study

I would like to personally, thank my humble family in Durban, especially my brother Jafar Bux and his lovely wife (Fathima). I lack words to measure the hospitality and assistance you rendered during my experimental process. Only Allah can pay you back. Jazakhallah.

I would like to express my gratitude to all members of the chemical engineering staff for their assistance and the friendly environment, with special thanks going to the HOD secretary (Khanyisile) and the entire technologist team, particularly Vishnu, Sheshna, and all others whose names not listed.

I am extremely grateful to all postgraduate students in chemical engineering Department of DUT for creating an incredibly friendly atmosphere as well as the helpful discussion. I would like to particularly, acknowledge the fuel and petrochemical research group for the remarkable relationship and for an extremely satisfying feeling of fitting to the group.

Finally, the financial support grant by Umgeni water treatment plant Durban, KZN province, Republic South Africa, is appreciated and acknowledged.

JOURNAL AND CONFERENCE PAPERS

Journal Papers published/accepted/under review

- ✓ **Aliyu, U. M.;** Rathilal, S.; Isa, Y. M. 2018 Membrane desalination technologies in water treatment: A review, IWA Publishing 2018, 13(4), pp. 738–752.
- ✓ **Aliyu, U. M.,** Rathilal, S., and Isa, Y. M. 2020 Synthesis, Characterization and Application of Kaolin - Based ZSM –5 Zeolite for Water Desalination, Journal of the Nigerian Society of Chemical Engineers, 35(1), 2020.
- ✓ **Aliyu, U. M,** Sudesh. R, Ronald. M, Mustapha. S. I and Isa Y. M.: Hydrothermal synthesis of Kaolin based ZSM-5 Zeolite: Effect of synthesis parameters and its application for bioethanol conversion: European Journal of Engineering and Natural Sciences. Under review

Conferences.

- ✓ **U. M. Aliyu**, S. Rathilal, Y. M. Isa. Synthesis, Characterization, and Application of Kaolin-based ZSM-5 Zeolite for Water Desalination. Proceeding of the 49th NSChE Annual conference: KADA 2019; pp 94-100
- ✓ **Aliyu Mohammed, U**., Mustapha, SI, Rathilal, S., Isa, YM.: Synthesis and characterization of zeolite A from South African clay and its application in water desalination: GLOBAL TRENDS AND CHALLENGES IN RESEARCH AND INNOVATION 17 – 20 September 2019 4th Interdisciplinary Research and Innovation Conference DUT 2019
- ✓ **U M Aliyu**, S Rathilal, S I Mustapha and Y M Isa: Hydrothermal synthesis and characterization of zeolite A from Grahamstown South Africa kaolin: 18th SOUTH

AFRICA Int'l Conference on Agricultural, Chemical, Biological & Environmental Sciences (ACBES-20) Nov. 16-17, 2020 Johannesburg (SA)

ABSTRACT

Accessibility to potable water worldwide is threatene, despite 71% of the earth's surface being covered with water. However, 97% of the 71% is too saline for consumption. A usual way of treating salinity is by membrane desalination using reverse osmosis. The disadvantage of this approach is its high cost and short life span of the polymeric membrane used. Creating a new robust high-quality water treatment system using a ceramic membrane will address these challenges due to its robust mechanical properties.

In this work, we synthesized different zeolites from South African kaolin under varying conditions such as crystallization time, ageing time and temperature and their effects on the properties of zeolites synthesized was investigated. Sample characterization confirmed the successful synthesis of ZSM-5 and zeolite A.

In the synthesis procedure, metakaolin served as the alternative source of silica and alumina and was use to synthesize different types of zeolites under varying synthesis conditions. Synthesized samples were characterized using X-ray diffraction (XRD), scanning electron microscopy (SEM), Fourier transform infrared (FTIR) spectroscopy and Brunauer–Emmett–Teller BET surface area.

The properties of the synthesized ZSM-5 were influence by the synthesis parameters, typically, crystallization temperature, ageing time and crystallization time. Crystalline ZSM-5 zeolite produced at an ageing time of 24 hours, crystallization time of 48 hours and crystallization temperature of 180°C with Si/Al ratio of 43 and BET surface area of 282 m^2/g. After a 12-hour ageing period, Zeolite A produced at crystallization time of 20 hours, the crystallization temperature of 100°C, Si/Al ratio of 1.3 and BET surface area of 143.88 m^2/g. The findings indicate that aging influences the synthesis of zeolite A, as a relatively crystalline material formed at an

ageing time of 12 hours, which continued to decrease as the ageing time was increased. We do not exclude the possibility of Ostwald ripening playing a role in this relationship.

Subsequently, the efficiency of zeolite A and ZSM-5 zeolite in removing salt ions, Ca^{2+}, K^{+}, Mg^{2+}, and Na^{+} from synthetic seawater was investigated at room temperature using a batch adsorption system. The effect of adsorbent dosage, agitation speed and contact time were consider. Dosages varied from 2.5 to 6.0 g/100 ml while the contact time varied from 30 to 180 minutes. The results obtained showed that a zeolite dosage of 6.0g/100 ml and agitation speed of 140 revolutions per minute (rpm) yielded a maximum removal efficiency of 89.7 % for Ca^{2+} and minimum removal efficiency of 1.8 % for Mg^{2+} at agitation rates of 30 and 120 minutes, respectively. Ion exchange of Na^{+} by Ca^{2+}, K^{+} and Mg^{2+} in the zeolite framework was established. The preference of the overall ion-exchange selectivity of both zeolites A and ZSM-5 are in the order of $Ca^{2+} > K^{+} > Na^{+} > Mg^{2+}$. Zeolite A showed higher removal efficiency compared to ZSM-5 zeolite. The results point out that the synthesized zeolite was able to desalinate the salt ions in synthetic seawater to a limit below the World Health Organization (WHO) recommended values. Consequently, zeolite synthesized from kaolin offers a cost-effective technology for the desalination of seawater.

The desalination and material characterization results used in selecting a potential zeolite for use in reverse osmosis (RO). The material successfully deposited on etched alpha-alumina support to produce zeolite membrane by a hydrothermal technique using a modified in-situ method. Zeolite A and ZSM-5 membranes produced and applied in the RO unit for desalination. The RO membrane experimental results show potential in desalination of synthetic seawater.

A machine-learning tool was use to predict the properties of the synthesized ZSM-5 as a function of the hydrothermal parameters. Finally, a techno-economic analysis of synthesizing zeolite using

locally available kaolin at a capacity of 5 x 10^5 kg/yr. has shown that the plant is economically viable with rapid break-even and the payback period is less than 4 years.

TABLE OF CONTENTS

LIST OF TABLES

LIST OF FIGURES

Nomenclature

List of Abbreviations and Acronyms

Abbreviation	Description
ANA	Analchime
BEA	Beta
ERI	Erionite
CHA	Chabazite
CAN	Cancrinite
LAU	Laumontite
EPI	Epistilbite
MAR	Marinellite
M F I	ZSM-5
LTA	Linde type A
FAU	Faujasite
AEL	AIPO-11
ABW	Li-ABW
ACO	ACP-1
BEC	Beta polymorph C
EMT	EMC-2

FAR	Farneseite
NAB	Nabesite
PAU	Paulingite
MOR	Mordenite
BET`	Brunauer-Emmett -Teller
SEM	Scanning electron microscopy
XRD	X-ray diffraction
FT-IR	Fourier transform infrared
RO	Reverse osmosis
TGA	Thermogravimetric analysis
ICP OES	Inductively coupled plasma optical emission spectroscopy
EDS	Electron diffraction spectroscopy
MED	Multi-effect distillation
MVC	Membrane vacuum distillation
MSF	Multi-stage flash distillation

CHAPTER ONE

1. Introduction to the study

1.1 Background

Water is a distinct and achromic chemical substance that is the primary component of the earth's rivers, ponds, and oceans, as well as the main component of the large proportion of living things. Water's chemical formula is H_2O, which indicates that it is made up of two hydrogen atoms and one oxygen atom linked together by covalent bonds. Water can be liquid at room temperature and pressure, but it can also be solid, known as ice, or vapour, known as its gaseous state. Water can be found in nature as glaciers, snow, ice packs, icebergs, clouds, fog, dew, and humidity.

Seawater is water from the seas or oceans that has an average salinity of 3.5 percent by mass. This means that there are 35 grams of salts dissolved in each 1000 mL. (Li *et al*., 2015). A typical seawater contains six salt ions: sodium ion (Na^+), chloride (Cl^-), sulfate (SO_4^{2-}), magnesium ion (Mg^{2+}), calcium ion (Ca^{2+}), and potassium (K^+). Other ions are insignificant and are not a focus of this research.

Drinkable freshwater is in short supply around the world, especially in dry and arid regions. It is exacerbated by population growth, industrialization, climate change, and drought (Subramani and Jacangelo, 2015). Despite the fact that water covers 71% of the world in the form of sea, ocean, and ice at the poles, a lack of fresh water is threatening (Khawaji, Kutubkhanah and Wie, 2008). This problem persists because 97% of it is too salty to eat. As a result, resolving the salinity issue requires 97 percent freshwater from the earth's surface.

Furthermore, Imbrogno *et al*. (2017) estimated that more than 1 billion people worldwide do not have access to safe drinking water, and nearly 2 million children die each year as a result of a lack

of safe water and proper hygiene. Drinking water shortages are becoming critical in many places, including the Middle East and other arid regions. To increase water availability, it is proposed that technicians and researchers develop new and improved methods of dissolving seawater and purifying low-quality water, such as brackish groundwater, storm water, greywater, and sewage.

Although climate change continues to have an effect on the greenhouse effect and sea-level rise, water demand for urban, agricultural, and industrial uses is expected to rise dramatically. As a result, in order to resolve these issues, it is necessary to investigate the development of new sources of high-quality water through water recovery, recycling, and reuse.

Natural water sources are dwindling due to Changes in the atmosphere and overexploitation, and Water recycling is one example of a potential remedy, water transportation, or the construction of new dams is inadequate to satisfy rising demand. As a result, the restoration of clean drinking water from salt is one of the most urgent concerns. or seawater, by far the most available global water source, and wastewater treatment and recycling (Lee, Arnot and Mattia, 2011).

1.2 Justification

Globally, the freshwater source designated for drinking is limited, especially in dry and arid areas. Desalination, a process that converts salt water to fresh water, is one of the most important solutions to these problems (Taylor and Stewart, 2012). One means of providing fresh water has been water treatment, such as desalination. More research is needed, however, to enhance its long-term efficacy and sustainability. The most common method for converting seawater to drinking water is reverse osmosis (RO). Desalination is now commonly performed using reverse osmosis (RO) membrane technology, but RO has limitations such as problems with fouling.

As a result, fundamental research of substitute membrane technology such as nanoparticles could allow further desalination choices in areas where current membranes are limited. Conserving South African inorganic locally - sourced resources (Kaolin) for the construction of desalination membrane might be a more reliable option, avoiding the expensive pretreatment conditions needed to meet the RO restriction content. The intrinsic ability of the zeolite membrane to repel salt ions while allowing water to pass through is needed for desalination. High ion rejection characteristics are critical, with the zeolite benefiting from increased water diffusion.

1.3 Membrane technology processes.

The membrane is a thin layer of organic or structured that is protected by a fibrous system that is impenetrable to solution components. There are several desalination technologies like reverse osmosis mode and thermal structures, for example membrane vacuum distillation, multistage flash distillation and multi-effect distillation. However, reverse osmosis, forward osmosis, pervaporation, membrane distillation, ultrafiltration and microfiltration are among the most frequent applied processes for the desalination of brackish and salt water (Greenlee *et al.*, 2009; Voutchkov, 2010; Pérez-González *et al.*, 2012; Swenson *et al.*, 2012; Sahebi *et al.*, 2015; Sun *et al.*, 2015). The features and membrane morphological characteristics influence the membrane's contaminant leakage, fouling proclivity, and water permeability (Tijingmkiii *et al*. 2015). Membrane advances in science present new processes, techniques, and modified production cycles. Membrane systems are much more efficient than the standard separation method, like those of sedimentation and filtration.

1.4 Problem Statement

Water treatment, such as desalination, has emerged as one method of supplying fresh water. However, more research needed to enhance its long-term efficacy and sustainability. Desalination is now widely accomplished using membrane technology in the reverse osmosis (RO) mode, but RO has limitations such as fouling issues. Because of these, fouling issues, research and development of alternative materials such as zeolites to improve membrane performance could allow for more desalination possibilities where current membranes are limited (Lee *et al*., 2010).

Desalination now done using reverse osmosis (RO) technology. However, due to the polymeric nature of the membrane content, RO is a membrane-based method of desalination that requires stringent pretreatment of contaminants such as oxidant, unpleasant material, and feed temperature regulation (Zhu *et al*., 2014). Without this pretreatment, the membrane can be harm and polluted by the foulant, or chemicals can be use to reverse and rejuvenate it. Despite the stringent pretreatment requirements, polymeric membranes need replacement every 5 to 7 years. Organic membranes are the name given to these types of membranes.

Research into different membrane materials could pave the way for a new technique to overcome the limitations of current membrane technology based on RO. Since it is ceramic-based and versatile when compared to the polymer membrane, the inorganic membrane can be investigated.

Zeolites are hydrated silica and alumina that usually occur as a secondary mineral used due to their molecular sieve characteristic where they undergo desiccation with no crystal structure transition.

They are commonly use as catalysts in a variety of industries, including fluid catalytic cracking (FCC) additives, ion exchangers, desalination, industrial separations, catalysis, adsorbents, and membranes. Zeolite frameworks are made up of various free $[SiO_4]^4$ and $[AlO_4]^5$ tetrahedral

configurations (Gougazeh and Buhl, 2014). Using both single layers and a novel bilayer theory, experimental and theoretical research showed that porous inorganic membranes reject ions through filtration. However, recent research indicates that zeolites are use for salt separation from aqueous solutions (Zhu, Kim, *et al*., 2013).

This is a completely new field of study at Durban University of Technology and in the Republic of South Africa in general. It is our intention in this research to provide insight into how to solve the pervasive water shortage in our local communities, in collaboration with our vicinage partners from waterworks. The most pressing problem in desalination is determining what the required technique is that contributes to the cost and how these costs can be efficiently minimize. The six major challenges in desalination and water production are saline feed water, the actual process and technology, chemicals, electricity, property, and concentrate. Any factor influencing the cost of the above challenges will influence the cost of desalination (Sheikholeslami, 2009).

1.5 Aim and objectives of the study

The main goal of this work is to apply zeolites membrane synthesized from South African Kaolin in desalination

The following specific objectives were investigated in order to address the overall aim:

- To investigate the effect of synthesis parameters on the properties of the zeolite.
- To investigate the efficiency of different synthesized zeolites in the removal of different salt ions. Prediction of the properties of the synthesized zeolite as a function of the hydrothermal parameters.
- To investigate the use of the zeolite as a RO membrane for water desalination.
- To conduct a techno-economic analysis of producing the synthesized zeolite.

1.6 Research approach.

The research carried out is in five phases. The beneficiation of the clay was the first stage. G&W Mineral Resources in Grahams Town, Western Cape, South Africa, donated the kaolin clay. Following the purification of the clay, it was use to synthesize the two forms of zeolite (zeolite A and ZSM-5 zeolite). The second stage involved testing the efficiency of the synthesized zeolites in removing salt ions from seawater using a batch experiment. The third stage included depositing the synthesized zeolite on the surface of a -alumina disk membrane and using this membrane to desalinate water using a RO unit. A techno-economic study of the proposed system's application for a water treatment plant performed, and finally, an attempt was made to predict how the type of zeolite affects water desalination.

1.7 Thesis structure.

This thesis is designed and structured into seven chapters, the individual chapter study separate features of the findings, data analysis, discussion and summaries of results presented below:

Chapter 1:

In this chapter a short introduction and motivation for the need to use desalination as an alternative technology of solving the problem of water shortage across the globe presented. Different types of membrane desalination technology with their fouling problems outlined. The justification of the study, aim and objectives, and the thesis structure are discussed briefly

Chapter 2:

This chapter presents a review of the relevant literature to the study. An outline of desalination technology was discussed.

Chapter 3:

This chapter introduced the methodology applied in this research. The chapter outlines the experimental materials and methodology applied for the hydrothermal synthesis and application of the synthesized zeolite to desalination using batch adsorption techniques.

Chapter 4:

This chapter presents the results and discussions of the synthesis and characterization of zeolite A and ZSM-5 zeolite produced using South African kaolin clay. Various approaches to characterizing the synthesized zeolites (ZSM-5, and zeolite A) are describe. The results obtained from the various analytical methods like X-Ray diffraction (XRD), Scanning electron microscopy (SEM), Thermogravimetric Analysis (TGA), Fourier transform infrared (FTIR), Brunauer-Emmiter-Teller (BET), Inductively coupled plasma optical emission spectroscopy (ICP OES) and Electron diffraction spectroscopy (EDS) are discussed.

Chapter 5:

In this chapter, the kinetic studies were discussed to investigate the performance of adsorbents to understand the desalination mechanisms involved in the investigation of adsorption. The factors affecting the effectiveness of the synthesized zeolites in the removal of salt ions (Na, K, Mg, and Ca) from seawater investigated and presented in detail. Investigating the efficacy of various synthesized zeolites in the absorption of various salt ions.

Chapter 6:

In this chapter, we presented the modification of zeolite support and the Zeolite accumulation on the substrate and the utilization of the deposited membrane in a reverse osmosis filtration unit to investigate the membrane performance in desalinating water. The impact of applied pressure was

studied. and the efficiency of the membrane in salt ions removal and the permeation fluxes was deduced.

Chapter 7:

In this chapter, the techno-economic analysis for the production of kaolin-based ZSM-5 zeolite is examine using the abundance of South African kaolin deposit as an alternative source of silica and alumina from expensive used of chemical. The economic analysis was establish using the cost estimation method. The profit analysis was perform to calculate the techno-economic feasibility of the proposed ZSM-5 zeolite production process to established production capacity and selling price and net profit of the production was obtained.

Chapter 8:

General conclusion and recommendation presented in this chapter

CHAPTER TWO

2. Literature review

2.1 Introduction.

The literature review of water desalination and zeolite synthesis presented here. An overview of water scarcity in the abundant and availability of oceans and seawater was assessed. An assessment of the historical background of zeolites and their types and nature as well as their synthesis method presented. Various desalination technologies and their application are presented. Different types of zeolite characterization technique reviewed.

2.2 Water scarcity

Affordability to freshwater has been at risk in many parts of the world. Climate change and drought are becoming more severe because of population changes and industrial growth. (Shannon *et al.*, 2008; Von-kiti, 2012; Zhao and Ho, 2014; Akther *et al.*, 2015; Burn *et al.*, 2015; Sari and Chellam, 2016). It is under pressure, despite the fact that water covers 71% of the earth in the form of sea, ocean, and ice at the poles (Khawaji, Kutubkhanah and Wie, 2008). This problem persists because 97 percent of it is too salty to drink.

Almost half of the water on Earth is salty and contained in the sea, with a small volume of freshwater. Only a small amount of this portion is available to support life, as it can be seen in the three bars in Fig. 2-1. The first bar shows the total earth's freshwater amounting to 2.5% and the second bar is the breakdown of freshwater, which mostly found to be in ice and in-ground with about 1.2% that is useful to life. The last bar shows the breakdown of surface freshwater which is also stacked up in ice while some little portion of about 20.9% found in lakes and 0.49% is river water.

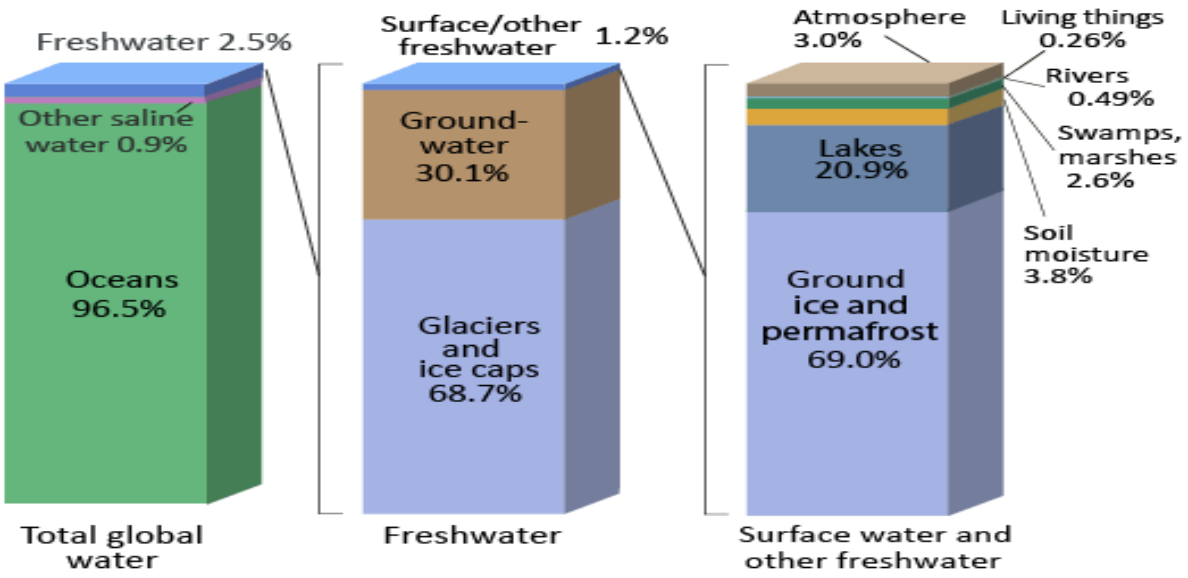

Figure 2-1 Distribution of earth's water (US Geological survey) (Mayere, 2011)

To reduce and restrain ever-increasing drinking water needs, various schemes such as wastewater treatment and desalination of seawater have been utilised (Jiang, Li and Ladewig, 2017). Global water shortage has progressively become a great opposition to human exploit, agricultural growth and industrial activities (Zhu *et al.*, 2016). Availability of potable water is vital for human needs and the scarcity of water is threatened in many areas across the globe more especially in developing countries and arid regions (Shannon *et al.*, 2008; Zhao and Ho, 2014). Water from oceans and seas comprise of more than 71% of the earth surface and 97% of it is saline and cannot be used as potable water as well as for agricultural purposes (Von-kiti, 2012). To curb and subdue this salinity problem and ensure the accessibility of freshwater, a right strategy has to be adopt. South Africa is located in between two great oceans, Atlantic and Indian and water crisis is usually emanating in some parts of the Cape Town province. Therefore, seawater desalination is a choice and potential technology to subjugate the water crisis in the future (Wibowo *et al.*, 2017).

Desalination of seawater is the removal of dissolved salts and minerals in order to create new potable water. (Zhao, Chang and Ho, 2013; Tang *et al.*, 2016; Wenten and Khoiruddin, 2016). There are several forms of seawater desalination systems available today, including RO (Greenlee *et al.*, 2009) and thermal processes like multi-effect distillation (MED) (Abu-Zeid *et al.*, 2015). membrane vacuum distillation (MVC) (Pérez-González *et al.*, 2012) and multi-stage flash distillation (MSF) (Khawaji, Kutubkhanah and Wie, 2008) These processes produce potable water but the technology is expensive to operate, so a cheaper way of alternative methods cannot be an overemphasis

2.3 Historical background of zeolites

The ancient Romans found zeolite and used it to filter water in their aqueducts. Cronstedt, a Swedish polymer chemist, officially recognized zeolites as a new generation of minerals in 1756, composed of hydrated aluminosilicates of alkali and alkaline earth metals. He coined the term "zeolite," which was taken from two Greek terms, zeo and lithos, which mean "to boil" and "a stone," respectively.

In the 1950s, the first commercial quantities of synthetic zeolite manufactured in the United States. It was use to process wastewater ammonia and hazardous substances in the 1970s. People began using the mineral in pools in Europe and the United States when the mineral's impressive filtration and adsorption potential became better understood. Since the 1980s, zeolite is known for use in a wide range of applications, making it a highly valued mineral.

2.3.1 Natural and synthetic zeolites

Native zeolites can be present in a variety of geological environments such as alkaline deserts, lake sediments, ash ponds, and aquatic sediments at very low temperatures. Synthetic zeolites, on the other hand, are created by chemical reactions, are formed in a more uniform, and refined state than natural zeolites in terms of their lattice architectures, pore sizes, and cages in their frameworks. The raw materials used to make synthetic zeolites are silica and alumina-rich chemicals (Jha and Singh, 2016). Synthetics zeolites have several advantages over natural zeolites. These characteristics include, but are not limited to, pureness, consistent pore diameter, and appropriate ion-exchange abilities. (Von-kiti, 2012).

In recent years, the progress made in the synthesis and development of novel zeolites from kaolin and bentonite clay is enough accomplishment of R&D in the field of chemical engineering and materials science. The remarkable outcome achieved and the targets obtained in these processes are undoubtedly proportional to the progress made in the other field of chemical engineering such as ceramics, polymers and polymer-based compounds. Zeolites are identified using a general formula $M_{2/n}O.Al_2O_3.xSiO_2.yH_2O_2.O$ where M is an interchangeable cation of valence n and it's either a member of group I or II ions while x and y represent stoichiometric coefficients of Al^{3+} and Si^{4+} in the case of the tetrahedral structure (Von-kiti, 2012).

Zeolites are characterized by physical and chemical properties, adsorption properties, ion exchange, mineralogical and morphological characteristics, thermal characteristics, crystal structure, the framework of the crystals, acidic medium characteristics as well as surface properties (Singh, 2016).

2.3.2 Zeolite nomenclature

To organize the nomenclature, international zeolites association structure commission and IUPAC designate each zeolite structure with a three-letter code. These codes are derive from the zeolite's name or material form for example, ZSM-5 from zeolite Socony mobile five. The novelty year, IUPAC name and zeolite name presented in table 2-1.

Table 2-1: Few zeolite IUPAC nomenclature and zeolite novelty year

Zeolite name	IUPAC name	Novelty year
Analchime	ANA	1978
Beta	BEA	1992
Erionite	ERI	1978
MCM-22	MWW	1997
SSZ-23	STT-23	1998
Chabazite	CHA	1998
Cancrinite	CAN	1987
AIPO-C	APC	1986
Laumontite	LAU	1994
Epistilbite	EPI	1985
Marinellite	MAR	2003
ZSM-5	MFI	1978
LTA	LTA	1978
Faujasite	FAU	1978
ALPO-11	AEL	1987
Li-ABW	ABW	1951
ACP-1	ACO	1997
Beta polymorph C	BEC	2000
EMC-2	EMT	1990
Farneseite	FAR	2005
Nabesite	NAB	2002
Paulingite	PAU	2005
Mordenite	MOR	1978

Source: Structure *Commission of the International Zeolite Association* (Flanigen, Broach and Wilson, 2010).

2.3.3 Classification of zeolites.

Zeolite is classified based on their chemical composition. They can be identify as low silica, intermediate silica, high silica and all silica with Si/Al ratio of 1.5-4, 4-20, 20-200 and infinity,

respectively. The pore size, chemical composition and existence are the major ways of classifying zeolite (fig. 2-2). Generally, all zeolite with small pore size is 8 membered rings with a free diameter ranging between 0.30 - 0.45 nm. Medium pore size zeolite has 10 membered rings with a free diameter ranging from 0.45 - 0.60 nm, large pore size with a membered ring of 12, free diameter ranging from 060 – 0.80 nm and extra-large pore size zeolite with 14 membered rings (Flanigen, Broach and Wilson, 2010).

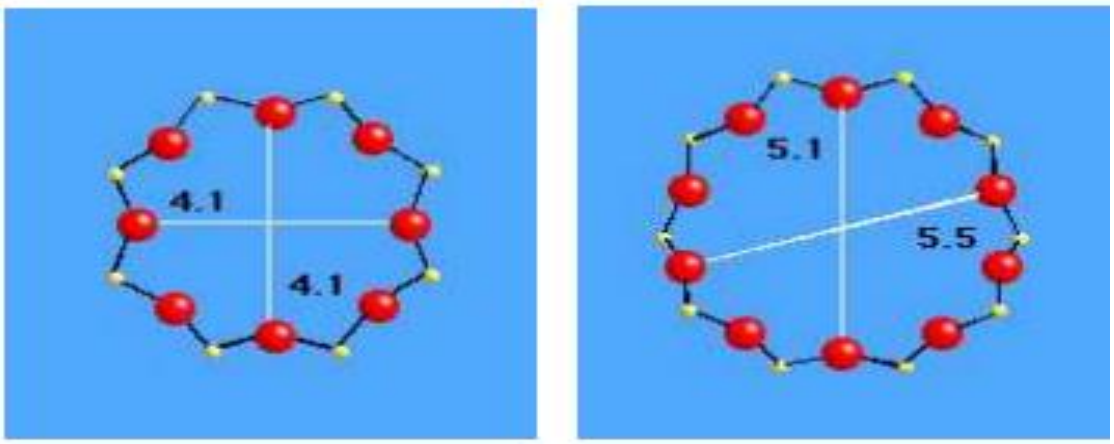

Figure 2-2: The pore structure apertures of 8-rings and 12-rings of zeolite A and ZSM-5 zeolite

2.3.4 Structures of zeolites.

Zeolites referred to as molecular sieve due to the size of its uniform pores. The pore diameter of zeolites is similar in size in which larger molecules cannot pass through, adsorbed while lesser molecules can pass, or fully adsorbed. Molecular sieve in zeolites refer to zeolites with a porosity between 0.3 nm to 2 nm diameter that is applicable for sieving molecules (Sánchez and García-Sánchez, 2011). They are classified as molecular sieves because porous materials like activated carbon and inorganic gel are grouped as disordered sieve structures, while zeolites and zeotypes are classified as ordered sieve structure material (Sánchez and García-Sánchez, 2011).

Zeolites are molecular sieves because particles with a kinetic diameter greater than the zeolite pores cannot pass through the aperture and enter the canal system while smaller ones can pass through. Dehydration and heat may affect molecular sieve quality because heating can create change in the lattice and heighten the void volume of the channels whereas cation interchange and charge diffusion in the structure is induce by dehydration. Zeolite framework is flexible at room temperature and pore diameter is control by the spatial array of the tetrahedral structure prompted by constant vibration of the molecule. The shape and size of the framework porosity is flexibility if the molecular vibration temperature increases.

Zeolites are essential in chemical industries because of their distinctive structures. Zeolites are applicable in catalysis, adsorption and in ion exchange because of their unique framework and pore structures. Therefore, zeolites structural framework characteristics knowledge is important in research involving their application (fig. 2-4). Zeolites are composed of tetrahedral AlO_4^{-5} and SiO_4^{-4} particles bound together by an oxygen atom held solidly with cation porous structure (Shabani, 2016).

The structure of zeolites is usually describe by their geometry, size or connectivity of the pore space, which translated by their framework. The pore size that curbs molecular entrance into the pore space is identified in respect of limiting ring size (Lijalem, 2016). Consistently, zeolites are divided into small, medium, large and moderate large pore substances. Small pore zeolite such as zeolite A carries a pore space aperture surrounded by 8 TO_4 tetrahedral with 4.2Å diameter. MFI is a moderate porosity zeolite with the characteristic of 10 ring pore aperture and a 5.5 Å diameter. Faujasite and Mordenite have pore aperture of 12 and about 7.5Å diameter. Any zeolite with an aperture of more than 12 T atom is classify as large pore zeolites. The most typical zeolites are 8-

ring and 10-ring. Figures 2-3 and 2-4 represent the most typical zeolite pore structures of the first two categories.

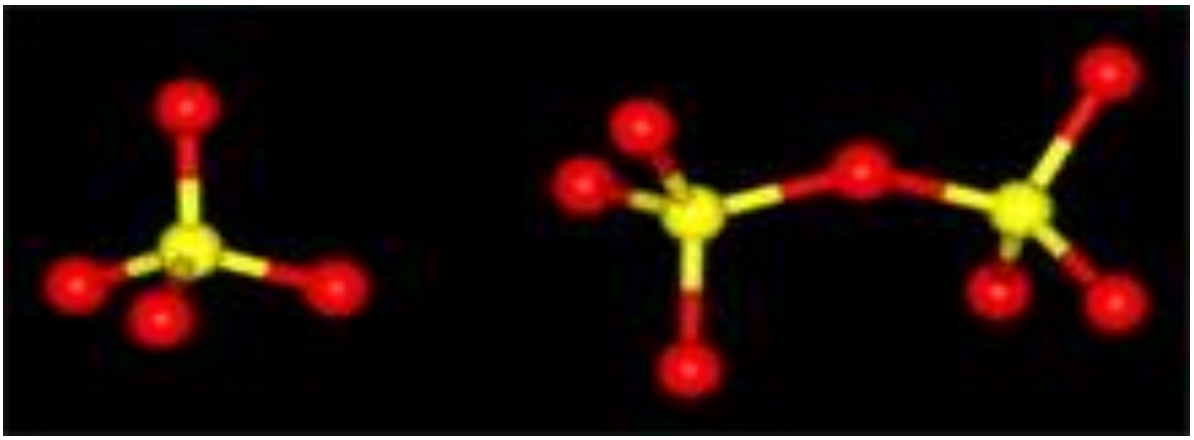

Figure 2-3 Primary building block unit and the two linked together to prove how they allied to formulate a larger structure (Ayele, 2016)

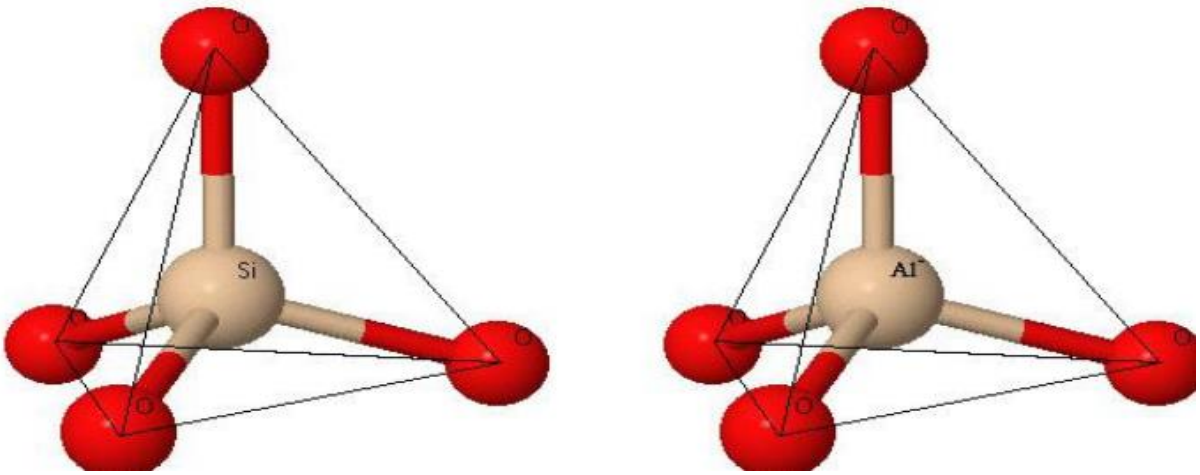

Figure 2-4 Sketch of the structure of zeolite representation of $\{SiO_4\}^{4-}$ or $\{AlO_4\}^{5-}$ tetrahedral (Ayele *et al.*, 2015).

Zeolites constitute more than 50 groups of aluminosilicate minerals. In this research, two typical zeolites (ZSM-5 and Zeolite A) are considered. The building block of zeolite is characterized by

[TO4] tetrahedral of primary and secondary units. The primary building unit (PBU) produces immeasurable lattice of matching building blocks of echoing unit referred to as secondary building unit (SBU). The secondary building unit is the one that defines the zeolite structure but excludes the water content and cation within the framework. Figure 2-5 describes all the recognized zeolite framework. The SBUs mentioned above are used to create zeolites, and often mixtures of SBUs are mixed to form zeolites. For example, zeolite A is made from four or six rings, or zeolite can be created from a binary four-ring building unit.

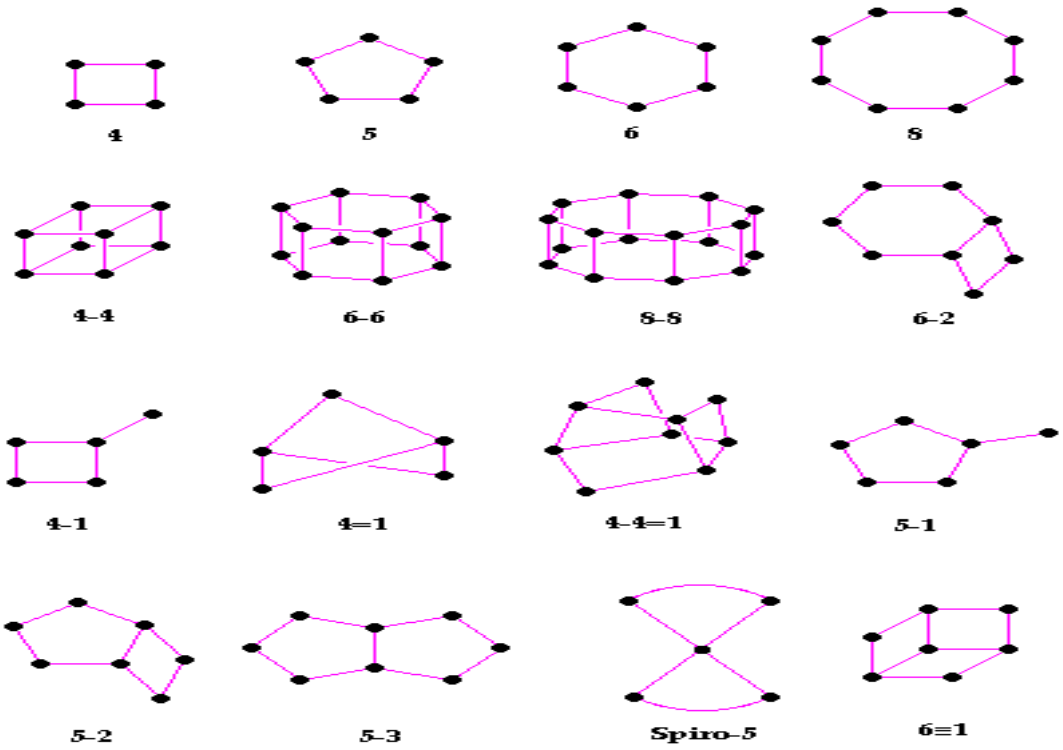

Figure 2-5 Secondary building units (SBU"s) present in a zeolite (Lijalem, 2016)

2.3.4.1 Zeolite A.

Zeolite A is among the various synthetic zeolite materials categorized under Linde type A zeolite (Lijalem, 2016). Zeolite A has the highest ion exchange potential of both synthetic and natural zeolites, making it ideal for use as an adsorbent and for ion exchange. (Ayele *et al.*, 2015). This

results in zeolite A taking the largest part of the overall manufacture of artificial zeolites (73 %) (Aarts *et al.*, 2004). Zeolites A (Fig. 2-6) is a microporous aluminosilicate material that is normally used as commercial adsorbents and s expressed by the equation $Na_{12}[(AlO_2)12(SiO_2)_{12}]27H_2O$. Zeolite A has an α-cage structure consisting of 8 cuboctahedra linked by 12 cuboids that result in excellent ion exchange potentials without any notable harmful consequences to the environment. Zeolite A is use in household detergents as a catalyst or molecular sieve to reduce water hardness by exchanging Ca-ions for Na-ions. The majority of phosphate-free household detergents rely on Zeolite A as a builder. (Petrov and Michalev, 2012).

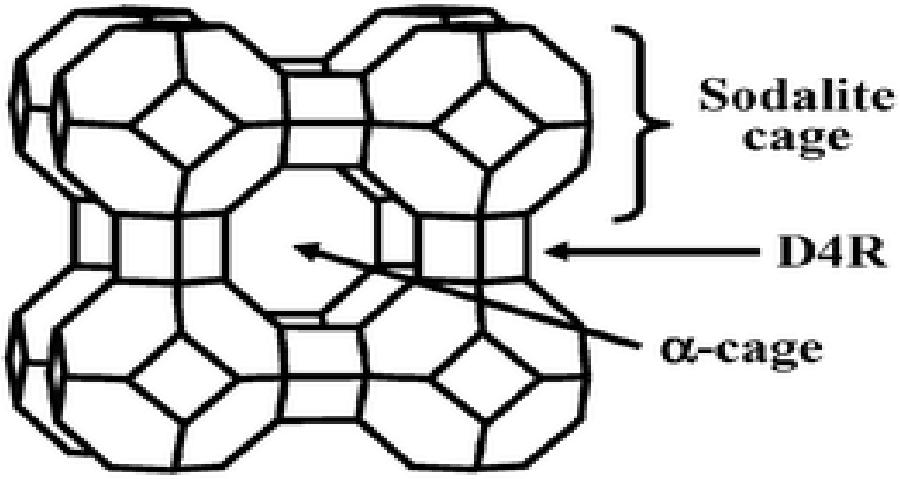

Figure 2-6 Structure of zeolite A; adapted from Petrov and Michalev (2012)

2.3.4.2 ZSM-5 zeolite.

ZSM-5 are crystalline aluminosilicates with a pore structure arranged in channels with a diameter ranging from 0.53 to 0.56 nm (fig 2-7) and are capable of adsorbing molecules up to the size of cyclohexane. The interconnection of tetrahedral SiO4 and AlO4, which form pores, and cages of

non-identical geometries make the structure of ZSM-5. This structure enables specific molecules to diffuse inside the pores (Greń *et al.*, 2010).

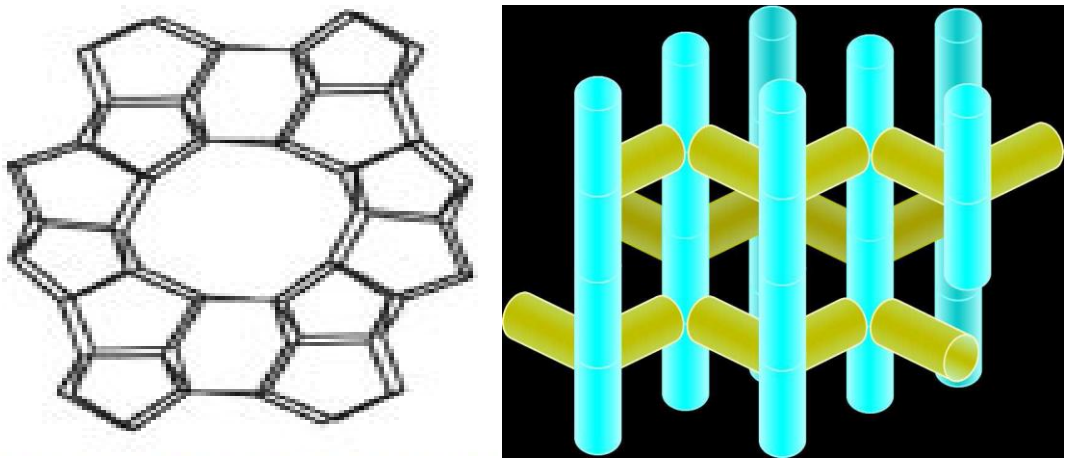

Figure 2-7 Structure of ZSM-5 (Mota and Rosenbach, 2011).

2.3.5 Zeolite Synthesis.

Zeolites can be produce by both natural means and synthetically. About 150 zeolite classes are synthetic types and 40 categories of naturally occurring synthetic zeolite are produced in the laboratory while natural zeolite is formed as a result of volcanic eruption ashes (Kiricsi, 1999; Aarts *et al.*, 2004; Von-kiti, 2012, 2016).

Zeolite synthesis is commonly perform using the hydrothermal method. Lately, the synthesis procedure is divided into salvo-thermal, ionothermal or hydrothermal. Ionothermal procedure applies to ionic liquids for the solvent and the template (structure-directing agent), in the synthesis of zeolite and the organic hybrids and it has been employed to manufacture zeolites and organic-inorganic hybrids like organic-metal frameworks (Parnham and Morris, 2007). The salvo-thermal

synthesis method applies to alcohols and amines with distinct structures and properties. Hydrothermal synthesis is commonly distinguish into mild reactions, where the reaction temperature is between 100℃ to 240℃ and high reactions where the temperature is up to 1000℃ and autogenous pressure. Almost all zeolite synthesis done at low temperatures and constant pressure. Both hydrothermal and salvo-thermal synthesis is used in the fundamentals of synthetic chemistry and preparation of porous material (Bedard, 2010; Von-kiti, 2016).

Metakaolinization or direct synthesis is use in the hydrothermal synthesis of zeolite from kaolin. Three stages are involved in the hydrothermal synthesis of zeolite.

a. Activation of kaolinite into metakaolinite.

b. The reaction of various alkali media with metakaolinite hydrothermally.

c. Washing/purification and activation of the zeolite.

Many experiments on the synthesis of zeolites conducted and recommended molar composition for each zeolite has been suggested. Some synthesized kaolin/clay-based zeolites presented in table 2-3. For example, synthesis of zeolite NaA from kaolinite as reported by Petrov & Michalev (2012) indicated a Na_20/AI_20_3 ratio of 1-2 and $Si0_2/AI_20_3$ ratio of 1-2.

Table 2-2. Some synthesized kaolin/clay-based zeolites

Zeolite	Kaolin Deposit location	Synthesis technique	Synthesis parameter	Comments	Reference
A	Bombowha Ethiopia	Conventional hydrothermal and alkali fusion followed by hydrothermal synthesis	Ageing and temperature	Zeolite A was produced from low-grade Bombowha clay using a traditional hydrothermal followed by an alkali fusion technique. Traditional hydrothermal synthesis produced cubic crystal zeolite A with a rounded edge and 75% crystallinity, while alkali fusion produced cubic crystal zeolite A with an 84 percent crystallinity. This show that alkali fusion followed by hydrothermal crystallization is more effective compared to conventional hydrothermal crystallization.	(Ayele *et al.*, 2016)
A	Jordan	Hydrothermal synthesis	Metakaolinization and NaOH concentration	The synthesis revealed zeolite A as the major phase with hydroxyl sodalite (HS) and quartz as minor impurities from the kaolin. XRD pattern presented an excellent relative crystallinity and SEM showing cubic images, which confirmed the morphology of zeolite A. Both XRD and SEM suggested that Jordanian kaolin can be used to synthesize zeolite A.	(Gougazeh and Buhl, 2014)
ZSM-5	G&W mineral	Hydrothermal synthesis	Temperature and time	The technique involved beneficiation using sieving and filtration to upgrade the kaolin.	(Mohiuddin *et al.*, 2016)

	resources South Africa			Temperature and time of crystallization varied. The optimization confirmed that both XRD and SEM show excellent SEM images and crystallinity. Finally, established that temperature and time of crystallization are critical in converting kaolin to ZSM-5 zeolite.	
Y	Ahoko Nigeria	Hydrothermal synthesis	Ageing and novel metakaolinization of kaolin	Kovo and his co-workers developed a novel metakaolinization technique and effectively applied in the synthesis of crystalline zeolite Y. Kaolin processed by metakaolinization at 600 with an exposure time of 50 minutes whereas 700 to 900--metakaolinization temperature reported by literature. The study concluded that ageing conditions significantly enhanced the crystallinity of the product.	(Kovo and Holmes, 2010)
Y	Elefun Nigeria	Hydrothermal synthesis	Silica/alumina starting materials	Zeolite Y was successfully synthesized using a new hydrothermal method by application of kaolin without calcination to transform it to metakaolin. After optimization, 8 M NaOH at 240°C for 8 hours was hydrothermally used for alkaline activation, converting kaolin and quartz to hydroxycancrinite, which readily dissolved in HCl solution to form silica/alumina gel. The gel was use to monitor the crystallization time of zeolite Y. The results remarkably confirmed that zeolite Y synthesis depends on the silica/alumina ratios of the initial materials though independent of the type of starting materials.	(Babalola *et al.*, 2015)

ZSM-5	Thailand lignite fly ash and rice husk ash	Conventional hydrothermal	SiO_2/Al_2O_3 mole ratio, the presence of TPABr	The influence of the SiO2/Al2O3 mole ratio, the presence of TPABr, temperature, and initial pressure on the yield of ZSM-5 zeolite investigated using a quick synthesis method (about 2–6 h). ZSM-5 zeolite could not be synthesize in the absence of sodium silicate solution. In the presence of TPABr, ZSM-5 zeolite could be synthesize in a SiO2/Al2O3 mole ratio range of 20–100. At a holding temperature of lower than many forms of zeolites were made. The highest production of ZSM-5 zeolite, 59 wt. percent, was produce at a SiO2/Al2O3 mole ratio of 40, reaction temperature of 210°C, holding time of 4 h, and initial pressure of 4 bar.	(Chareonpanich *et al.*, 2004)

2.3.6 Preparation of Zeolites from Kaolin

The preparation of zeolite from kaolin involves many variable parameters. The most imperative limitations for the formation of zeolite are the starting material composition like the amount of water, crystallization temperature, crystallization time, and ageing time. For the zeolite to be prepared from kaolin, kaolin should be beneficiated and purified to remove the impurities like iron, calcium, magnesium etc. Zeolite synthesized from natural kaolin have some traces of the impurities that are present in the kaolin. These impurities may have some advantage in the properties of the zeolite such as electrical properties, brightness, hardness and catalytic activity (Petrov and Michalev, 2012).

2.3.6.1. Chemicals and batch reaction composition for ZSM-5 zeolite synthesis.

Different methods have been use for the synthesis of ZSM-5 zeolite from various sources such as fly ash, kaolin, bentonite, bauxite etc., which are predominantly comprised of silica and alumina. However, the basic chemical source of silica is water glass ($Na_2O{\cdot}xSiO_2$), sodium silicate ($Na_2SiO_3{\cdot}_9H_2O$), colloidal soil (SiO_2 40 wt. per cent) and aluminium source include sodium aluminate ($NaAlO_2$), aluminium hydroxide ($Al(OH)_3$), aluminium nitrate ($Al(NO_3)_3{\cdot}9H_2O$). Other reactants are base, water, mineralizer, and metal ions. (Salou *et al.*, 2001; Iwakai *et al.*, 2011; Zhu *et al.*, 2013; Tang *et al.*, 2016). Crystallization (temperature, time and ageing time) are the parameters that the rate of zeolite crystallization, products type, morphology and crystals size distribution depend on. Generally, ZSM-5 crystallization is affected by reaction mixture composition, reactants nature and their pretreatments, crystallization temperature, time of crystallization, pH of the mixtures, pH of the mixtures, pH of the mixtures and other factors such as continuous or semi-continuous operation (Lijalem, 2016).

2.3.7 Application of zeolites

2.3.7.1 Ion exchange (IE)

Ion exchange is a water treatment process in which one or more unacceptable ions separated from water through exchange with another non-objective or less undesirable ion material. A common example of ion exchange is the method called "water softening" to decrease the calcium and magnesium content. Both the impurity and the exchanged material must be softened and have the same type (+, -) of electrical charge (Wang *et al.*, 2016).

2.3.7.2 Adsorption

Adsorption is the binding of electrons, ions, or molecules from a solvent called adsorbate to the surface of particles called adsorbent. A German physicist, Heinrich Kayser, first introduced adsorption in 1881. Adsorption is the mechanism by which atoms, ions, or molecules bind to the surface of the adsorbent, while absorption is the process by which atoms, ions, or molecules migrate through the solid body known as adsorbate to form a solution (Salih and Salih, 2017). Figure 2-8 shows Adsorption and Absorption processes

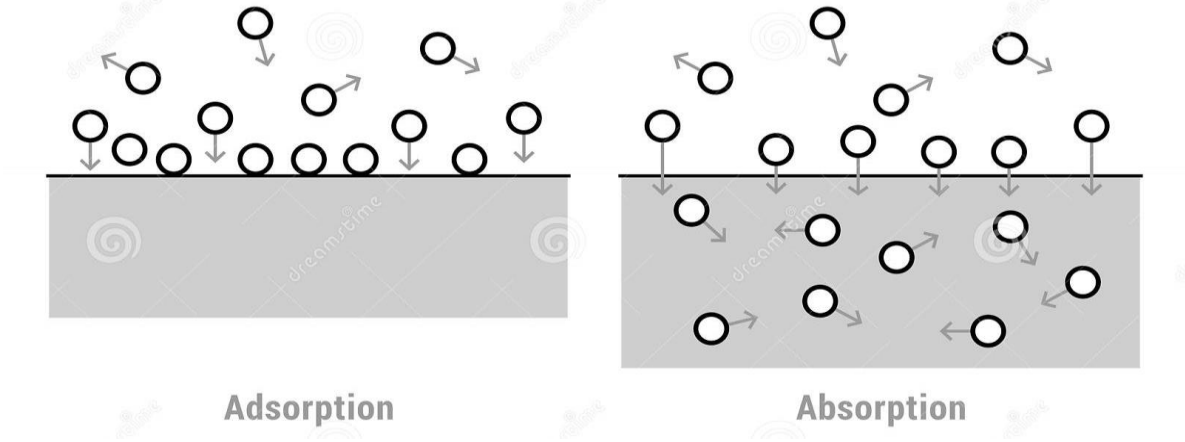

Figure 2-8 (a) Adsorption and (b) Absorption processes

Figure 2-8. (a) Shows the adsorption system, in which atoms, ions, or molecules adhere to the adsorbent's surface, and (b) Shows the absorption mechanism, in which atoms, ions, or molecules penetrate the volume of the absorbing material. Based on the design of the processes involved, there are two basic forms of adsorption (1). Physical adsorption, also known as physio sorption, and (2.) Chemical adsorption is known as chemisorption. (Demirbas, 2008).

2.3.7.3 Physical adsorption or physio sorption

This adsorption mechanism takes place when a multilayer of adsorbate forms on adsorbent with a low enthalpy of adsorption due to weak vanderwaal forces of attraction between adsorbate and adsorbent. Physical adsorption occurs at room temperature or temperatures colder than the adsorbate's boiling point. Increasing the process temperature slows down the physio sorption process (Von-kiti, 2016).

2.3.7.4. Chemical adsorption or chemisorption

The chemisorption mechanism happens as chemical forces or chemical bonds serve as an attractive force between the adsorbate and the adsorbent, resulting in the creation of a single layer of adsorbate on the adsorbent. It takes place both at room and at elevated temperatures. If the process temperature increases, chemisorption increases (Von-kiti, 2016).

2.3.7.5. Types of adsorbents

There are two broad categories of adsorbents, natural and synthetic. Natural adsorbents are the ones that are produced by nature and not artificially made, for example zeolites and clay, whereas synthetic adsorbents are those that are produce from waste material such as agricultural waste and domestic waste. Other examples of adsorbents are activated carbon, activated silica, silica gel, molecular sieve zeolites and polymeric adsorbents (Hameed, Din and Ahmad, 2007).

2.3.8. Factors affecting zeolite synthesis.

Several factors affect the synthesis of zeolites either from expensive chemical sources (silica and alumina) or from cheaper raw materials like clay minerals (kaolin), coal ash, natural zeolites etc. These include:

2.3.8.1. Zeolite adsorbent characteristics

Adsorbent are porous the volume of the reference used determines materials with different density.

1. Densities: adsorbent density can be categorize into materials density, particle density and bulk density.

a. Materials density: this is the real density of the dense material and can be define as the ratio of adsorbent mass, $M_{A,}$ and volume of the solid material, *Vmat*, without pores.

$$\rho M = \frac{MA}{Vmat} \quad (2\text{-}1)$$

b. Particle density, $\rho_{p,}$ is the measure of adsorbent mass M_A and volume of adsorbent with $pores\, VA$.

$$fp = \frac{MA}{VA} = \frac{MA}{\text{Vmat+Vpore}} \quad (2\text{-}2)$$

c. Bulk density, $\rho_{B,}$ is defined as the ratio of adsorbent mass and the total volume of reactor full of liquid and solid, V_R

$$\rho B = \frac{MA}{VR} = \frac{MA}{VL+VA} = \frac{MA}{VL+Vpore+Vmat} \quad (2\text{-}3)$$

2. Porosity.

Porosity known as the proportion of void space in a material's total volume, which may be particle porosity p or bulk porosity ε_B.

a. Particle porosity, εp, This is the adsorbent with particle empty fraction volume and can be represented mathematically as

$$\varepsilon p = \frac{Vpore}{VA} = \frac{Vpore}{Vmat+Vpore} \quad (2\text{-}4)$$

Moreover, can be translate into particle density and material density by

$$\varepsilon p = \frac{Vpore}{VA} = \frac{VA-Vmat}{VA} = 1 - \frac{Vmat}{VA} = 1 - \frac{\rho p}{\rho M} \quad (2\text{-}5)$$

b. Bulk porosity, ε_B. This is otherwise called external empty fraction and is defined as the quotient of the liquid-filled empty volume between the adsorbent particle, $V_{L,}$ and the volume of the reactor, V_R (Worch *et al.*, 2012).

$$\varepsilon B = \frac{VL}{VR} = \frac{VL}{VA+VL} \quad (2\text{-}6)$$

This is related to particle density and bulk density

$$\varepsilon B = \frac{VL}{VR} = \frac{VR-VA}{VR} = 1 - \frac{VA}{VR} = 1 - \frac{\rho B}{\rho p} \quad (2\text{-}7)$$

3. External surface area

The mass transfer rate during adsorption affected by the external surface field. This can be seen and differentiate in the case of external and internal mass transfer of a porous material.

4. All porous adsorbents has internal surface areas (Table 2-3) which typically have to surpass the external surface areas by far and basically, the absorption capacity of a material is furnished by internal surface areas (Worch *et al.*, 2012).

Table 2-3 Few selected adsorbents internal surface area (Worch *et al.*, 2012).

Adsorbent material	BET surface area (m^2/g)
Activated carbon	600 to 1200
Aluminium oxides	150 to 350
Zeolites	400 to 900
Polymeric adsorbents	300 to 1400
Granular ferric hydroxides	150 to 350

5. The pore size distribution of adsorbent.

There are three types of pores with different shapes and sizes as indicated by the International Union of Pure and Applied Chemistry (IUPAC). Meso pore, Macropores and Micropores as summarized in Table 2-4 with their pore radii Meso and Macropores are usually applied for mass transfer into the interior of the adsorbents but Micropores is determining the internal surface size and the adsorbent capacity.

Table 2-4 Adsorbents IUPAC pore size specifications (Worch *et al.*, 2012).

Pore	Radius (nm)
Macro pores	Above 25
Mesopores	1-25
Micro pores	Less than 1

2.3.9. Catalysis

Zeolites have numerous applications and these include crude oil conversion to lighter beneficial hydrocarbon products. The typical reactions involved in catalysis are dehydrogenation, hydrocracking, and isomerization of the polymers. Zeolites have an advantage in catalysis because of their cage-like structural framework and selective due to their characteristic pore size. (Riittonen *et al.*, 2012). Zeolites have been use as precursors in the transformation of low-cost compounds like bioethanol to more valuable hydrocarbons. (Makarfi *et al.*, 2009)

2.4 Characterization Techniques

The characterization approaches for zeolite and membrane samples reviewed here. These approaches include X-ray diffraction (XRD), Scanning Electron Microscopy (SEM) and Brunauer-Emmett-Teller (BET).

2.4.1 X-ray diffraction (XRD)

X-ray diffraction is a non-annihilative investigative technique of determining and quantitative identification of the various crystalline configurations called phases. This was establish by measuring the X-ray diffraction pattern. This method validates the structural characteristics pattern by confirming the fingerprint of the investigating samples. Diffraction takes place when radiation penetrates the crystalline samples and disperses it. The diffraction intensity and direction is a

function of the crystal lattice orientation with the radiation. Roentgen and Laue 1915 theory to determine crystal structure from the diffraction pattern produced by Bragg was the first to discover X-ray diffraction in 1914. (Lijalem, 2016).

Sir W. H. Bragg and Sir W.L. Bragg established a relationship in 1913 to explain separated faces of crystals that represent x-ray beams at precise angles of incidence. They explained that crystalline solid waves are disperse by interplanar distances between lattice planes. These scattering waves interact with one another, and the path length of each wave is an integer multiple of the wavelength. The direction difference of a wave experiencing interference pattern is denoted by 2dsinϴ, where denotes the angle of scattering. As a result, the Bragg law came into existence explaining the condition for constructive interference successive crystal crystallographic planes (hkl) which is deduced by the equation $2d\sin\theta = n\lambda$. This equation called Bragg's equation; n taken as unity, d is the interplanar spacing of the atoms, λ is the wavelength of the incident x-ray figure 2-9.

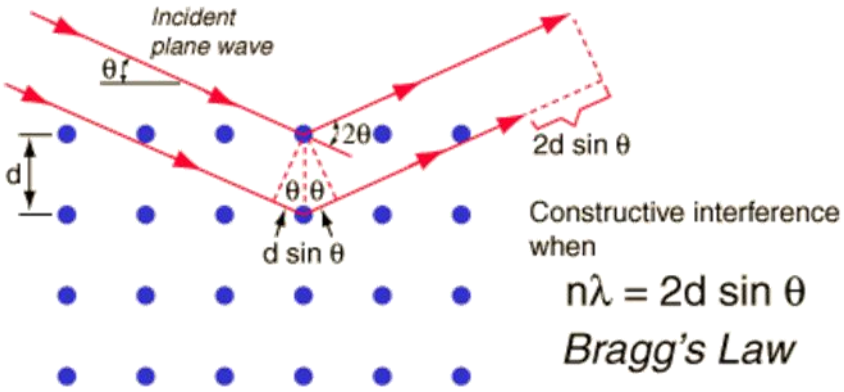

Figure 2-9 Reflection and diffraction from crystals lattice plane of X-Ray (Lijalem, 2016).

All crystalline materials have unlimited number of lattice planes and discrete Miller indices, from which numerous d spacing is deducted by modification of the Bragg equation and its application to all crystal systems (Fig. 2-10). Delineating the amplitude of scattered waves as a function of

scattering angle yields the diffraction pattern. As the dispersed waves satisfy the Bragg condition, Bragg peaks extracted in the 32-diffraction pattern. Bragg peaks can be apply to deduce the crystallinity of crystals. Diffraction of the x-ray is applied to estimate information about structural properties of all crystalline material (Lijalem, 2016).

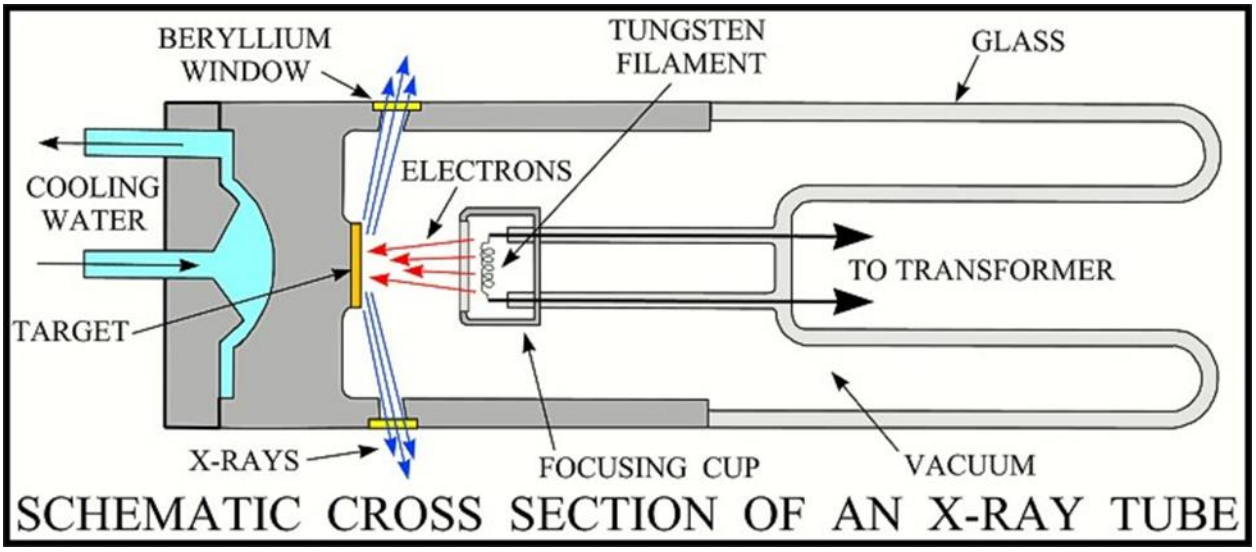

Figure 2-10 Schematic diagram of the cross-section of a typical X-Ray tube (Salih and Salih, 2017)

The XRD apparatus (Fig. 2-10) consists of an x-ray tube where the electron is discharge to the cathode and are surge through the vacuum where they hit the target metal anode. Metallic elements such as copper (Cu), molybdenum (Mo) and cobalt (Co) are usually applied as the anode (Lijalem, 2016).

2.4.2 Scanning Electron Microscopy (SEM)

This is the fantastically flexible mechanisms available for the assessment of the morphology of solid substances such as zeolites and kaolin (Radetié, 2011). The design of a common SEM shown on (Fig. 2-11) unveil that it is made up of an electron gun located on the upper side of the column that gives rise to an electron with energy level ranging 0.1-30 eV. A high vacuum influences

electron transport in the absence of interference or scattering by air. SEM performance is subject to the concept of interaction between the sample and the electron beam that gives rise to a signal from secondary electrons backscattered electron which commences triggering images (Lijalem Ayele Regassa, 2016).

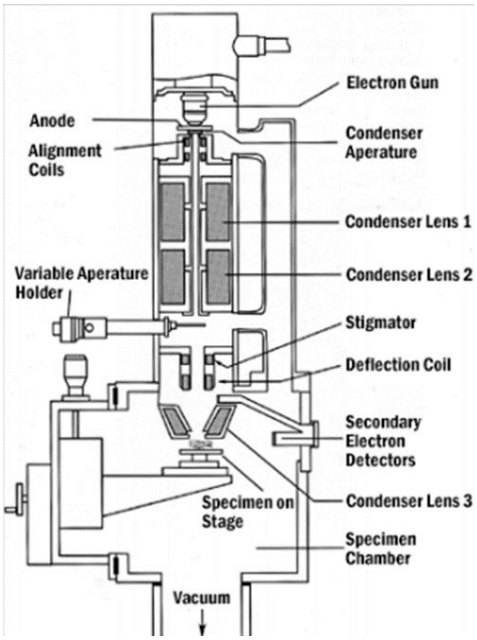

Figure 2-11 Schematic diagram of the cross-section of a typical scanning electron microscopy (SEM) (Salih and Salih, 2017)

2.4.3. X-ray fluorescence (XRF)

X-ray fluorescence is a procedure whereby electrons evacuated from their microscopic orbital locations, discharging a surge of energy that is typical of a specific element. The sensor in the XRF instrument, which in turn labels the energies by element, then, records this discharge of energy.

2.4.4. Brunauer-Emmett-Teller (BET).

The measurement of surface area, pore volume and porosity of a material specifically carried out by the theory of gas adsorption founded by Brunauer, Emmett, and Teller called BET analysis. The surface area and porosity analysis for this study are achieve by N2 adsorption and desorption isotherms at −196°C employing the Micrometrics Tristar 3000 analyzer. Before N_2 physisorption samples were degassed at 150 °C for 4–5 h using helium.

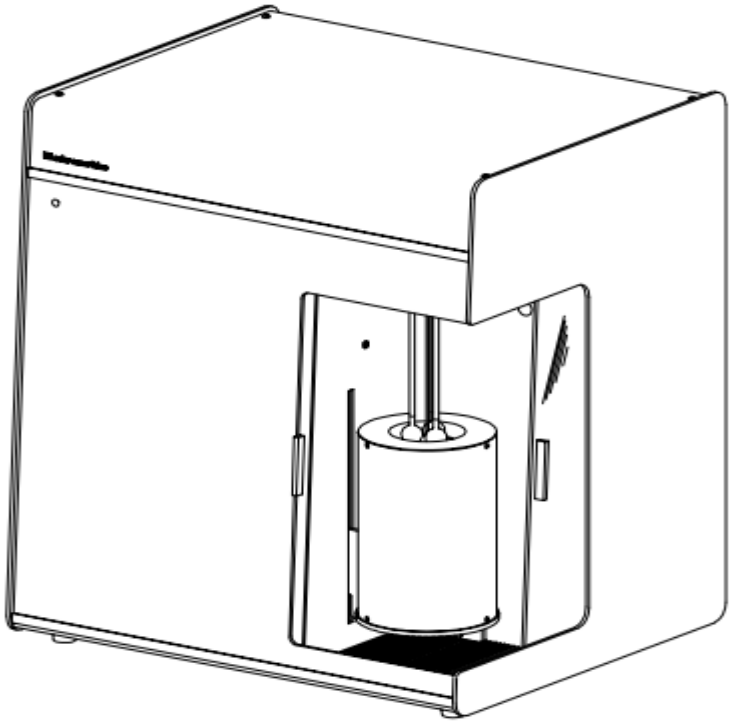

Figure 2-12 Simplified schematic diagram of Tristar 3000 analyzer (Micromeritics, 2007)

The Trista micromeritics 3000 analyzers (Fig. 2-12) are programmed gas adsorption machines with three ports that can operate up to three specimens simultaneously. The TriStar 3000 device includes the TriStar analyzer, an optional Smart Prep degasser for sample preparation, a vacuum pump, and a control module for entering study and documentation options. (Micromeritics, 2007).

2.4.5. Thermogravimetric analysis (TGA)

This is a mechanism in which, the consequences of the heart rate of the mass of a sample is examine to acquire quantitative information. The process involves the thermal decomposition of the sample. In this aspect, kinetic and engineering knowledge and judgement is applied and these require the tenacity of prime temperature region for the industrial process application, forecasting the yield after the thermal operation and time required to reach a specific yield (Czarnecki and Šesták, 2000). The operation is usually done in the air and sometimes under inert gas such as helium or argon and the data is documented as the temperature is rising (Lijalem, 2016).

2.4.6. Inductively coupled plasma emission (ICPE).

Inductively coupled plasma emission (ICPE) is use to analyze elements and determine their concentration in a different form. This emission spectroscopy is define as a synergy of light and matter with physical and analytical uses. The physical spectroscopy emission uses emitted, absorbed and scattered light to interpret the chemical system mechanics, whereas analytical spectroscopy emission applies a physical mechanism to resolve the content and concentration of molecular and atomic species in a chemical system. The ICP mechanism emits photons from the ionized mixture of gases compiled by a special concave lens. ICP comes in different methods and technologies for elemental analysis. ICP-AES stands for inductively coupled plasma optical emission spectroscopy. ICP-AES as atomic emission spectroscopy and ICP-MS as mass spectroscopy, which is competent of identifying elements of the periodic table at nano size scale.

2.4.7. Calculation of Crystallites (grain) size

Calculation of crystallites (grain) size and average crystallites from XRD data are perform using the Scherrer equation

$$D = \frac{K\lambda}{\beta cos\Theta} \quad (2\text{-}8)$$

Where D = crystallites size (nm)

K = 0.9 (Scherrer constant)

λ- 0.15406 (wavelength of the X-ray sources)

Θ = peak position (radians)

The peak position full width at half maximum (FWHM) from XRD data must be measured and entered into the Scherrer equation to calculate the crystallite size of the zeolite.

2.5. Membrane Technology Processes

There are many methods of seawater desalination techniques, including reverse osmosis membrane (RO) and thermal distillation techniques such as membrane vacuum distillation (MVC), multi-stage flash distillation (MSF), and multi-effect distillation (MED). Osmosis is a process in which solvent molecules tend to move across a semipermeable membrane from a less saturated to a more concentrated solution. Reverse osmosis employs the osmosis theory to desalt water and other pollutants through the use of a semi-permeable membrane succession.(Nair and Kumar, 2013; Goh *et al.*, 2016; Kaplan *et al.*, 2017). Some of these technologies outlined here.

2.5.1. Multi-effect distillation (MED)

MED is the most historic and thermodynamically efficient form of desalination process (Khawaji, Kutubkhanah and Wie, 2008). Fig. 2-13 represents the concept of MED. The process of MED arises because of lowering the atmospheric pressure in the series of evaporators referred to as effects. The seawater feed undergoes a series of transformation without a high demand for heat in the first set of the effects. After preheated in the tubes, the water in the first effect is raise to boiling

temperature. The temperature of the tubes is increase by the power plant's supply of steam, and the steam is cooled on the other side of the tubes while its condensate is returned to the power plant to boil feed water. (Khawaji, Kutubkhanah and Wie, 2008).

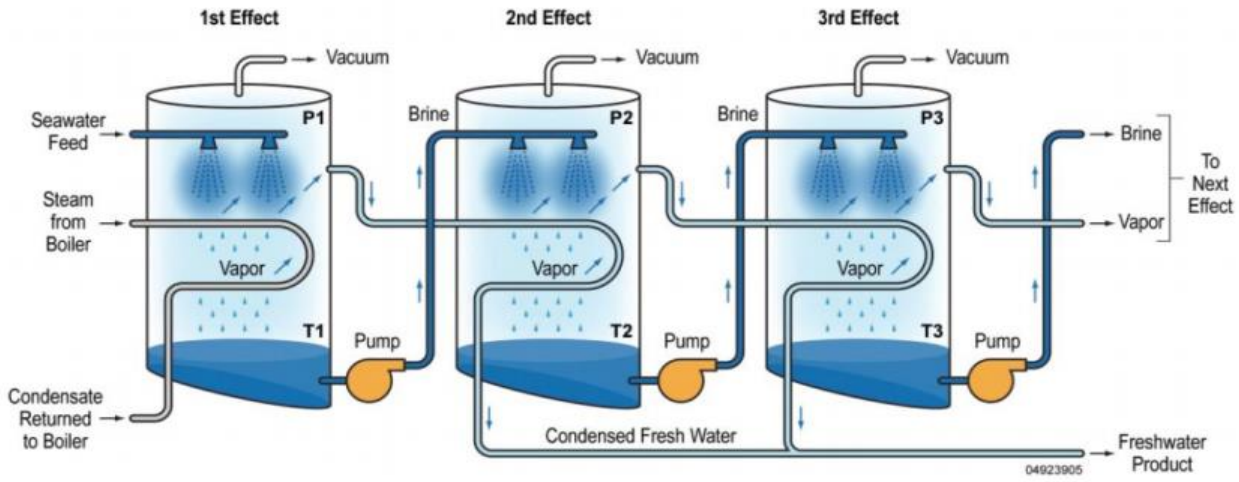

Figure 2-13 Concept of multi-effect distillation (Mayere, 2011).

2.5.2. Multi-stage flash distillation (MSF).

MSF is a method of desalination that driven by heat Fig. 2-14; the heated feed seawater is pressurized in the saline boiler and circulated into the stages. Because of the lower pressure in the room, some of it flashes into steam, and the brine pushes from one chamber to the next, flashing constantly with no additional heat. The flickering vapour is convert into freshwater by being concentrated on a tube of heat exchangers that runs through all of the chambers. The feed water flowing through the furnace cools the pipes and, as a result, heats them, reducing the amount of thermal heat used in the heater.

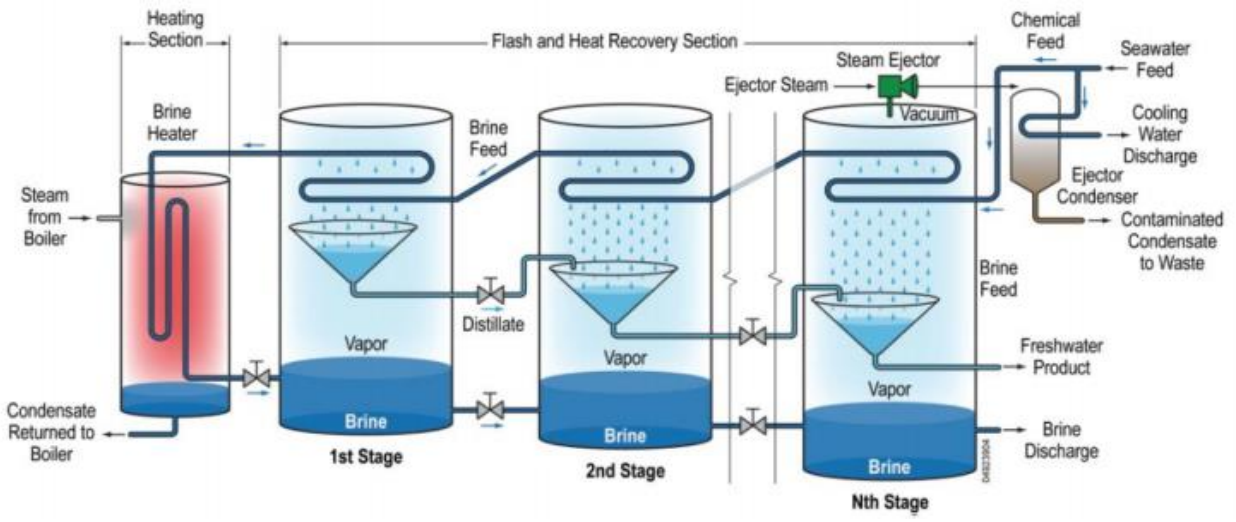

Figure 2-14 Concept of multi-flash distillation (Mayere, 2011)

A MSF plant can have up to 40 stages and typically operates at temperatures ranging from 100 to 110°C to yield 6-11 kg of distillate per kg of steam added. For a 40-year life cycle, the performance ratio can be as high as 12. A plant with an output ratio greater than 7 will absorb 290 kJ/kg of thermal energy when only 4 to 6 kWh/m3 of electricity is used to power auxiliary components. However, the total capital and electricity costs are very high. The Shoaiba Desalination Plant in Saudi Arabia is the largest MSF plant. It was finished in 2003, with a gross capacity of 450,000 m3 per day and a total project cost of $1.06 billion (Mayere, 2011).

2.5.3. Forward Osmosis

The difference in concentration gradient through semi-permeable membranes opposing the substance controls osmotic processes. (Cath, Childress and Elimelech, 2006).

The FO process concentrates a feed stream while diluting a highly concentrated one. FO, as opposed to RO, based on an osmotic pressure differential rather than a hydrostatic pressure differential. The FO process concentrates a feed stream while diluting a concentrate one (often known as the extraction solvent)

The dosages are link by Equation 2-12.

$J_\omega \Delta p = A(\Delta\pi - \Delta P)\Delta P$ (Lee, Baker and Lonsdale, 1981) (2-9)

Which can be transform to

$J_\omega = (\sigma\Delta\pi - \Delta P)$ (Cath, Childress and Elimelech, 2006) (2-10)

Where $J\omega$ is the water flux, A the water permeability constant of the membrane, σ the reflection coefficient, and P the applied pressure. For FO, P is zero; for RO, $P > \Delta\pi$.

FO draw solutes can be replenish with a minimal amount of energy. If the reverse/backward flux of draw solutes is inhibit by the membrane support surface, deterioration of the FO membrane can be decreased (Cath, Childress and Elimelech, 2006).

While various osmotic agents can be use, draw solutions are less expensive and can be replenished using current technology. To mitigate precipitates, draw solutions must be stable, non-toxic, and affordable, as well as have a neutral pH. (Cath, Childress and Elimelech, 2006; Achilli *et al.*, 2009; Subramani and Jacangelo, 2015).

Concentration polarization (CP) closely related across all membrane separation techniques. The consequent pressure difference at the membrane-solution interface allows selective species transfer across a semi-permeable membrane (Pendergast and Hoek, 2011).

Internal concentration polarization (ICP) is reduced as molecules and ions are added to extractions solution while causing backwards salt diffusion. To mitigate solution reversal and achieve high forward flow, Future research in FO desalination should look into this. The draw solute properties influence ICP, concentration polarization, and reverse solute diffusion (Baker. 2012).

Water treatment is one of the processes for FO membranes (Goh *et al*., 2016), waste management (Shaffer *et al*., 2015), water filtration (Shannon *et al*., 2008), generic drug applications (Khawaji, Kutubkhanah, and Wie, 2008), food manufacturing, and energy production (Shaffer *et al*., 2015).

Because of its universal nature, FO piqued the attention of researchers from a wide range of disciplines. However, since it is not rigorously implemented and destroys membrane components, more scholarly analysis is needed to study both hollow-fibre and flat-sheet FO membrane systems to facilitate handling at extreme temperatures with the highest solute resistance, chemical and mechanical stability, and ICP. A draw solution is required to achieve high FO operational efficiency (Lee *et al*., 2010; Chekli *et al*., 2015; Kaplan *et al*., 2017) (Lee *et al*., 2010; Chekli *et al*., 2015; Kaplan *et al*., 2017)

The FO method has the advantage of requiring little to no mechanical pressure to work, with fluid flow created by membrane modules and the device. (Achilli, Cath and Childress, 2010). Cath *et al*. (2006) discovered that filtration bags were commercially viable, did not need strength, and had low fouling characteristics even if used in dark water. They also said that the purified water was devoid of contaminants.

Finally, incorporating FO-hybrid systems with renewable energy will enhance and make water production and draw solution recovery more sustainable (Akther *et al*., 2015). According to thermodynamic principles, FO necessitates little energy effort to achieve separation because the process takes place instantaneously (Baker. 2012).

2.5.4. Reverse osmosis (RO)

Figure 2-5 shows an example of a RO process. That can be accomplish by increasing the pressure above the osmotic pressure of the water. Consequently, water travels through the membrane in the

opposite direction, trapping soluble minerals behind and increasing the concentration of the solution. Heat or phase transition are not needed (Akther *et al*., 2015).

When various amounts of ionic aqueous systems are segregated, an intrinsic phenomenon known as osmotic pressure causes water from the lower concentration solution to dilute the more concentrated solution, resulting in equal unique ecosystem on both sides of the membrane (Greenlee *et al*., 2009). Water molecules cross the membrane towards the more dilute side when hydrodynamic force is exert to the concentrated liquid above the osmotic pressure. This allows for the separation of water from ions and low-molecular-weight chemical constituents. (Bush, Vanneste and Cath, 2016).

RO processes have four phases: pre-treatment, high-pressure pumping, membrane isolation, and post-treatment (Ayyash *et al*., 1994). In this segment, only the membrane separation section is considered.

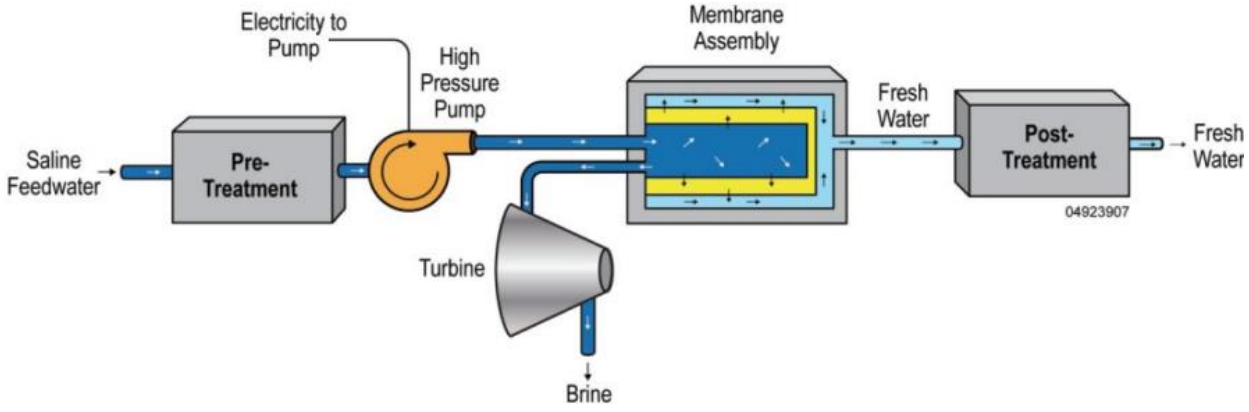

Figure 2-15 Concept of reverse osmosis process (Mayere, 2011)

The two most commercially successful module types are hollow fine fiber and spiral-wound membranes (Bou-Hamad *et al*., 1998). In U-shaped, pressure vessels, hollow fine fiber membranes made of cellulose triacetate and polyamide ar carried. They, High water flux, high salt rejection,

strict adherence to public health rules, and environmental protection are all advantages of spiral-wound membranes.

Despite their advantages and ability, RO membranes have disadvantage of low pervade flux, low selectivity, moderate resilience, fouling potential, and high machinery and operating costs, which make the method inefficient (Wenten and Khoiruddin, 2016).

Since the mid-twentieth century, efforts made to refine RO technologies and reduce both capital and operational costs, especially through advances in membrane process. These advancements included enhanced flux, long lifespan, enhanced salt flow, higher compression resistance, and increased potential recovery (Subramani and Jacangelo, 2015).

Despite membrane fouling and operational cost concerns, many researchers suggest RO is by far the most efficient membrane separation technique. Fouling affects desalination and other water treatment procedures in pressure drive and membrane-based systems (RO, NF, UF). Fouling is described as accumulation on the membrane's surface and/or in its pores, which reduces resistivity and effectiveness, as well as water flux capacity (Tijing *et al.*, 2015; Majeed *et al.*, 2016).

The main fouling issues in RO secondary treatment processes are microorganism colonization and the deposition of undesirable materials. They can cause serious membrane damage, raise operating costs, and reduce performance if not managed properly. Colonies of microorganisms can permanently damage cellulose acetate membranes (Shannon *et al*., 2008). About the fact that polyamide membranes cannot be degradable, there seems to be a possibility that membrane efficiency will be impaired. (López-Ramrez *et al*, 2006). When compared to cellulose acetate membranes, the surface morphology and roughness of polymeric polyamide aromatic membranes have a high influence on colloidal fouling in RO (Elimelech *et al*., 1997).

2.5.5. Membrane Distillation (MD)

This technique is thermally motivated (fig.2-16), centered on the influence of the thermal gradient on the total vapour pressure differential at the liquid-vapor interface (Tomaszewska *et al*, 1995). At low temperatures, MD extracts water vapour from aqueous solutions (Abu-Zeid *et al*., 2015). Vaporization produces pure water distillate, which concentrates the solution in the feed vessel.

MD membranes are hydrophobic and porous. Most are polymeric, such as polypropylene (PP), polytetrafluoroethylene (PTFE), polyvinylidene fluoride (PVDF), zeolite, and ceramic materials. The process runs at temperatures ranging from 50 to 80 degrees Celsius and can be power by waste heat or solar energy. Because of the low concentration polarization effect, it can operate at very low pressures in comparison to pressure-driven membrane techniques such as RO and use very concentrated feed solutions. MD membrane separation has a well-established and documented potential value (Al-Ansari, Ettouney and El-Dessouky, 2001; Alkhudhiri, Darwish and Hilal, 2012). MD membranes act as a barrier amongst the processes feed) and permeate sides (Fig. 2-16) Mass transfer and separation exist as membrane characteristics only in MD, where the membrane serves as a support. The vapour pressure gradient that exists amongst the input and output streams cause mass transfer.

MD is a comparatively new, low-cost procedure that is being study worldwide. It uses less energy than RO, distillation, or other hydraulic separation processes, resulting in substantial energy savings (Lawson and Lloyd, 1997).

When running at a low temperature, MD produces almost 100% salt rejection and a high performance (permeate) flux that is unaffected by salt concentration, etc. (Maab *et al*., 2013). It is

a rising desalination technique for producing potable water from seawater, but it has a high-energy consumption due to substantial heat loss by conduction through the membrane (Lee *et al*., 2015).

Unlike RO, MF, and UF membranes, are use for separation; the MD membrane is usedto assist the liquid-vapor interface. The MD membrane does not function as a sieve or use to distinguish between solution compositions concentrations. As a result, these membranes can be produced of corrosion - resistant composites such as PTFE, PP, which PVDF, and have large diameter pores that do not readily foul (Lawson and Lloyd, 1997).

The MD idea can take many different procedures. The goal is to create a vapour pressure gradient that will allow vapour to pass through the membrane. The following methods were used to reduce vapour pressure on the permeate side: (a) direct contact MD (DCMD); (b) air gap MD (AGMD); (c) sweeping gas MD (SGMD); and (d) vacuum MD (VMD). Each approach has benefits and drawbacks based on the feed solution to be processed (Imdakm, Khayet and Matsuura, 2007).

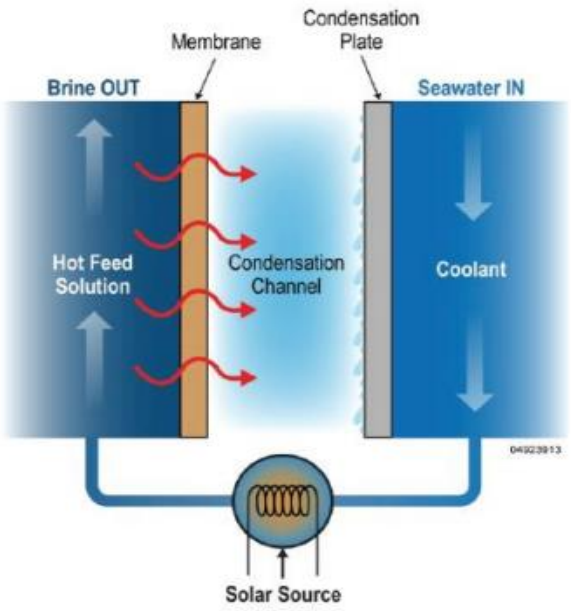

Figure 2-16 Concept of membrane distillation (Mayere, 2011)

MD is a thermally controlled process that operates at concentration gradient ranging from zero to a few kilopascals – a bit slower than pressure-driven systems such as RO. As a result, equipment costs are minimal, and process safety is high. (Lawson and Lloyd, 1997). Because they have similar applications, MD is comparable to pressure-driven systems like UF, MF, and RO (Lawson and Lloyd, 1997).

2.5.6. Direct Contact Membrane Distillation (DCMD)

In DCMD Fig. 2-17, the (saline) feed temperature of the water must be above 80°C and isolated from the cold filtrate by a porous, hydrophobic membrane (Maab *et al*., 2013). DCMD uses membranes with high porosity and pore sizes ranging from 0.1 to 0.6 m. If the solution pressure is less than the breakthrough pressure, hydrophobic membranes with this amount of porosity cannot wet by aqueous non-wetting solutions such as saline water under continuous operating conditions. (Sirkar and Qin, 2001). Conduction through the pores transports vapour and heat from the hot brine side to the cool distillate side. Evaporation is the process by which heat is lost. By minimizing conductive heat transfer, DCMD performance is maintain. Thermal condensation across polymer base walls often exceeds heat resistance through a vapour space, meaning that high porosity; thick-walled membranes have a lower heat loss conductive propensity (Li and Sirkar, 2005).

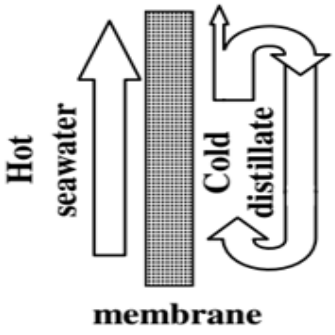

Figure 2-17 Schematic diagram of DCMD

Since the condensate and cooling surface of the film are in close contact with the membrane, they are the process effects in DCMD (unlike in AGMD).

2.5.7. Air gap membrane distillation: (AGMD)

In AGMD Figure 2 – 19 A thin air gap formed between the membrane and the freezing surface. Vapour molecules can pass through the membrane and condense on the cooling surface thanks to the air gap and membrane (Lee *et al*., 2010; Wang and Chung, 2015). The air gap acts as a barrier to the transfer of vapour.

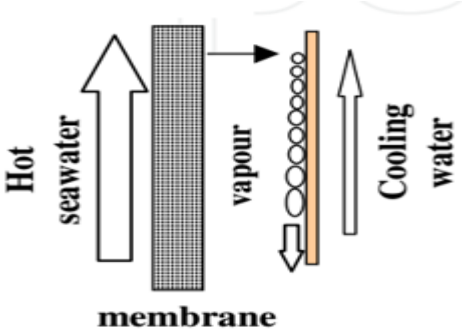

Figure 2-18 Schematic diagram of AGMD

AGMD formations have a lower water flux than DCMD formations (Warsinger *et al*., 2015). The integrated cooling plate of AGMD has enabled comprehensive research into multi-effect or multi-stage membrane modules with improved thermal performance (Wang and Chung, 2015; Wang *et al*., 2016).

2.5.8. Sweep gas membrane distillation (SGMD)

An inert gas is added into the permeate stream in SGMD Fig. 2-19 to sweep into the permeate flow and absorb vapour molecules from the membrane surface. Typically, the vapour cooled in a different condenser outside of the membrane configuration (Burn *et al*., 2015). The machinery can be very expensive (Wang and Chung, 2015).

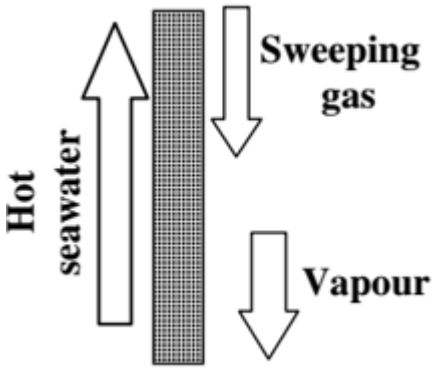

Figure 2-19 Schematic diagram of SGMD

2.5.9. Membrane vacuum distillation (MVD)

The input temperature and the pressure of the vapor are the operative variables affecting the permeation flux in vacuum membrane distillation (MVD) (Fig. 2-20). There is less effect on other operational conditions. The MVD membrane materials are the same as those used in MD, but are configure differently. In MVD, the impermeable area of the membrane is vacuum using a pump by applying hydraulic pressure. There is no thermal loss. The membrane area is condensed (Achilli, Cath and Childress, 2010; Alkhudhiri, Darwish and Hilal, 2012).

The reports from Banat and Simandl (1999) and Imdakm *et al*. (2007) show a significant influence on performance and achieve the great driving force throughout the membrane, toruosity, membrane stiffness, pore size distribution, and permeability are all factors to consider. It requires low mechanical membrane performance and can achieve strong salt rejection for non-volatile solutes (Abu-Zeid *et al*., 2015). MVD is a modern desalination technology that uses little resources. The transmembrane process that is base on the difference of vapour pressures that may be held on the permeated side of the membrane (Pérez-González *et al*., 2012). On one side of the membrane, in MVD, cold distillation is produce with a vacuum for the extraction by vaporization (Li and Sirkar, 2005). In contrast to DCMD, the extracted steam liquefied into another condenser.

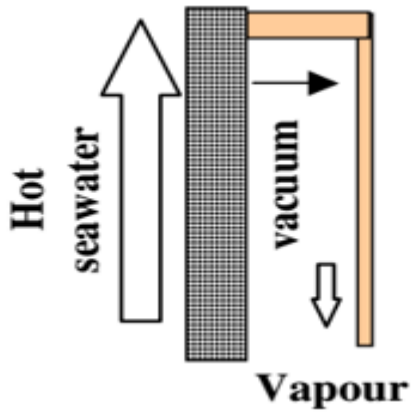

Figure 2-20 Schematic diagram of MVD

2.5.10. Membrane Modules:

2.5.10.1 Plate and Frame

In plate and framework membrane modules, spacers are located between pairs of identical flat sheets. Such membrane normally used for simplicity in laboratory configurations. The MD used to treat water and desalination plates and frame modules (Alkhudhiri, Darwish and Hilal, 2012). The modules and their operation shown in Figures 2-21 and 2-23.

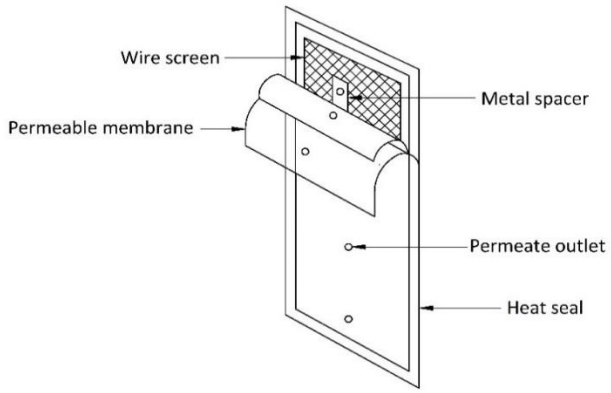

Figure 2-21 Schematic model of plate and frame membrane modules (Aliyu, 2018)

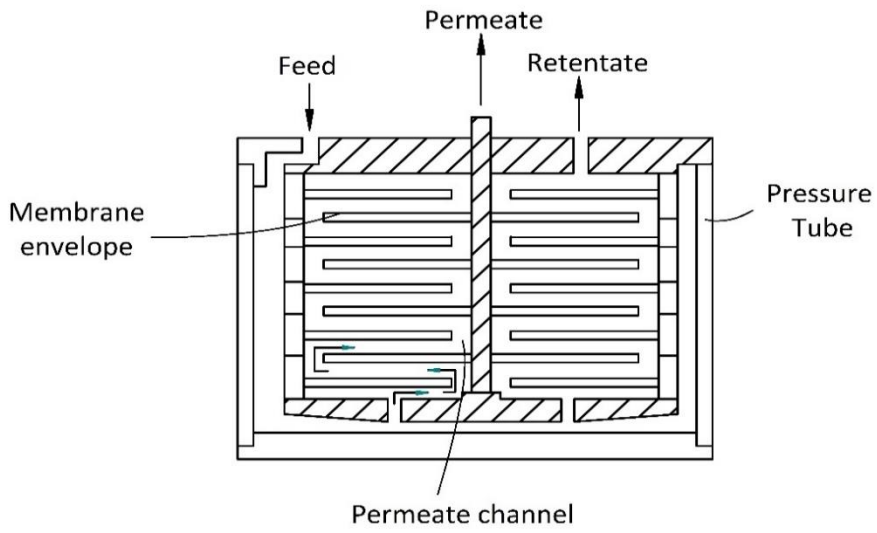

Figure 2-22 Plate and frame membrane module operation (Aliyu, 2018)

2.5.10.2. Hollow Fiber

Figure 2-23 of this module has a hollow fiber, which has a tubular shell and is secure. The feed enters the shell and the filter released via the membrane. This module used to treat apple juice and alcohol in their independent studies by Laganà *et al* (2000) and Fuji & kigoshi (1992) and Elimelech *et al*. (1997) used capillary, polypropylene membranes to treat saline water.

The high packing density and low energy usage of hollow fiber membrane modules is an advantage. The downsides are high tendency to deflect, maintenance and a possible replacement after damage (Lee, 2008).

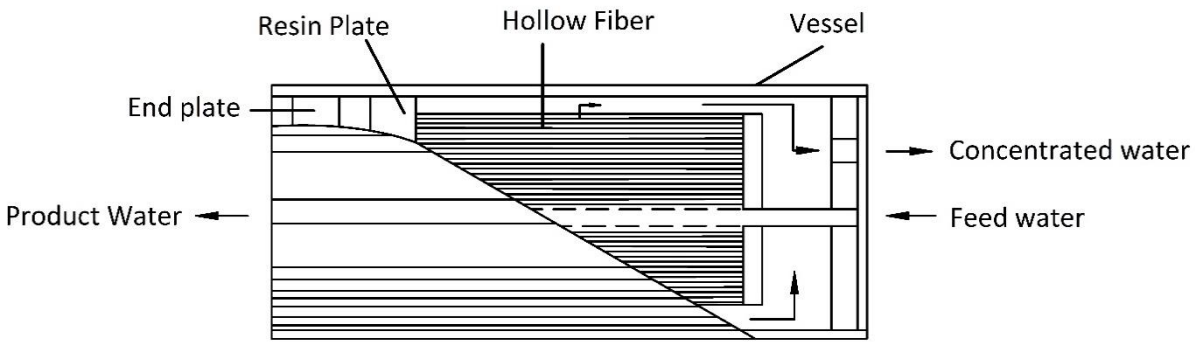

Figure 2-23 Cutaway model of the hollow-fibre membrane module (Baker., 2012)

2.5.10.3. Tubular Membrane

The membrane structure of this tube are place between warm and cold parallel cylinders. The tube-shaped membrane component has the benefits of low propensity to foul, easy repairs and good areas for contact, making it attractive for business applications. It also covers MD but also has a low packaging density and high operating costs. In many MD systems (DCMD, AGMD & VMD) ceramic membranes were apply to treat aqueous NaCl – with salt rejections of more than 99%. (Cerneaux *et al*., 2009; Alkhudhiri, Darwish and Hilal, 2012).

2.5.10.4. Spiral Wound Membrane

Spiral wound membranes are construct to pack and wound a flat sheet and spacers around a punctured collection area. The feed solution axially crosses the membrane and the filter moves radially through the collection area into the centre. Spiral membranes with a low fouling tendency (figures2–24 and 2–25), moderate energy consumption and decent packing density. Two fundamental methods, cross-flow and dead-end flow, apply to microfiltration processes and both apply to MD. For example, crossflow when the feed is tangently move to the membrane, with the treated water crossing the membrane while recirculating the feed solution (Lee, 2008).

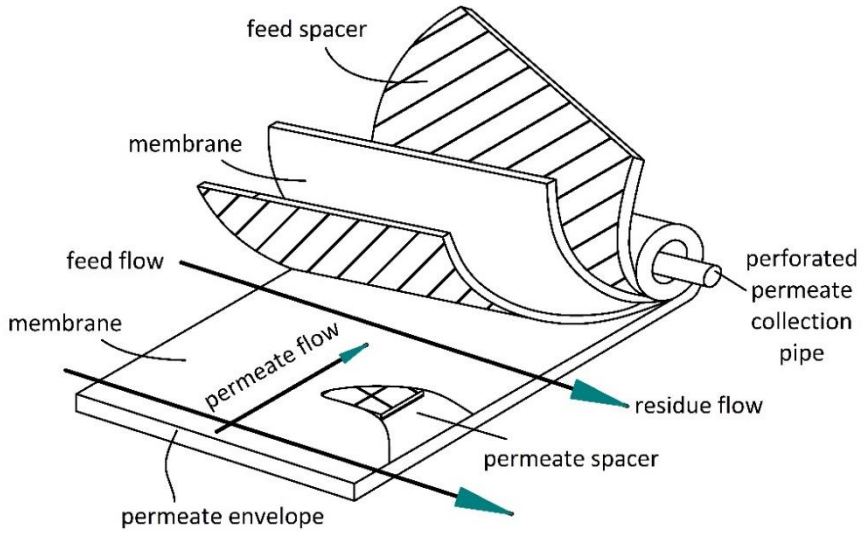

Figure 2-24 Spiral wound membrane module and filtration operation (Aliyu, 2018)

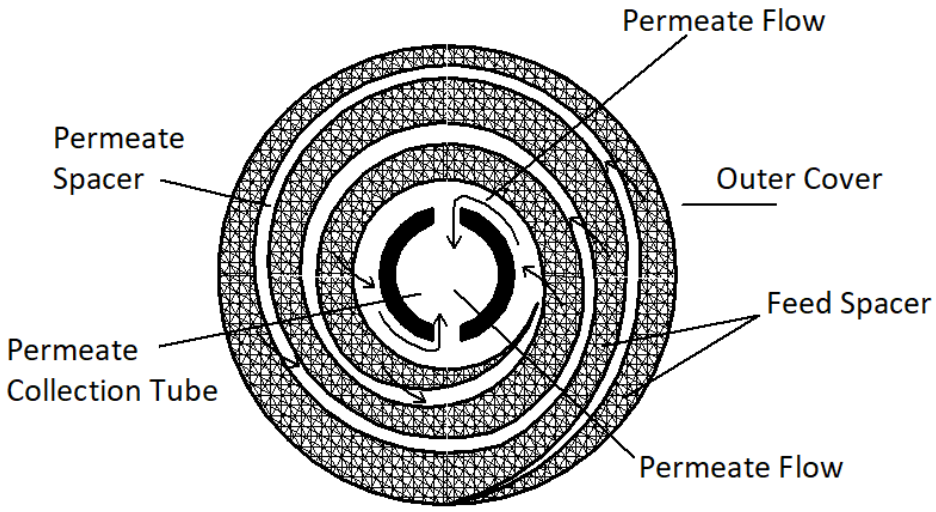

Figure 2-25 Cross-section of the spiral wound membrane module (Aliyu, 2018)

2.5.10.5. Pervaporation (PV)

V is a desalination process of high salt content for sea and brackish waters (Wang *et al*., 2016). In academia and industry, extensive work were been done to establish a Thin Composite Film TFC membrane for better efficiency and sensitivity, chlorine, solvents, and fouling resistance (Lau *et*

al., 2012). In PV, the membrane behaves as a molecular sieve between the feed and permeate while in MD, it merely serves as a support (Semiat, 2008). Polyethene and cellulose were use for membrane technology in the 1960s, but the researchers began paying attention to Silica zeolites since the turn of the century. The synthesis of new composite membranes from organic inorganic sources and high-water flux TFCs has progressed in the desalination of PV membrane by organic and non-organic membrane. (Lau *et al*., 2012; Wang *et al*., 2016). With continued growth in both industry and academia, membranes projected to remain the most feasible options for extracting cheap fresh water from seawater.

2.5.10.6. Microfiltration/Ultrafiltration/Nano filtration

These processes mainly vary in pore size of the membrane. MF membranes have bigger pores and only reject microorganisms that are relatively larger than UF membranes, whose pores are much larger. UF can reject super molecules and bacteria. NF, sometimes known as "loose RO" membranes, is new and is limited to RO applications (Chollom *et al*., 2015).

In the 1960s, water treatment and purification MF and UF low-pressure membrane technology were established. Their membrane sizes range from 0.08 to 0.5 to 0.001 to 0.01. (Fig. 2-26). MF allows effective colloidal suspension separation and treatment, while UF is use to separate and treat moderate molecular solutions/suspensions (Buffle *et al*., 1998; Wu *et al*., 2017).

MF is a water treatment technique in which contaminated solutions treated with a membrane with a specific pore size. It allows microorganisms and suspended solids to be isolated from a feed solution and is usually used in conjunction with other separation techniques such as RO and UF (Chollom *et al.*, 2015).

Development in UF and MF membrane technologies for water recycling has resulted in a membrane pretreatment breakthrough in seawater desalination (Busch, Chu and Rosenberg, 2010; Voutchkov, 2010). Several aspects highlight the need to take into account MF/UF rather than conventional pretreatment (fig. 2-27). These include the ability to handle harsh water, reliability, design and operation easy, and lower cost of operation and capital (Busch, Chu and Rosenberg, 2010; Wu *et al*., 2017). Tuberculosis can restrict UF and/or MF pretreatment, resulting in low plant yield. However, since UF and MF have low salt rejection, RO membrane biofouling cannot be avoid.

NF can divide colloidal parts between UF and RO and the pores are between 0.5 and 5 nm. It is pressure-driven and can tolerate differential pressures ranging from 500 to 2000 kPa, making it less permeable than RO but with greater permeation. (Chollom *et al*, 2015). NF can limit divalent (Ca2+, Mg2+), monovalent ions (Na+, K+ and Cl-).

NF is similarly use as RO, but it is different in the structure of the network. It used extensively in water treatment and organic removal, as well as treatment and rehabilitation of wastewater (Elimelech *et al*., 1997; López-Ramir, Oviedo and Alonso, 2006).

NF and RO low-pressure processes often use laws and regulations concerning drinking water treatment with minimal health risks for surface water treatment.

By combining the above methods, a new technical phenomenon known as an integrated membrane system has been developed (IMS). The use of IMS reduces the problem of membrane fouling (Lee, 2008).

The rating of desalination processes affected by IMS (Figure 2-27), for example:

1. The MF/UF filter efficiency is strong and stable over time, and the colloidal fouling and turbidity load on the RO can be reduce.

2. The colloidal RO/NF fouling frequency is decrease.

3. Compared to chemically improved, traditional pretreatment operations, the concentrates from MF/UF can easily be discharge (Kabsch-korbutowicz, 2005).

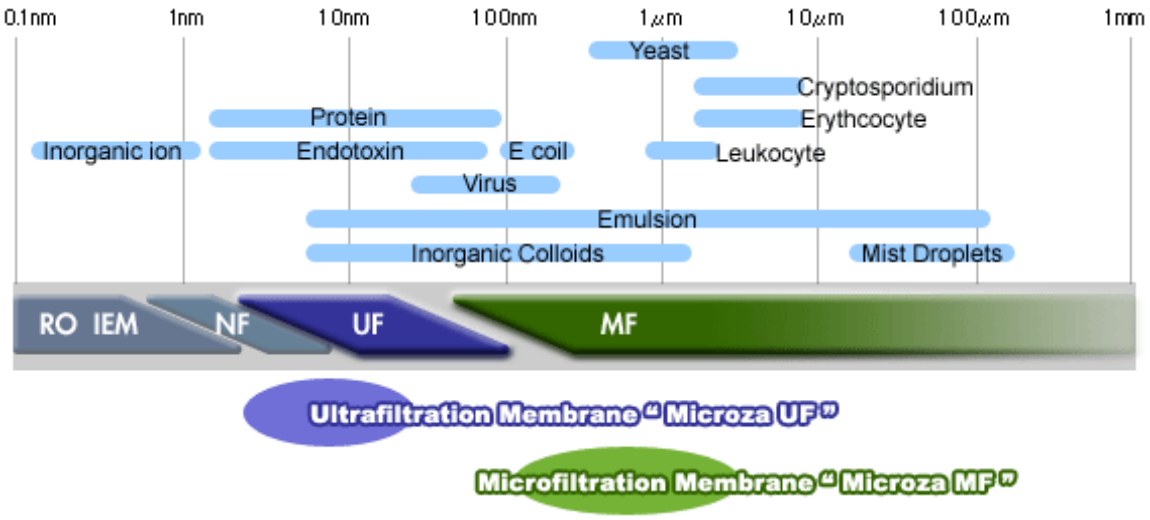

Figure 2-26 Membrane types and corresponding pore sizes (Lee, 2008)

2.5.10.7. Membrane Integration in Desalination Processes

Integration of membrane desalination processes may reduce salt release and increase water recovery (Godino *et al*., 1996). Several studies report on the efficacy and economic feasibility of energy consumption and flow with MD/NF or MD/RO integration (Yun *et al*., 2006; Qu *et al*., 2009; Chunrui *et al*., 2010; Ji *et al*., 2010; Mericq, Laborie and Cabassud, 2010). De Andrés *et al*., (1998) have reported a 7.5 percent increase in yield/flux and a 10 percent increase in energy efficiency because of MD incorporation.

By integrating MD into desalination operations, a fouling problem can be apparent due to inorganic species deposition e.g. Ca^{2+} on the membrane surface (Wang and Chung, 2015).

Fresh water collected from saline water by capturing and melting freeze crystals formed during freezing desalination (FD) (Manwell and Mcgowan, 1994; Guan *et al*., 2012). Während FD little water recovers, Wang & Chung (2012) suggest that an FD-MD desalinisation technology could improve recovery and efficacy, by concentrating the saline reject from FD through MD processing. Both processes produce 71.5 percent of salt-free water.

2.5.11. Membrane Classification

2.5.11.1. Organic Membranes

The organic membranes are made up of either celluloses or altered organic polymers – e.g. PE (Xie, Ng, *et al*., 2011), or polyether-amide (Zwijnenberg, Koops and Wessling, 2005) polyether-esters (Xie, Ng, *et al*., 2011), cellulose-based membranes (Xie, Ng *et al*., 2011), polyesters (Wang *et al*., 2016), nanostructures (Krzeminski *et al*., 2017) or polyvinyl alc. (Krzeminski *et al*., 2016). (Wang *et al*., 2016).

As described in Table 2-5, common organic membrane materials are:

• PE - Polytetrafluoroethylene. polyethylene (PE) (PTFE)

- Polypropylene (PP) - polyacrylonitrile cellulose acetate (CA) (PAN)

- Polysulfones - polyimides (PI) - polyether sulfones - polyimides (PES)

Table 2-5 Typical organic membranes, with process types, driving force, technology, membrane types and permeation fluxes

Process	Driving Force	Potential use	Membrane material	Typical fluxes $L/M^2.h$	Temperature	References
RO	Induced Pressure	Desalination	PA, CA	90	60°C	(Greenlee *et al.*, 2009; Pérez-González *et al.*, 2012; Antony *et al.*, 2016)
FO	Osmosis	Desalination	Cellulose triacetate (CTA)	3.1	50°C	(Wang *et al.*, 2014; Sahebi *et al.*, 2015; Majeed *et al.*, 2016)
MD	Thermal	Desalination, brine concentration	polyvinylidene difluoride (PVDF), PTFE, and PP.	n.r.	50°C-80°C	(Al-Ansari, Ettouney and El-Dessouky, 2001; Alkhudhiri, Darwish and Hilal, 2012; Maab *et al.*, 2013; Wang and Chung, 2015)
PV	Thermal	Desalination	PVDF, Polyether amide	0.03	90°C	(Swenson *et al.*, 2012; Zhu *et al.*, 2014);
MF	Induced Pressure	Desalination	PTFE, Acrylonitrile polymer	n.r.	25°C	(Lee, 2008; Bush, Vanneste and Cath, 2016)
UF	Induced Pressure	Desalination	PTFE, PVDF and CTA, regenerated cellulose	91.2×0^3	75°C	(Lee, 2008; Busch, Chu and Rosenberg, 2010; Chekli *et al.*, 2015)

NF	Induced Pressure	Desalination	CTA	≤ 17.4	25-55℃	(Noghabi *et al.*, 2011; Chekli *et al.*, 2015)
ED	Electric current	Brackish water desalination	CTA	≤ 3.5	Ambient temperature	(Greenlee *et al.*, 2009; Pérez-González *et al.*, 2012; Burn *et al.*, 2015)
MED	Thermal	Desalination, brine concentration	PVDF, PTFE, and PP.	n.r.	50℃	(Maab *et al.*, 2013)

*n. r (not relevant)

2. 5.11.2. Inorganic Membranes

There is currently considerable focus on PV research on inorganic membranes such as zeolites. Good thermal and chemical stability, good separation and low fouling propensity, offer inorganic membranes (Zou *et al*., 2011). Moreover, their rigid ceramic shape and so-called "definite porosity" means they are suitable in processes of separation based on molar shapes and size. Desalination processes dominated by the morphology of the membrane (Wang *et al*., 2016).

Zeolites are the most effective inorganic membrane material with 0.3 to 1.3 nm of porosity. Synthesized A and ZSM-5 zeolites on a support membrane for alumina (Malekpoour, Millani and Kheirkhah 2008), and created a perfect MFI membrane using the secondary growth method without template and Si / Al ratio.

Wang et al. (2016) used the silicalite-zeolite membrane. Salt rejection has increased from 97 per cent to more than 99 per cent with aluminum/silica ratios between 20 and 500 with zeolite membrane Al/Si. RO Na+ 17% refusal recorded with an Al/Si ratio of 100 ZSM-5 zeolite membrane while the negative Na+ refusal with other membranes recorded. Different Al/Si ratios

can influence water streaming in PV processes with hydrophobicity or membranes thickness, as the surface charge is not link to Al/Si.

Molecular screening is the ideal technique in the use of inorganically porous membranes for desalination by size exclusion. Sometimes, the ion exchange between the membrane and the feed solution produces higher membrane flow rates for concentrated salt than for freshwater (Wang *et al*., 2016).

Wang (2016), has also confirmed the conversion of a limited amount of salt across inorganic and polymeric membranes. Finding better methods to handle this in PV desalination requires more research.

2. 5.12. Energy Consumption and Salt Rejection Efficiency

The energy consumption of a RO device varies between 6 and 8 kWh/m3 depending on salinity and system capacity, with efficiencies of up to 99.75 percent (Lee, Arnot and Mattia, 2011; Mayere, 2011) as the feed must be pressurized to the best performance over the saline's osmotic pressure.

FO's power consumption and efficiency are lower than RO, as FO does not drive energy. Its effectiveness is therefore only reasonable (Chung *et al*., 2012; Kaplan *et al*., 2017).

With moderate efficiency MSF energy consumption range from 2.5 to 5 kWh/m3 (Blank, Tusel and Nisan, 2007; Semiat, 2008).

MED uses 2-2.5 KWh/m3 of energy and achieves a rejection of the salt of over 90%. (Blank, Tusel and Nisan, 2007; Semiat, 2008; Thiel *et al*., 2014; Chekli *et al*., 2015; Kaplan *et al*., 2017).

While energy not driven by PV, MF, UF and NF, the efficiency of salt rejection is between 90 and 99.99 per cent (Zwijnenberg, Koops and Wessling, 2005; Blank, Tusel and Nisan, 2007; Lee, 2008; Semiat, 2008; Ge *et al*., 2011; Chekli *et al*., 2015; Fasano *et al*., 2016; Kaplan *et al*., 2017).

2.5.13. Materials for Inorganic Membranes

Inorganic membranes made up of the following basic materials:

1. Aluminium oxide is a chemical compound (Al2O3)

2. Zirconium oxide is a chemical compound (ZrO2)

3. S/S (stainless steel)

4. (Shirasu Porous Glass) (SPG)

In comparison to inorganic membranes, organic membranes have relatively low structural properties, thermal tolerance, and chemical inertness. However, these advantages are often compound by higher initial capital costs.

2.5.14. Hybrid organic-inorganic membrane modification:

The benefits of marine desalination include high flows, ion exclusion, and high selectivity through zeolite membrane processes (Zhu *et al*., 2014). Fouling membrane can significantly increase operating costs as energy demand increases and productivity is reduce and quality is permeated (Jiang, Li and Ladewig, 2017). Fouling, removal of foulant and membrane cleaning as well as maintenance can be controlled and the membrane life reduced by pre-treatment (Achilli *et al*., 2009; Tang *et al*., 2016; Jiang, Li and Ladewig, 2017).

There has been a new hybrid membrane consisting of a combination of chemically bonded organic and inorganic phases. It is stable and has a good flow of penetration. A sol gel-mechanism was use to synthesize PVA with organic silica spread on it (Hoang, *et al*., 2011). This improved PVA water stability and PV desalination efficiency. The flow increases from zero to 10% from 4.29 to 5.51L/m^2·h at 22°C and vacuum from 800 Pa if the silica content is increased during PVA/malic

anhydrides/silicate diaphragm synthesis. This may be due to the increase in the volume of free silicone nanoparticles due to their size (Hoang, *et al*., 2011). The flow rose to 11.7 $kg/m^2 \cdot h$ when the feed temperature rose to 65°C (Xie, *et al*., 2011). Due to the chemical and thermal strength of the Zeolite inorganic phase, the hybrid membrane is robust.

CHAPTER THREE

3. METHODOLOGY AND EXPERIMENTAL STUDIES.

3.1 Introduction

In this chapter, the methodology used in the synthesis of candidate zeolites A and ZSM-5 is been presented. After synthesis, the resulting powder sample was analyze based on XRD, SEM, BET, TGA, FTIR, etc., to confirm the samples produced are the targeted zeolites. Furthermore, an investigation into their performance in desalinating seawater performed using batch experiment. Based on this the candidate zeolite was a screen and selected for the deposition on the surface of the α-alumina sheet membrane. Experiments conducted to find a solution to the membrane-fouling problem. The experiment focused on three major aspects. The first part was the synthesis and characterization of the candidate zeolites and the second part is the deposition of the zeolites on the membrane support while the last part is desalination using the RO unit.

3.2 Beneficiation of G&W kaolin.

For this experiment, the source is silica and alumina from commercial Kaolin from mineral resources of G&W, Eastern Cape, South Africa. The raw tone (kaolin) was disperse directly from the source into a deionized water and slurry by manually mixing for around an hour with an iron stirrer without applying any scattering agent or changing the pH, the solution was allowed to gravitate for 10 minutes before decanting. Before decanting, the slurry was transfer to a titanium funnel and left to relax for 48 hours and the solution was allow to gravitate for 10 minutes before decanting.

3.3. Metakaolinization.

Conventionally, kaolin is transformed into metakaolin by calcination at a temperature range of 550 to 900℃. In this work, the kaolin from G&W was calcined using a muffle furnace. The crucible containing the kaolin to be calcined was first loaded into the furnace and heated to 650℃ (Gougazeh and Buhl, 2014) at a heating rate of 10℃/min for 3 hours.

$$2Al_2\,2Si_2O_5(OH)_4 \xrightarrow{650℃} 2Al_2 2Si_2O_7 + 4H_2O$$

Kaolin Metakaolin

Thereafter, the crucible allowed cooling naturally without opening the furnace. The calcined kaolin (metakaolin) was then recover from the furnace and characterized using XRD, SEM and TGA analysis.

3.4. Synthesis of ZSM-5 zeolite

The sol or precursor solution was organize using the required amount of Kaolin, which spread in predetermined deionized water called solution 1. The calculated NaOH pellets dissolved in 10 g of deionized water called solution 2. The two solutions (1&2) added to form solution A. The required volume of sodium silicate solution (Na_2SiO_3.9H2O) formed solution B. TPABr was dissolved into another calculated amount of deionized water and stirred to form solution C. Mixtures A and B were simultaneously added to solution C while stirring continuously. The pH was regulated using nitric acid. The batch composition mixture for this synthesis has the following molar ratio: $50SiO_2$:Al_2O_3:$20Na_2O$:2TPABr:$2000H_2O$. These steps presented in a schematic process diagram in (Fig. 4-6). The precursor achieved was aged for 0, 24 and 48 hours at room temperature before hydrothermal crystallization for 24, 48 and 96 hours with crystallization time and crystallization

temperature of 120, 150 and 180℃ using a Teflon-lined autoclave. At the end of each experiment, the autoclave was quenched with cool tap water before being washed with deionized water through vacuum pump filtration until the pH reached 8. The sample was then dried in a 90°C oven overnight before being calcined at 550°C for 5 hours to extract the structural directing agent (SDA) using a muffled furnace at a heating rate of 10°C/min. The sample was packaged and characterized with XRD, SEM and BET surface area. The procedure optimized as presented in Table 3-1

3.4.1. Hydrothermal Teflon-lined stainless-steel autoclave

This is the reactor uses to conduct hydrothermal synthesis reaction at high temperature and high pressure. It usually comes with a cup made up of polytetrafluoroethylene (PTFE) known as Teflon-lined hydrothermal autoclave reactors. Hydrothermal synthesis is a technique of synthesis of single crystals that governed by the solubility of minerals in boiling water under high pressure.

3.4.2. Hydrothermal synthesis of zeolite A.

The hydrothermal synthesis procedure was used to produce zeolite A using calcined kaolin as a source of silica and alumina. The kaolin activated to metakaolin using the muffled furnace at 650℃ for 3 hours. The effect of synthesis parameters (crystallization temperature and time, and ageing) was controlled and studied to optimize for the best synthesis condition of zeolite A synthesis (Table 3-1). 3 M sodium hydroxide concentrated solution (3M NaOH) was use to augment sodium oxide (Na_2O) in the molar composition ratio. Metakaolin was dissolve in a 3 M solution of sodium hydroxide (3M NaOH). The mixture was homogenize by stirring slowly for 10 min at room temperature. The metakaolin and sodium hydroxide solution ratio was 1.0g/25 ml (Gougazeh and Buhl, 2014). The reaction mixture slowly stirred for 30 min. The obtained sol-gel was aged for 0, 12, and 24 hours at room temperature. The aged sample crystallized at 80, 90 and

100℃ for 20 hours under autogenous pressure. Using a vacuum filtration pump setup, the items purified and washed three or four times with pure water. The zeolite dried at 80℃ overnight. The products packaged in a container for characterization with XRD, SEM, FTIR, and BET surface area, pore size and volume.

Table 3-1 Optimized experimental conditions for zeolite A synthesized zeolite from G&W kaolin

Experimental run	Crystallization temperature (°C)	Crystallization time (Hour)	Ageing time (Hour)
A1	80	20	0
A2	80	20	24
A3	80	20	12
A4	90	20	0
A5	90	20	12
A6	90	20	24
A7	100	20	0
A8	100	20	24
A9	100	20	12
A10	100	24	6

3.4.3. Screening of adsorbent using batch sorption technique

The preliminary study on the time of agitation and dosage of zeolite required for batch experiment carried out. The results not presented shows that 120 min was the optimum time and 6g/100ml is the optimum dosage of the zeolite adsorbent. After obtaining the results, the optimum values of both ZSM-5 and zeolite A applied in batch sorption experiments to screen the best adsorbent out of the range of the best synthesis of the sample. ZSM-5 had 27 sets of the synthesized sample, while zeolite A had 5 sets of the synthesized sample under various synthesis parameters. The zeolite quantity of adsorbent to synthetic seawater ratio of 6:100 made use of in this screening exercise as

confirmed from the preliminary study. The pH of the seawater sample adjusted to 7.8 by 0.1 M NH_4Cl and 0.1 M HCl solution. The concentration of the elements at constant time 120 min and constant agitation 174-rpm using linear shaker presented in table 7.

3.4.4. Characterization and analytical procedures of ZSM-5 and zeolite A,

3.4.4.1. Scanning electron microscopy (SEM)

The morphology of the synthesized zeolites described using scanning electron microscopy FEI Nova NanoSEM 230 with a field emission gun equipped with a high-resolution immersion lens. The Oxford X-Max EDS detector regulated by INCA program.

3.4.4.2. X-ray diffraction (XRD)

X-ray diffraction (XRD) patterns and average crystallite size were obtained using a Bruker AXS, D8 Advance fitted with a Tube (Cu-Ka radiation (lKa1=1.5406) and Detectors LynxEye (Position sensitive detector) at 40 kV, 40 mA, and V20 variable slit. The measurements taken with a phase width of 0.5° to 130° 2, an increment (2) of 0.034°, and a scan rate of 0.5 sec per step. The diffraction data were analyzed using March 2 software to estimate the sum of each step in the sample.

3.4.4.3. X-ray fluorescence (XRF)

X-ray fluorescence is a procedure whereby electrons evacuated from their microscopic orbital locations, discharging a surge of energy that is typical of a specific element. The sensor in the XRF instrument, which in turn labels the energies by element, then, records this discharge of energy**.**

3.4.4.4. Brunauer-Emmett-Teller (BET).

The measurement of surface area, pore-volume, and porosity of material specifically carried out by the theory of gas absorption founded by Brunauer, Emmett, and Teller called BET analysis. The

surface area and porosity analysis for this study were achieve by N_2 adsorption and desorption isotherms at −196°C employing the Micrometrics Tristar 3000 analyzer. Before N_2 physisorption samples were degassed at 150°C for 4–5 h using helium.

3.4.4.5. Thermogravimetric analysis (TGA)

In this study, the thermal stability of the kaolin, metakaolin, zeolite A, zeolite Y, and ZSM-5 zeolite was undertaken by an air Thermogravimetric analyzer (TA instruments, Model: SDT Q600) at a temperature range of 25 to 900℃ and heating rate of 10℃/min.

3.4.4.6. Inductively coupled plasma emission (ICPE).

Inductively coupled plasma emission (ICPE) used to analyze elements and determine their concentration in a different form. It's used in this work to analyze the concentration of elements in the seawater sample from both batch and RO experiments conducted. This emission spectroscopy is define as a synergy of light and matter with physical and analytical uses. The physical spectroscopy emission uses emitted, absorbed and scattered light to interpret the chemical system mechanics, whereas analytical spectroscopy emission applies the physical mechanism to resolve the content and concentration of molecular and atomic species in a chemical system. ICPE is a method of emission spectroscopy that excites atoms and ions with a plasma, causing it to emit electromagnetic radiation at wavelengths characteristic of a particular element. It's an analytical technique used for the detection of chemical element.

3.4.4.7. Fourier Transform Infrared (FTIR) spectroscopy

The product's functional group identified using Fourier Transform Infrared (FT-IR) Spectroscopy (BRUKER FTIR spectrometer ALPHA II). The instrument was designed with ALPHA II's platinum ATR single reflection diamond module and the pressure applicator that can be rotated

360° to provide unobstructed access to the sampling area with ergonomic one-finger clamp mechanism simplified with sample positioning. The ALPHA II was equipped with an integrated panel PC and dedicated OPUS-TOUCH software.

3.4.5. Kinetic studies

The equilibrium studies conducted by mixing 6 g of ZSM-5 and zeolite A separately with 100 ml of seawater solutions. The concentrations of the initial elements level were 378.40, 198.02, 153.62, and 1348.28 ppm of K, Ca, Mg and Na respectively. The pH of the water was adjusted using 0.1 M HCl and NH_4Cl. A linear shaker was use to agitate the solutions for 180 minutes at 174 rpm. The samples were separated using Whitman filter paper no.1 after equilibrium was achieve.

3.4.6 Prediction of the properties of the synthesized zeolite as a function of the hydrothermal parameters using Artificial Neural Network (ANN)

The predictive model for hydrothermal parameters based on the properties of synthesized zeolites (crystallization temperature, crystallization and ageing times) was generated with the MATLABR2015a Artificial Neural Network (ANN) toolkit (Math Works, Inc. Nitick, MA, USA) to predict ZSM-5 and zeolite A relative crystallinity, crystalline size, and Si/Al ratio. To achieve the desired goals, the set of data was establish into three groups such as 70%, 15% and 15%. The 70% used for training, 15% used for validation and the last 15% was use for model reliability.

Back-propagation based on the Levenberg-Marquardt algorithm used to train a multi-layered perceptron (MLP) feed forward neural network. The ANN system was used, with three neurons in the input layer (crystallization temperature, crystallization and ageing times), one neuron in the output layer (relative crystallinity), and a secret layer. The number of neurons in the MLP's hidden layer was determined by identifying the number of neurons with the lowest mean square error

(MSE) value among a variety of neuron numbers tested. The hyperbolic tangent sigmoid was use as the transition function for input layer to hidden layer mapping and hidden layer to output layer mapping (tansig).

3.4.7 RO Process

Figure 2-15 depicts a diagram of the RO framework. The zeolite membrane installed in a stainless steel cell facing the feed stream and sealed with silicone O-rings. The cell's feed and permeate chambers had identical small volumes of around 0.5 cm^3. To save the membrane from breaking when subjected to high pressure, a porous stainless steel disc (sintack valve) mounted underneath the alumina substrate. The feed pump maintained the feed pressure, and a pressure pump located at the feed chamber exit regulated the flow rate throughout this sequence of experiments. A small Sample bottle was used to collect the liquid permeate for examination.

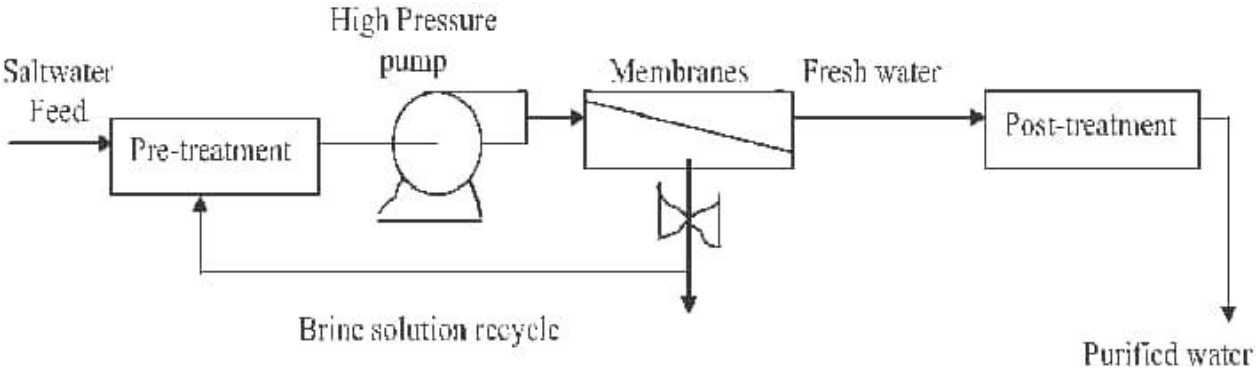

Figure 3-1 Schematic diagram of RO process

CHAPTER FOUR

4 Effect of synthesis parameters on the properties of the zeolite

In this chapter, the synthesis and characterization of the candidate zeolites from G&W kaolin from South Africa are considered. The detailed procedure of synthesis from beneficiation of the as-received kaolin through metakaolinization, synthesis of precursor, crystallization and characterization presented.

4.1. Introduction

Zeolites are use in both natural and synthetic forms (Colella *et al*., 2012). Zeolites made up of hydrated silica and alumina, which are widely used as secondary minerals and are use because of their molecular sieve property, which allows them to desiccate without changing their crystal structure. (Coronas, 2010). They are commonly use in the industry as catalysts (Aarts *et al*., 2004). Zeolite frameworks are made up of various free $[SiO_4]^{4-}$ and [AlO4]5-tetrahedral configurations of $[SiO_4]^4$ (Gougazeh and Buhl, 2014).

4.2. Kaolin clay

Kaolin is a commercial term used to describe white natural clay minerals that are predominantly kaolinite ($Al_2Si_2O_5(OH)_4$) and halloysite with a small number of impurities such as quartz and feldspar (Mineralogy, 1976). Kaolin chemical composition can vary from one deposit to another or from one location to another in terms of the Si/Al molar ratio and the concentration of impurities. Kaolinite composition (%) has been reported to theoretically comprise SiO_2 (46.5), Al_2O_3 (39.6) and H_2O (13.9) (Lijalem, 2016). The chemical composition of kaolin indicates the considerable amount of silica, alumina and other impurities in the clay. These minerals are commonly use in industrial processes such as additive in paper and adhesive in paper surfaces, as well as in the paint

and pharmaceutical industries. Kaolin clays are the principal ingredients in ceramic and refractory products, plastics and rubber industries. Kaolin clays are also used in cement, glues, and paper manufacturing, and have recently been used in the synthesis of zeolites (Mineralogy, 1976; Saikia *et al.*, 2003; Lijalem, 2016). Table. 4-1 shows a typical kaolin clay composition, it can be seen that silica and alumina are among the major constituents. The structure of kaolin layer is represented by the general chemical composition of $Al_2Si_2O_5(OH)_4$. This is depicted in Fig. 4-1 as a continuous two-dimensional framework with a silica tetrahedral sheet and a central cation of octahedral alumina linked to four shared oxygen atoms.

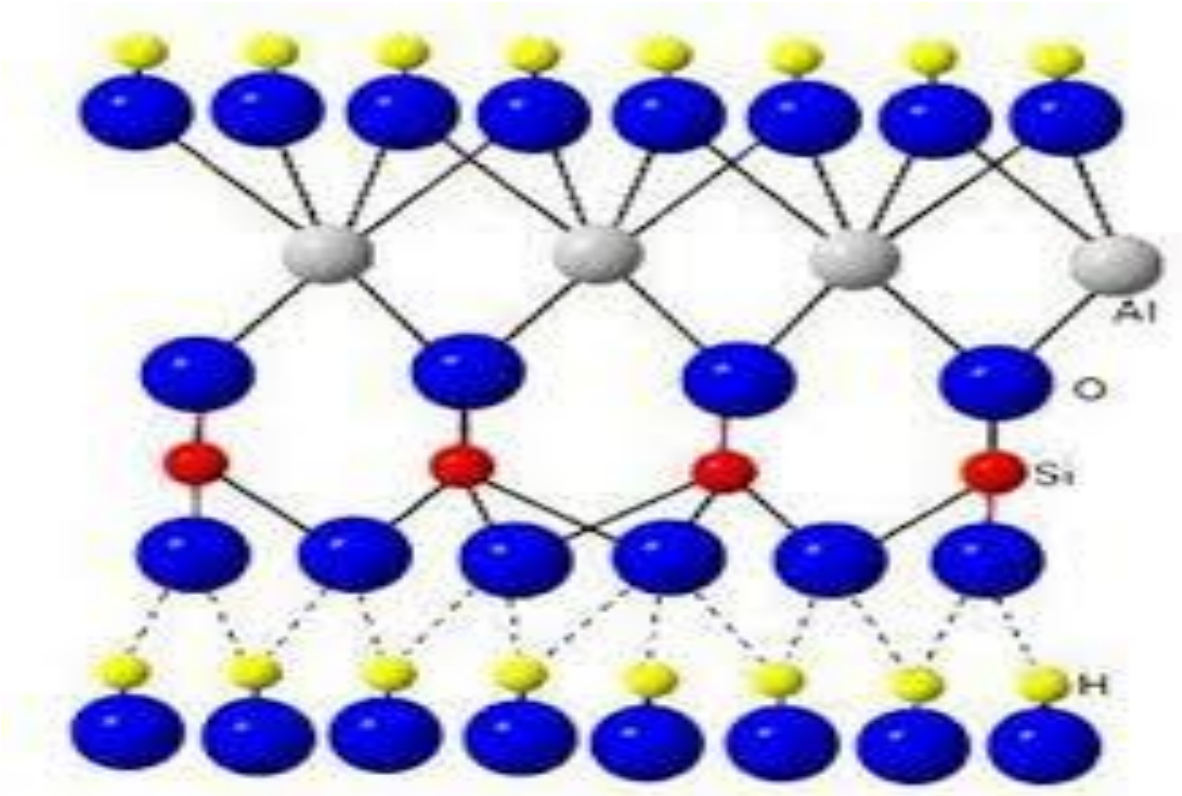

Figure 4-1: Structure of kaolinite (Kovo, 2011)

Table 4-1: Chemical composition of the typical kaolin clay mineral

Oxide	Conc. wt.%	Mineral	Percentage (%)
SiO_2	48.79	Kaolinite	40.00
Al_2O_3	33.58	Quartz	52.28
Fe_2O_3	2.65	Illite/Mica	6.89
CaO	2.98	Palygorskite	0.18
MgO	0.58		
SO_3	0.04		
Na_2O	0.07		
K_2O	0.01		
TiO_2	1.48		
P_2O_5	0.10		
Mn_2O_3	0.01		
Si/Al (Wt.%)	1.45		
Na_2O	0.07		

Source: (Adeoye *et al*, 2017)

4.3. Metakaolinization

Kaolin is naturally less reactive in its original form and can be modified to hydrosodalite as a result of the dihydroxylation process. Metakaolinization is accomplished by calcining kaolin to produce metakaolin at temperatures ranging from 550 to 900°C (Granizo *et al*, 2000). Loss of hydroxyl groups and the repositioning of the metakaolin octahedral layer to the tetrahedral position accompany metakaolinization. (Kovo and Holmes, 2010; Lijalem et al, 2016).

Generally, the synthesis of ZSM-5 and A zeolites involve two stages: metakaolinization and zeolitization processes. Metakaolinization is the high-temperature calcination of clay minerals to produce stable chemical reactive kaolin, whereas zeolitization is the hydrothermal alteration of metakaolin with zeolite minerals. Metakaolinization or dihydroxylation is a process of reactivation

of kaolin before zeolitization takes place. Calcination of kaolin at a temperature range of 550 to 900℃ (equation 4-1) was documented by many researchers (Publishers, 2000; Gougazeh and Buhl, 2014; Morsy *et al.*, 2014). Metakaolinization essentially entails the loss of hydroxyl groups, which is accompany by the rearrangement of the calcined clay's octahedral layer to tetrahedral orientation. (Kovo, 2011; Holmes, Alomair and Kovo, 2012; Aliyu *et al.*, 2017). Raising the temperature of calcination to 950℃ (equation 4-2) causes the transformation of the metakaolin to produce a spinel of aluminium-silicon, which referred to the gamma-alumina type structure. With increasing the temperature further to 1050℃ (equation 4-3) the spinel structure transforms into mullite and crystalline cristobalite as presented in the following transformation reactions.

$$2Al_2\,2Si_2O_5(OH)_4 \xrightarrow{550-900℃} 2Al_2 2Si_2O_7 + 4H_2O \qquad (4\text{-}1)$$

Kaolin Metakaolin

Increasing the heating temperature to 925℃ a defected structure called spinel formed.

$$2Al_2 2Si_2O_7 \xrightarrow{925-950℃} Si_3Al_4O_{12} + SiO_2 \qquad (4\text{-}2)$$

Metakaolin Spinel

Stable Mullite and Cristobalite are form on a further increase in heating temperature to 1050℃.

$$3Si_3Al_4O_{12} \xrightarrow{1050℃} 2Si_2Al_6O_{13} + 5SiO_2 \qquad (4\text{-}3)$$

Spinel Mullite Cristobalite.

4.4. Methodology

4.4.1. Beneficiation of G&W kaolin.

Commercial kaolin from G&W mineral resources Eastern Cape Province, Republic of South Africa, with low oil absorption, low iron, and high alkali content, used in this experiment as the source of silica and alumina. The beneficiation of the kaolin as shown in figure 4-2 obtained by gravity settling of clay slurry in separating funnel (40cm height and 4.2cm diameter). The kaolin slurry made by mixing the necessary amount of kaolin in 450ml of deionized water and allowing it to settle for a while. The abrasive constituents settled by gravity and the kaolin fractions remained in the slurry as supernatant and then decanted into a beaker and left to settle for a period of 48hour. The refined kaolin fraction obtained from the beneficiation process was dried overnight using TRILAB support model 1339 oven and then characterized using SEM, XRD, and XRF. Process flow of G&W kaolin beneficiation presented in fig. 4-2 and the beneficiation glass funnel used for gravitational settling of the kaolin slurry presented in fig 4-3.

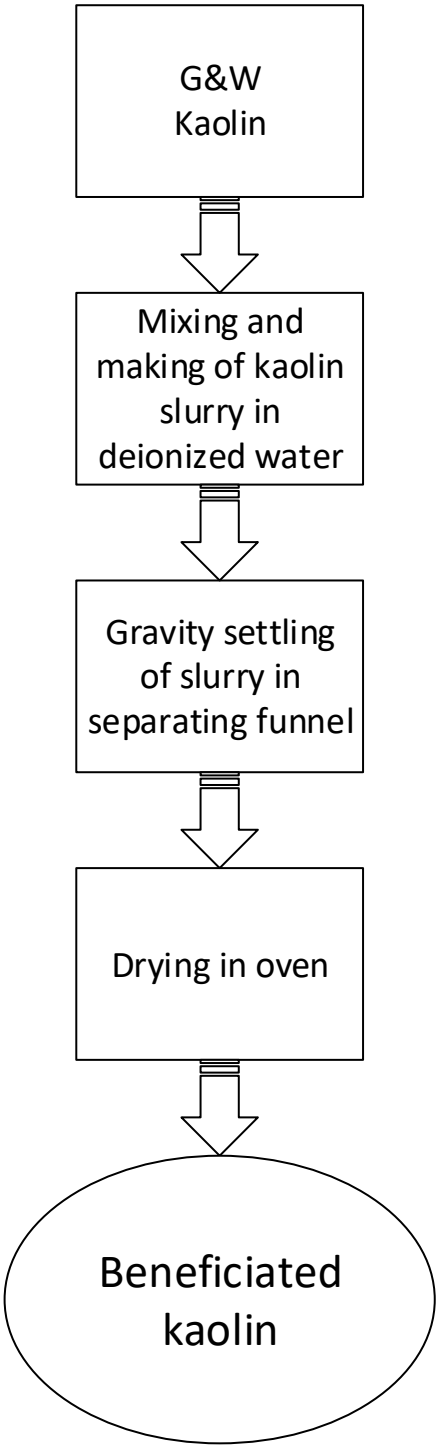

Figure 4-2 Process flow diagram of G&W kaolin beneficiation

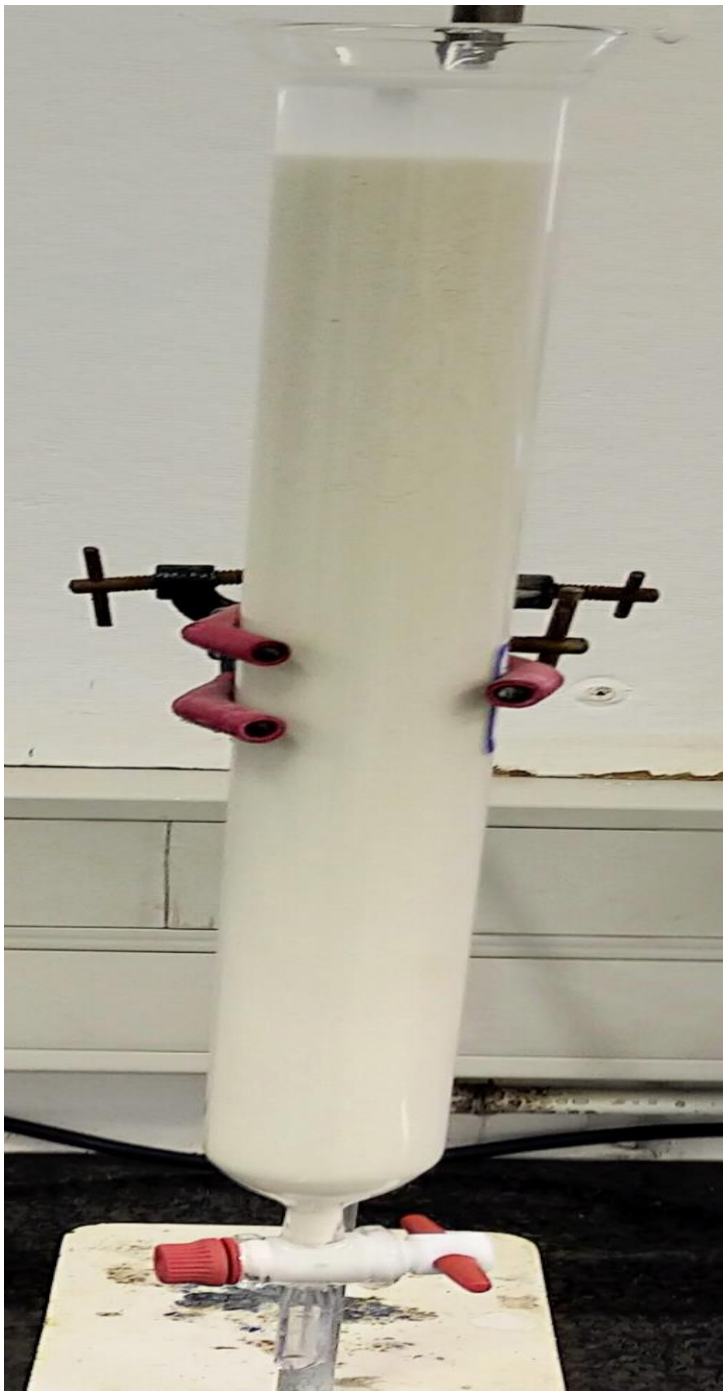

Figure 4-3 Beneficiation glass separation funnel.

4.5.2 Metakaolinization.

Conventionally, kaolin is transformed to metakaolin by calcination at a temperature range of 550 to 900℃. In this work, the kaolin from G&W was calcined using muffle furnace figure 4-5. The crucible containing the amount of kaolin to be calcine was first loaded into the furnace heated to 650℃ at a heating rate of 10℃/min for 3 hours after which the furnace was stopped. Thereafter, the crucible allowed cooling naturally without opening the furnace. The calcined kaolin (metakaolin) recovered from the furnace and characterized using XRD, SEM and TGA analysis.

4.5.3 Synthesis of zeolites from Grahamstown kaolin

4.5.3.1 Hydrothermal synthesis of ZSM-5 zeolites

The ZSM-5 zeolite synthesized using the molar composition of

$50SiO_2:Al_2O_3:20Na_2O:2TPABr:2000H_2O$.

Kaolin clay obtained from G&W mineral resources South Africa used as a combined source of silica and alumina. As additional sodium oxide sources, the reagents used for the synthesis of ZSM-5 are sodium silicate solution/water glass (Sigma Aldrich) with SiO percent formulations of 26.5 and Na_2O 10.6wt percent, respectively, and 98 percent purity NaOH (Sigma Aldrich). The structure-directing agent (SDA) for ZSM-5 synthesis was tetrapropylammonium bromide (TPABR) from Sigma Aldrich. To change the pH, Ace Enterprises Chemical Association used AR grade nitric acid (55 percent). All of the reagents were use exactly as they were given to us, with no modifications. The zeolites were produced hydrothermally after mixing the required amount of raw materials (Mohiuddin *et al.*, 2016). . The resulting mixtures were aged at various times (0, 24, and 48-hours). After ageing, the mixtures we moved into stainless steel Teflon-lined hydrothermal reactors and processed under autogenous pressure at various crystallization temperatures and times.

The reactors quenched with tap water before washed with deionized water through a vacuum pump filtration process until the pH of the filtrate matched that of the washing water. The samples then dried in a 90°C oven overnight before calcined at 550°C for 5 hours in a muffle furnace at a heating rate of 10°C/min to eliminate the structural directing agent (SDA). XRD, SEM, and FT-IR used to classify and identify the samples.

The synthesis steps presented in a schematic diagram in fig. 4-6. The stainless steel Teflon-lined autoclave used for the hydrothermal synthesis shown in figure 4-7. The procedure carried out as presented in appendix A

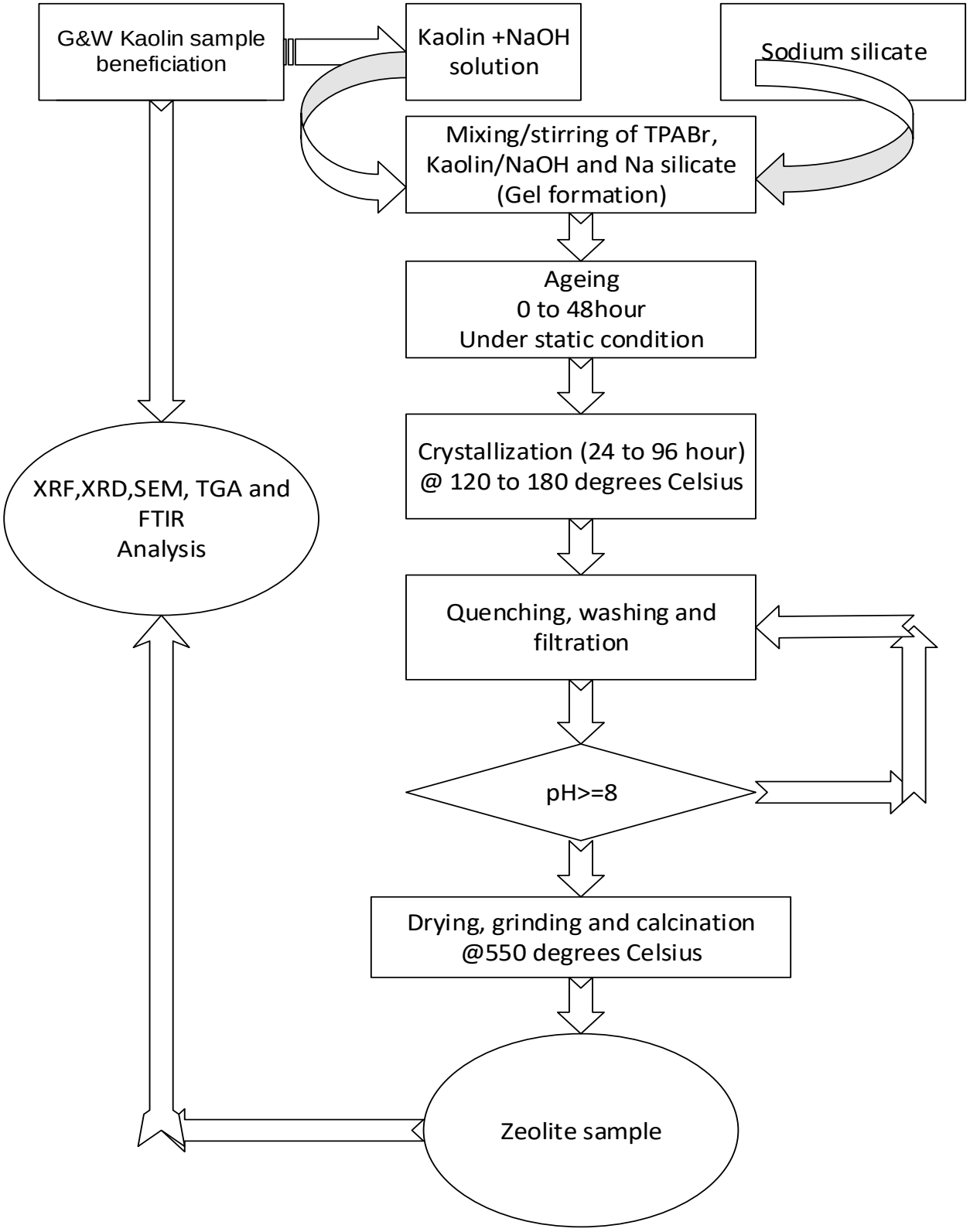

Figure 4-4 ZSM-5 zeolite synthesis schematic flow diagram

Figure 4-5 stainless steel Teflon-lined hydrothermal reactor

4.5.4 Hydrothermal synthesis of zeolite A.-

Hydrothermal procedure was used to produce zeolite A using calcined G&W kaolin as a source of silica and alumina. The kaolin activated to metakaolin using a muffle furnace at 650℃ for 3hours. The effect of synthesis parameters (crystallization temperature and time and ageing) was controlled and studied. 3M Sodium hydroxide solution (3M NaOH) used to augment sodium oxide (Na_2O) in the molar ratio of the batch mixture. Metakaolin dissolved in a 3M solution of sodium hydroxide. The mixture was homogenize by stirring slowly for 10 min at room temperature. The metakaolin and sodium hydroxide solution ratio of 1.0g/25 ml (Gougazeh and Buhl, 2014) was used. The sample solution was then shake vigorously for 30 minutes. The obtained sol-gel was aged at ambient conditions for 0 and 24 hours. The aged specimen was autogenously crystallize for 20 hours at 80, 90, 100, 120, 140, and 180°C. Using a vacuum filtration pump, the products were wash thoroughly three to four times with distilled water. The zeolite dried at 80℃ overnight. The products were stored in a container for characterization using XRD and SEM.

4.6. Results and Discussion

4.6.1. Beneficiation of G&W Kaolin.

Pretreatment of kaolin is the basic requirement in any industrial application because kaolin in its natural state accompanied by common impurities such as quartz and mica. The XRD patterns of the raw kaolin from Grahamstown and the calcined kaolin were analyze and compared, the two diffractograph presented in figure 4-8. The samples' XRD data corresponds to that of kaolinite, with characteristic 2 peaks at = 12.4, 24.6, and 38.3°. These are the characteristic peaks of kaolinite and are in good agreement with similar work reported by several other researchers (Kahraman, 2005; Gougazeh and Buhl, 2014; Ayele *et al.*, 2016). Given the availability of kaolinite's characteristic peaks, the XRD analysis reveals the presence of a significant amount of quartz impurities at peak positions 2= 20.9 and 26.5°. Geological surveys have shown that the Kaolin deposit is commonly associated with kaolinite and quartz and other oxide impurities (Zegeye *et al.*, 2013). Kaolin from Grahamstown has such a high concentration of quartz, mica and iron oxide. The XRF analysis presented in table 4-2, shows the chemical composition and their respective weight %. The result shows a very high percentage of silica and alumina. High silica content indicates the presence of high content of quartz in the G&W kaolin, which agree with the XRD result. It shows a typical mineralogical weight % of 49, 37 and14 for quartz, kaolinite and mica respectively.

Table 4-2 XRF analysis of beneficiated Graham's town kaolin

Compound	Raw kaolin %	Beneficiated kaolin %	Typical mineralogical weight %	Raw	Beneficiated
SiO_2	66.58	64.87	Mica	14	11
TiO_2	0.57	1.26	Quartz	49	34
Al_2O_3	22.81	21.64	Kaolinite	37	39
Fe_2O_3	0.87	0.57			
MnO	0.010	-			
MgO	0.61	0.57			
CaO	0.12	0.16			
Na_2O	0.29	0.31			
K_2O	2.01	1.46			
P_2O_5	0.289	0.205			
Cr_2O_3	0.361	0.288			
L.O.I.	6.10	7.12			
Total	99.98	98.19			
H_2O	1.57	-			

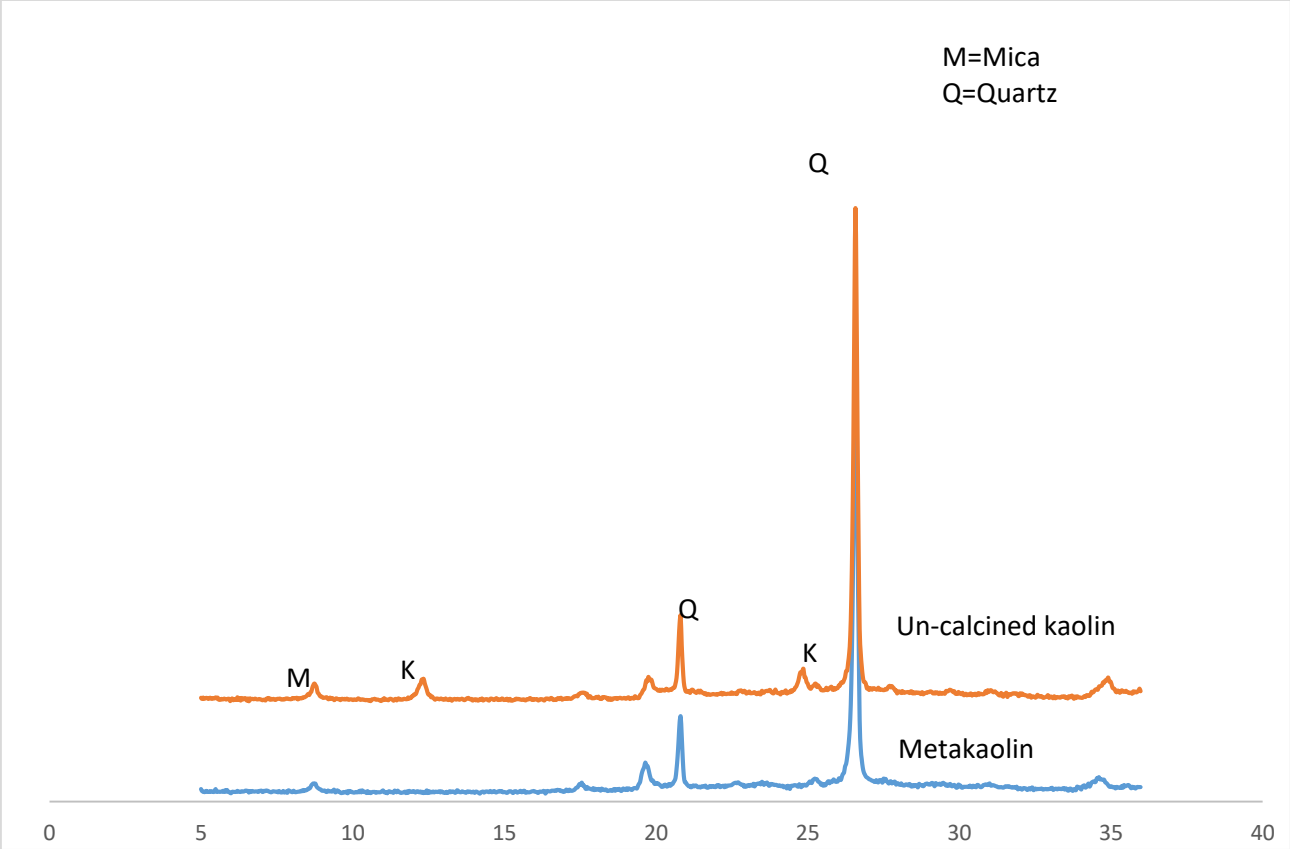

Figure 4-6 XRD pattern of beneficiated kaolin and metakaolin calcined at 650 degrees

The SEM micrograph of the G&W kaolin reveals crystalline particles with randomly hexagonal platy structure kaolinite (Mineralogy, 1976; Hartanto *et al.*, 2016; Bortolatto *et al.*, 2017). The physical examinations of the SEM image in Figure 4-7. shows that the clay mineral is associated with quartz impurities as reported by Colella (2012). With this impurity, it is pertinent to beneficiate the minerals before the synthesis of zeolite and membrane deposition. Quartz and other impurities are naturally occurring together in kaolin as a source of silica and alumina and the presence of these impurities needs to be reduce to a minimum level before zeolite synthesis. The high silica content in the XRF analysis demonstrates the presence of high quartz content in the kaolin sample. For successful application in the synthesis of zeolite, the content of quartz needs to be reduce to an acceptable level. There are several beneficiation methods of kaolin and in this

study; a simple technique of particle sedimentation by decantation was use. The kaolin clay (G&W) was beneficiated by simple dispersion in deionized water and decantation technique (Pereira *et al.*, 2018).

4.6.2 Metakaolinization

Numerous studies on the synthesis of zeolites from kaolin have been recorded in the literature using diverse metakaolinization temperature (Kovo, 2011; Holmes, Alomair and Kovo, 2012; Mohiuddin *et al.*, 2016). Table 4-2 shows that G&W kaolin is rich in oxides of potassium which implying that there are huge amounts of quartz in the sample and oxides of titanium, iron, calcium and magnesium oxides. The XRF results confirm the presence of SiO_2 and Al_2O_3 in un-calcined kaolin. The kaolinite clay from G&W minerals resources has the SiO_2/Al_2O_3 ratio of 2.92 which is in agreement with the theoretical value of silica/alumina ratio of the study on kaolinite of the same area (Jacob, Mitha and Macpherson, 2004; Mohiuddin *et al.*, 2016).

Figure 4-6 indicates the X-ray peak intensity of the calcined (metakaolin) and un-calcined kaolin. The un-calcined kaolin shows the presence of quartz and mica as main impurities with the characteristic peaks of quartz at $2\Theta = 20.9$ and 26.4°, and mica with characteristic peaks at $2\Theta = 8.9°$. However, the kaolinite characteristic peaks were identified at $2\Theta = 12.4$ and 24.8°.

Figure 4-7 shows the SEM image of un-calcined kaolin, depicting the kaolinite concealed by quartz impurities in its typical pseudo-hexagonal shape. As shown by the XRD analysis result, the diffractogragh peaks intensity of quartz of metakaolin decreases compared to un-calcined kaolin sample. This is an indication that kaolin has transformed to metakaolin. The metakaolinization of kaolin at 650℃ resulted in collapsing of the kaolinite lattice crystal structure and converted it to

the amorphous and disorderly structure (Belviso *et al.*, 2013). This confirmed the conversion of kaolin to metakaolin.

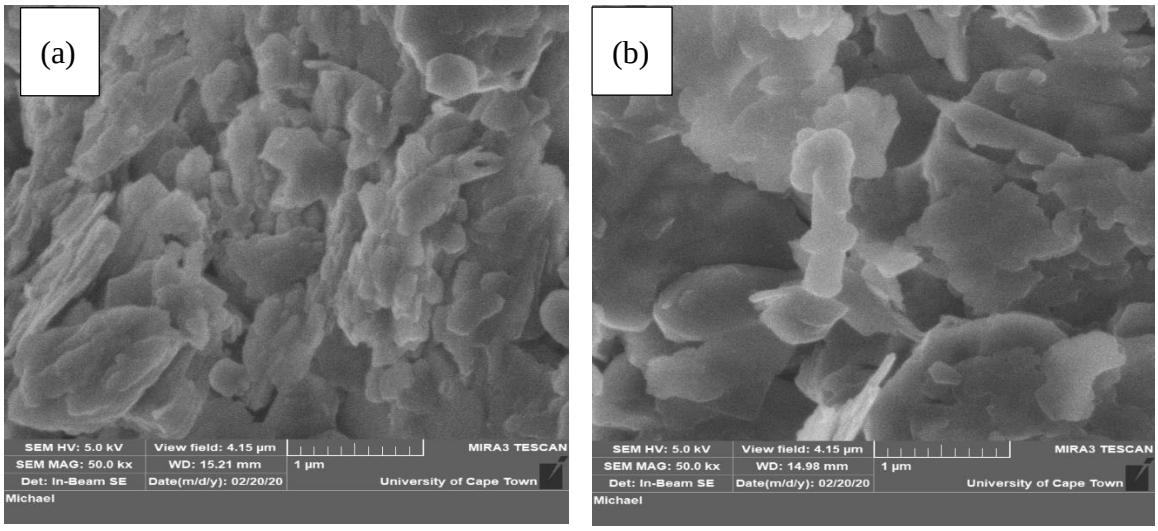

Figure 4-7: SEM images of beneficiated as-received (a) and calcined (b) G&W metakaolin sample

4.6.3. Hydrothermal Synthesis and characterization of ZSM-5 Zeolite and zeolite A from Graham's town clay

The conventional hydrothermal technique was use to synthesize these two types of zeolites after the beneficiation of the clay from Grahamstown and the result of the study on the production of the candidate zeolites is presented here.

4.6.3.1. Effect of crystallization temperature

Figure 4-10 depicts the XRD pattern of the kaolin-based ZSM-5 zeolite synthesized at 120°C, 150°C, and 180°C under the same crystallization conditions. The 120°C synthesis XRD peaks reveal no ZSM-5 peaks and a less extreme quartz peak with a crest of unreacted silica and alumina. The XRD pattern (Fig 4-b) shows a significant rise at 150°C, with ZSM-5 peaks forming at 7.93^{o}, 8.84^{o}, 23.04^{o}, and 23.93^{o} 2, as well as sharp quartz intensity peaks at 20.9^{o} and 26.57^{o} 2. This is due to the crystallization temperature being too low to completely dissolve and transform the

precursor gel to zeolite. When the synthesis temperature was raised to 180°C (Fig 4-8c), the peak intensities rapidly increased, revealing that ZSM-5 was produced at this temperature, with extreme peaks at 2 = 7.8, 8.8, 23.0, 23.9, and 24.3°. The presence of quartz peaks at 20.9 and 26.5 2 can be linked to the clay beneficiation phase, which was a basic gravity settling of the slurry followed by decantation. To remove quartz impurities from the process, extensive beneficiation needed.

Figure 4-9 shows the SEM micrograph of the ZSM-5 synthesized products after 4 days at temperatures ranging from 120 to 180°C. At 120°C, the presence of amorphous solid with asymmetrical form crystals can be seen in Fig 4-9a. It's hard to imagine ZSM-5 being synthesized at a lower temperature of 120°C and under the conditions described. SEM images of the products synthesized at 150°C show the presence of ZSM-5 zeolites as well as some amorphous undissolved crystals of quartz, whereas cubic crystals of ZSM-5 were obtained at 180°C, with mica and quartz impurities present. This means that the temperature of crystallization governs the synthesis of zeolite metastable phases (Kovo, 2011). SEM images of ZSM-5 transformation from amorphous aluminosilicate gel to crystal micrograph after treatment with different crystallization temperatures of (a) 120°C, (b) 150°C, and (c) 180°C are shown in Figure 4-9. The SEM images verified that the optimum temperature for crystallization in the synthesis of ZSM-5 zeolite from Grahamstown kaolin is 180 degrees Celsius.

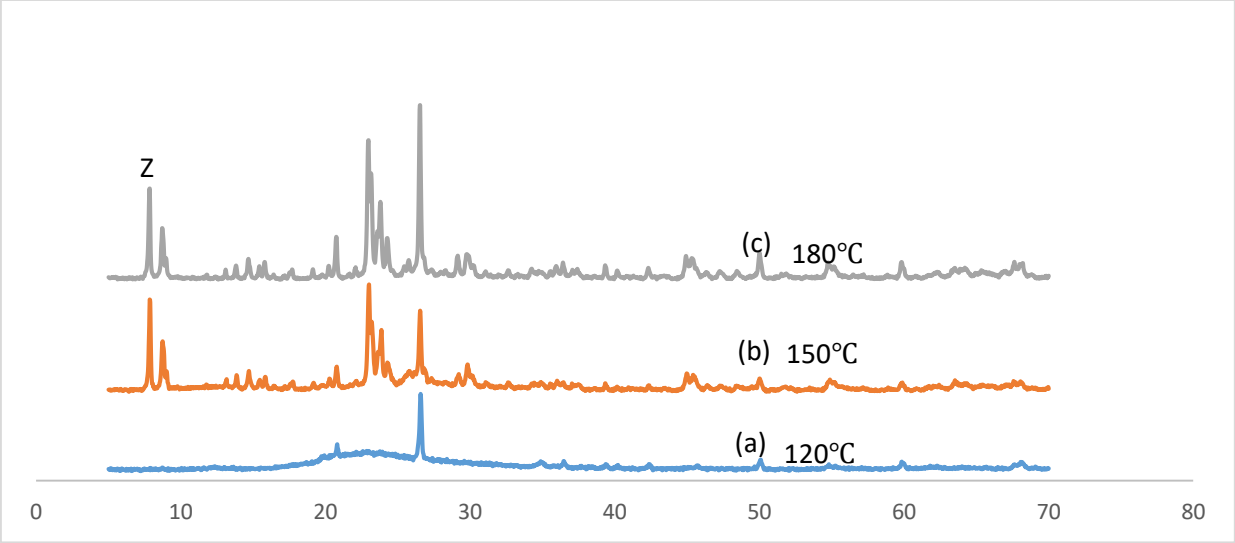

Figure 4-8 XRD pattern of ZSM-5 synthesized under (a) 120 (b) 150 and (c) 180 degrees Celsius.

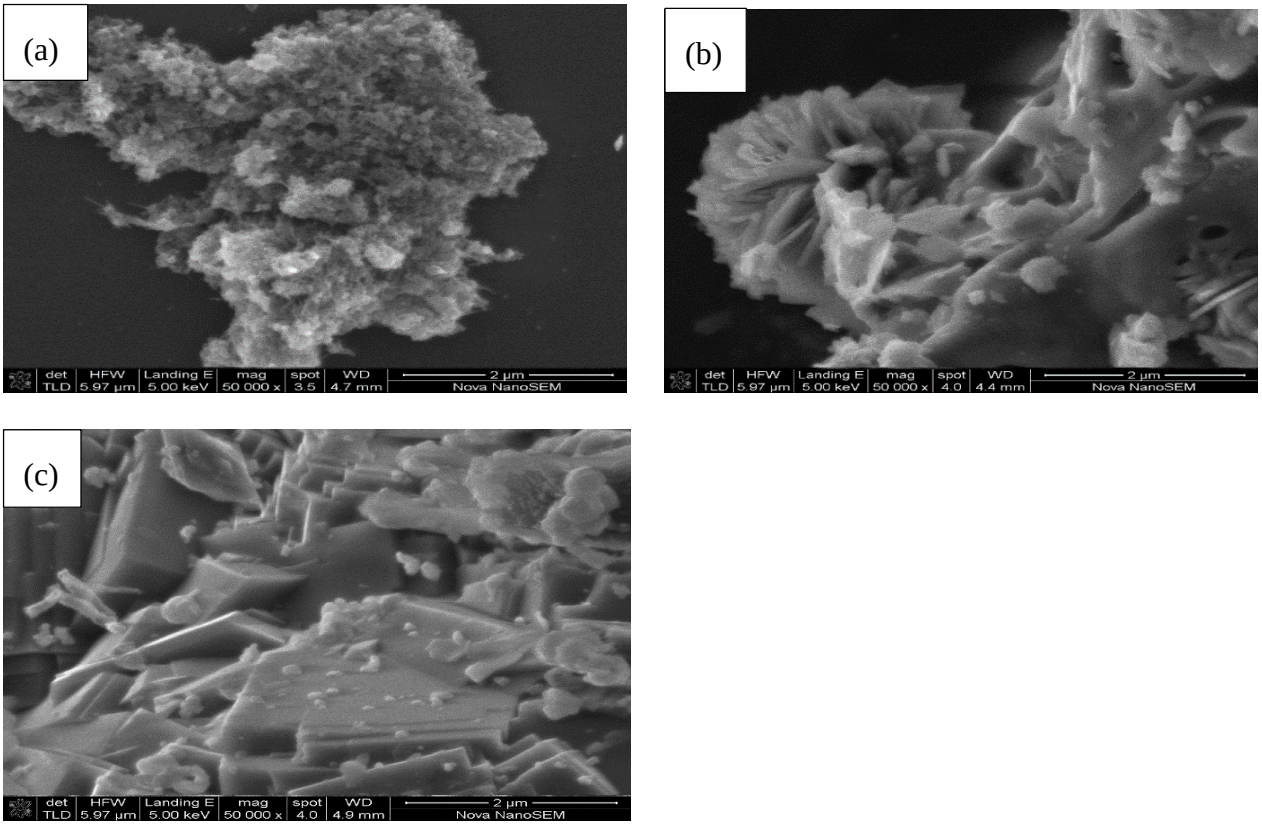

Figure 4-9 (a, b, c): SEM images of ZSM-5 synthesized at (a) 120°C, (b) 150°C, and (c) 180°C after 48 hours of crystallization and no ageing.

Figure 4-10 shows the XRD pattern of ZSM-5 synthesized at various temperatures. The characteristic diffraction of samples synthesized at 120, 150, and 180°C reveals peaks at 2 theta equal to 7.91, 8.84, 23.07, 23.91, and 24.41°, which correspond to the five most extreme peaks in the XRD analysis. The peaks at this 2 ° correspond to the typical peaks of ZSM-5's MFI structure (Kovo, 2011). Table 4-3 shows the corresponding crystallinity under these conditions. The formation of ZSM-5 at a lower temperature of 120°C was not possible, according to the table, because no peaks were established. The appearance of extreme peaks at 150°C indicates that as the temperature of crystallization rises to 180°C, ZSM-5 with relative crystallinity of 40.5 and 46.5 percent formed. The relative crystallinity of ZSM-5 was affected by the temperature of crystallization.

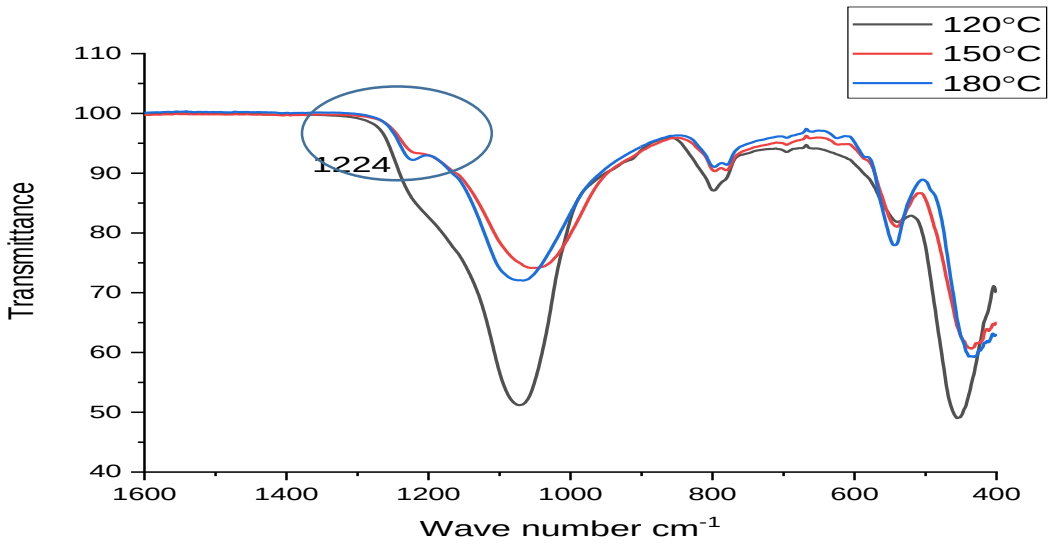

Figure 4-10: FT-IR Spectra of ZSM-5 Crystallinity as a Function of Crystallization Temperatures

Figure 4-10 represent the FT-IR spectra on the consequence of temperature of crystallization on the crystallinity of ZSM-5 zeolite. As it can be seen from the legend, there is a presence of crystal peaks at 1224 band, which is the characteristic of ZSM-5. The peaks significantly raise as the

crystallization temperature rises from 120 to 180°C. This demonstrates that the best temperature for crystallization in this study is 180°C. Physical analysis of the FT-IR spectra reveals the absence of peaks at 1224 cm-1 in the amorphous band of the zeolite synthesized at 120ºC. The presence of 1224 cm^{-1} stretch vibration band caused by external TO4 tetrahedral linkages and it is a distinctively sensitive feature of ZSM-5 zeolite IR band structures. (Dey, Ghosh and Naskar, 2013).

Table 4-3. The influence of crystallization temperature on the crystallinity of synthesized ZSM-5 zeolite

The temperature of Crystallization (℃)	∑ 5 most intense peaks at 2Θ 7-25	Crystallinity (%)
Reference sample	29,211	100
180	13,468	46.1
150	11,828	40.5
120	No ZSM-5 characteristic peaks observed	NA

4.6.4. Effect of ageing time

Figure 4-11 depicts the XRD pattern of ZSM-5 synthesized under various ageing conditions. The characteristic diffraction peaks of the samples synthesized at 0, 12, 24, and 48 hours ageing period show peaks at 2 theta equal to 7.91, 8.84, 23.07, 23.91, and 24.41°, which correspond to the XRD analysis's 5 most extreme peaks. The peaks at this 2° correspond to the characteristic peaks of the ZSM-5's MFI structure (Kovo, 2011). The presence of intense peaks in the XRD pattern of the synthesized ZSM-5 zeolite at 2 = 7.9; 8.8; 8.9; 23.0 and 23.1° under zero ageing time (Fig 4-11) indicated that ZSM-5 crystal was formed, though crystal formation was poor during the ageing time of zero with a relative crystallinity of 46.1 percent.

Table 4-4 Effect of ageing time on synthesized ZSM-5 zeolite crystallinity

Experimental Runs Aging Time (Hour)	∑5 most intense peaks at 2Θ (°) 7-25	Relative crystallinity (%)
Reference sample	29,211	100
0	13,468	46.1
12	17,689	59.5
24	22,357	76.5
48	19,032	65.1

The diffractogragh of samples synthesized under ageing periods of 0, 12, 24 and 48 hours shown in Fig 4-11. These samples tend to have the same XRD pattern as the ZSM-5 sample with an ageing period of 0 hours. To assess relative crystallinity, the 5 most extreme peaks produced at 2 = 7.8, 8.8, 23.0, 23.9, and 24.3° were used. The number of the five most extreme peaks in ageing time at 0, 12, 24, and 48 hours is 2 = 13,468, 17,689, 22,357, and 19,032, while the reference sample has 2 = 29,211. The sample aged for 24 hours had the highest pressure, implying the highest crystallinity at 0, 12, 24, and 48 hours, the relative crystallinity of the sample was 46.1, 59.5, 76.5, and 65.1 percent, respectively. As a result, the crystallinity of 76.5 percent is highest after 24 hours of ageing. SEM images of ZSM-5 synthesized at (a) 0 hour, (b) 48-hours, and (c) 96-hours are shown in Fig 4-12.

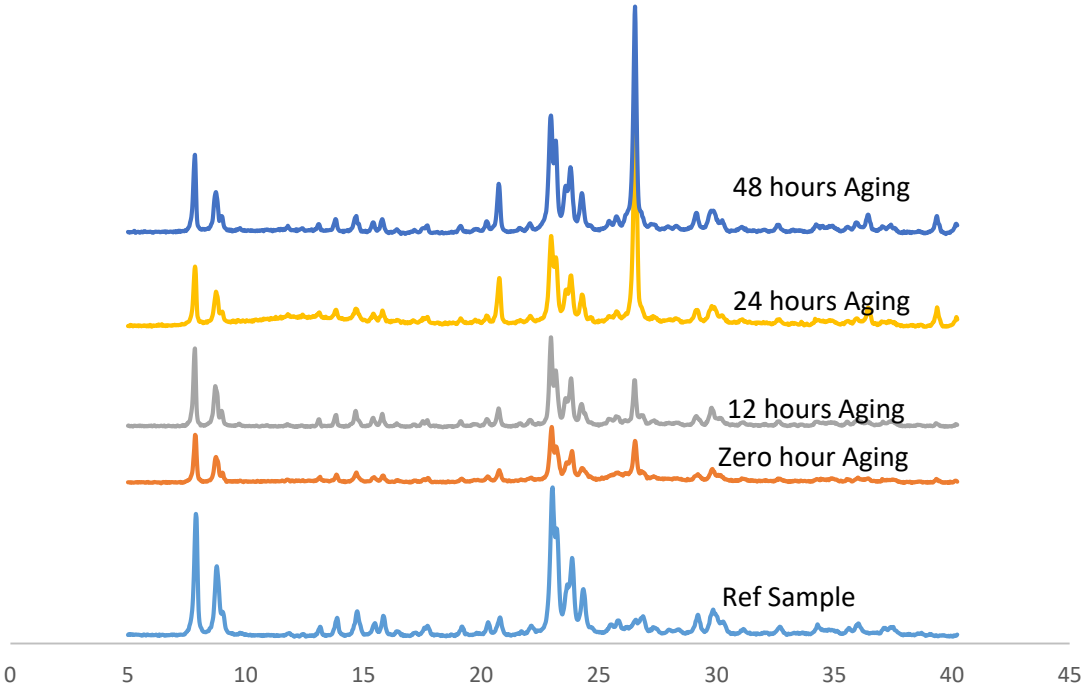

Figure 4-11: Effect of ageing time on the crystallinity of synthesized ZSM-5 zeolite

The XRD sequence of ZSM-5 aged for 48 hours has peaks at 2 = 7.8, 8.7, 23.0, 23.8, and 24.3° that are close to those observed at other aging periods. The peak amplitude of the XRD pattern decreases significantly after 48 hours of ageing as compared to the one after 24 hours of ageing. After 48 hours of aging, the $\sum 2\Theta$ = 19,032° with a crystallinity of 65.1 percent was obtained. The rise in crystallinity from 46.1, 59.5, and 76.5 percent, respectively, confirms that there is a crystal growth at aging periods of 0, 12, and 24 hours, as seen in Table 4-4. During the aging phase, zeolite crystal growth and nucleation occur (Kovo and Holmes, 2010). All of the samples have varying crystallinity, indicating that ageing time influences and regulates the formation of ZSM-5 crystals.

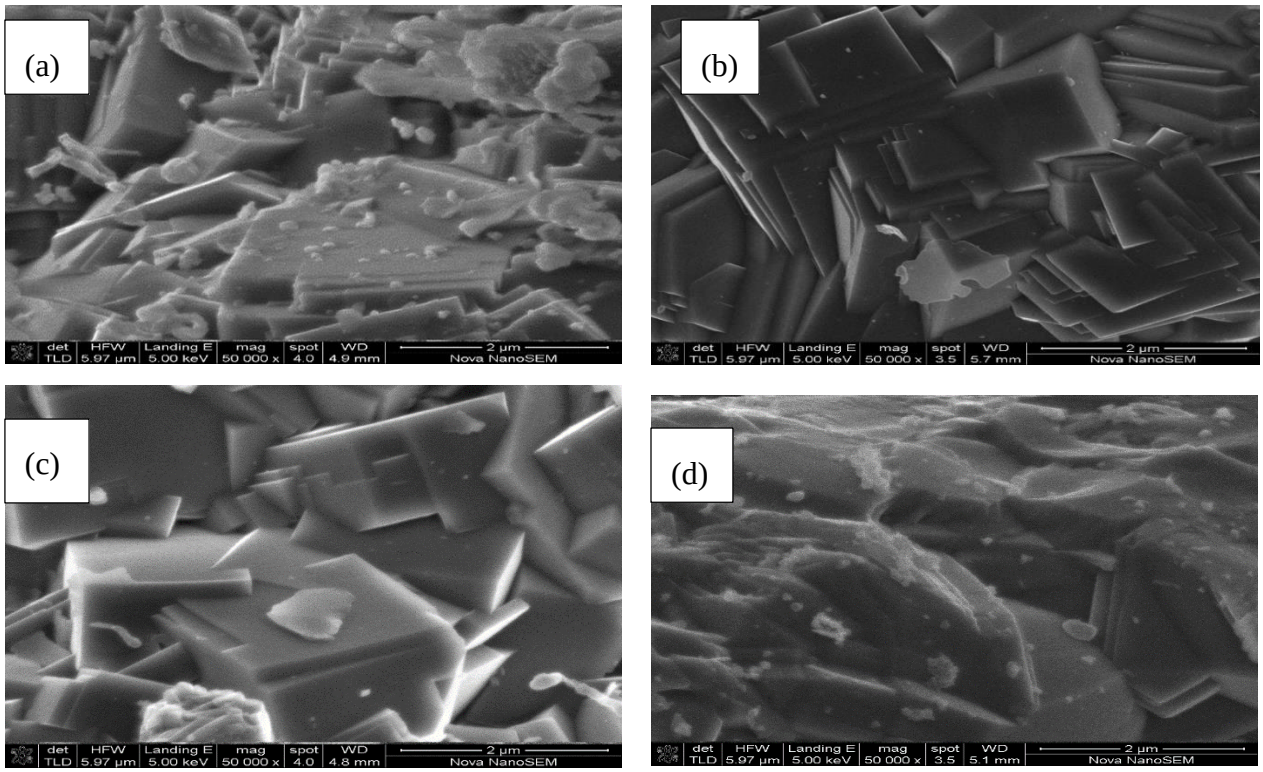

Figure 4-12: SEM images of ZSM-5 zeolite synthesized at (a) 0 hour (b) 12 hours (c) 24 hours and (d) 48 hours ageing time at 180℃ crystallization temperature and crystallization time of 48 hours.

Figure 4-12 depict the SEM images of ZSM-5 zeolite synthesized under various ageing time and at fixed temperature of crystallization of 180℃. It can be confirmed that there is a crystals growth from ageing time of 0, 12 and 24 hours, which in turn increases the crystallinity of the zeolite as presented in Table 4-4. As the ageing time increases to 48 hours, crystallinity decreases and this confirmed that the best ageing time of synthesis of ZSM-5 from this kaolin is 24 hours. This result is in agreement with the XRD pattern as depicted in figure 4-11.

Table 4-5 BET analyses of ZSM-5 zeolite samples at various ageing conditions

Sample ageing (Hours).	Surface area (m^2/g)	Pore volume (cm^3/g)	Pore size (Å)
0	74.817	0.019	14.239
12	174.277	0.072	31.367
24	282.887	0.117	31.850
48	146.154	0.056	59.121

Table 4-5 shows the surface properties of the synthesized ZSM-5 zeolite materials produced under different ageing times. It can be seen that the result that there was a linear relationship between the surface areas, pore volumes and pore sizes at from 0 to 24 hours ageing time. It can be seen that all the material was either micro or mesoporous under the different the ageing times. All the materials synthesized at 180℃ and at a varied ageing time showed a good surface areas as presented in Table 4-5, excitingly, the ageing time of 24 hours had showed the largest surface area compared to the other ageing times of 0, 12 and 48 hours. Observing the samples synthesized at 0, 12 and 48 hours, from table 4-5, showed that a longest synthesis ageing condition of 48 hours did not correspond to the largest surface area, it is worth noting that a similar observation was made when the relative crystallinities were considered; a maximum was reached at 24 hours and not 48 hours. Furthermore, it is observe that the synthesis parameter such as the temperature of crystallization and ageing time contributed to the surface properties of the zeolite materials. We however interpret the deviation observed between 24 and 48 hours to theories such as Ostwald ripening and raw kaolin impurities.

4.6.5. Effect of crystallization time

The XRD pattern results (Fig. 4-13) show that the crystallinity of ZSM-5 increases as the crystallization period increases from 24 to 96 hours. Crystal growth is influence by crystallization time, which is also affected by crystallization temperature. Crystallization time has an effect on nucleation and crystal formation, but crystallization temperature is unaffected. The XRD pattern

of the sample prepared at hydrothermal periods of 24, 48, and 96 hours reveals MFI zeolite peaks, indicating that nucleation of ZSM-5 was stable over the various crystallization times. Peak intensities rose from 24 to 48 hours of crystallization time, and then decreased from 48 to 96 hours of crystallization time. At the first step of hydrothermal synthesis, zeolite nucleation occurred, and crystal development resulted (Iwakai *et al.*, 2011). At crystallization periods of 24, 48, and 96 hours, the percentage relative crystallinity was 51.37 percent, 74.66 percent, and 66.24 percent, respectively. In this study, the crystallization period of 48 hours was the best.

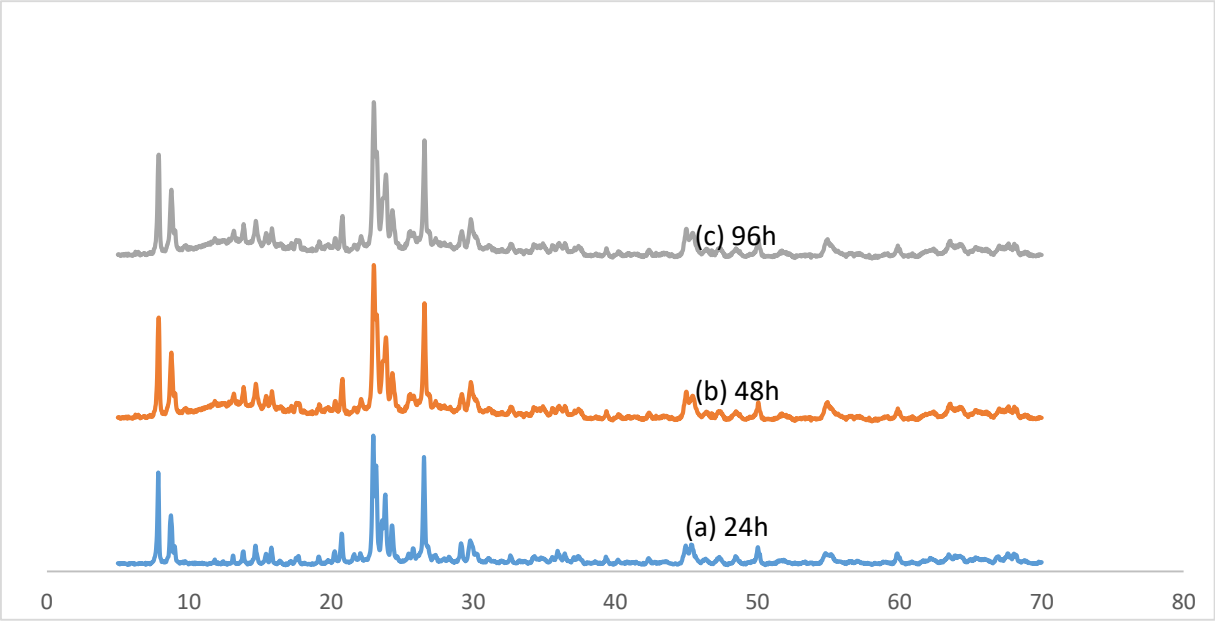

Figure 4-13: XRD patterns of ZSM-5 zeolites synthesized at 24h, 48h and 96h crystallization time

Table 4-6 Relative crystallinity of ZSM-5 samples synthesized at crystallization time of 24h, 48h and 96h.

Experimental Runs Crystallization Time (Hours)	∑5 most intense peaks at 2Θ (°) 7-25	Relative crystallinity (%)
Reference sample	29,211	100
24	15,067	51.6
48	21,808	74.6
96	19,349	66.2

Although the XRD patterns showed that ZSM-5 phase powder was collected, SEM images indicated that the nucleation rate had a cognitive effect on the morphology of the samples (Fig 4-14), indicating that the crystallization period of 24 hours is insufficient for nucleation and crystal growth as compared to the hydrothermal time of 48 hours. The excess hydrothermal period of 96 hours results in the gel converting to amorphous crystals with irregular shapes and undissolved aluminosilicate during the zeoilitization process. The agglomeration of zeolite caused by crystallization time promotes the growth of nuclei and octahedral morphology, which is consistent with the work of Kovo (2011) and Mohiuddin *et al* (2016).

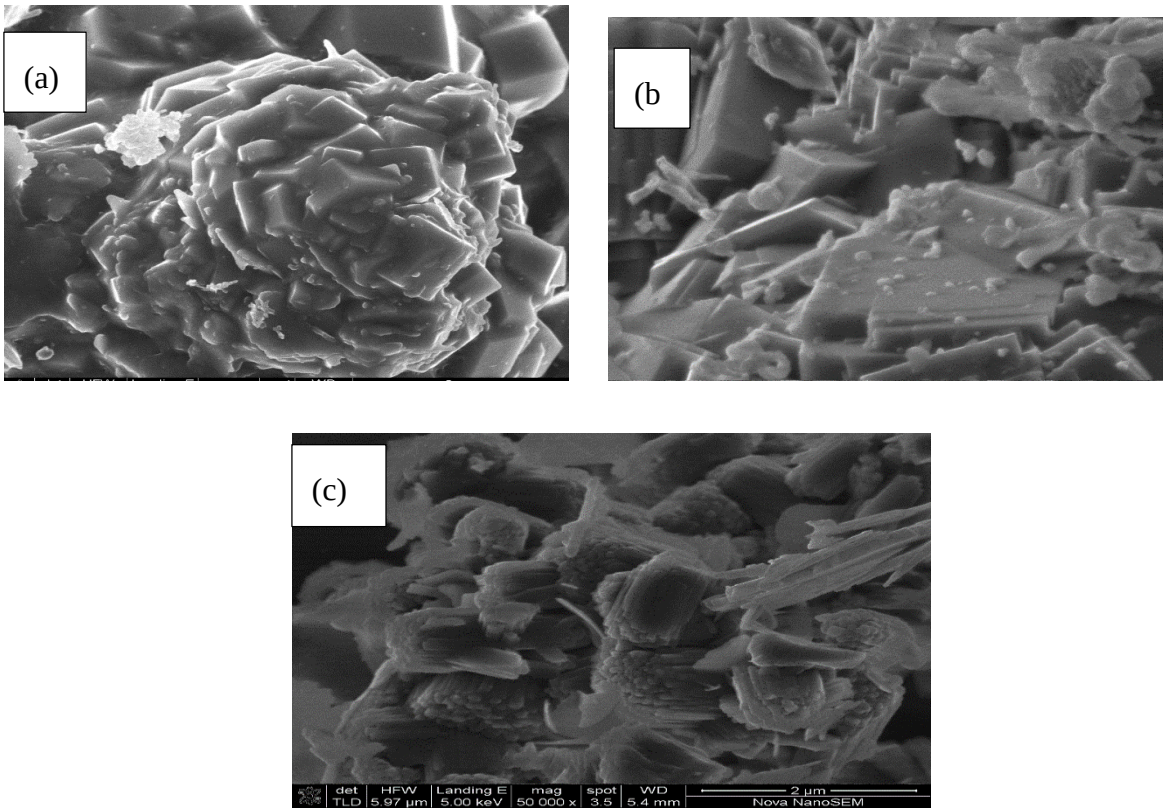

Figure 4-14: SEM images of ZSM-5 zeolite synthesized at different crystallization times (a) 12 hours (b) 48 hours (c) 96 hours at 180℃ crystallization temperature and 0 ageing time.

Figure 4-14 present the micrograph of ZSM-5 zeolite synthesized at dissimilar crystallization time under fixed temperature of crystallization of 180℃ and 0 ageing time. The SEM images of the sample synthesized at the hydrothermal time of 24 and 48 hours show the crystals growth as the time of crystallization increases from 24 to 48 hours but the crystals decrease as the time increases to 96 hours. We conclude that the optimum time of crystallization for synthesis of ZSM-5 from South Africa Kaolin is 48 hours

4.6.6. FT-IR spectra analysis

The FT-IR spectra of synthesized ZSM-5 samples made with Grahamstown kaolin were analyze and shown in Fig 4-15. The effect of crystallization temperature investigated under set ageing and

crystallization periods. Internal TO4 tetrahedral bending stretche assigned to the 436 and 457 cm^{-1} bands. Double ring vibration stretches assigned to the 545 and 550 cm^{-1} bands. External symmetric stretching is associated with the bands at 798 and 800 cm^{-1}. The external asymmetric stretching vibration assigned to bands at 1058 and 1080 cm-1 (Si-O-T Linkage). Asymmetric stretch vibration is associated with the band at 1224 cm^{-1}. The figure depicts the presence of bands at 550 and 1224 cm^{-1}, which are characteristics of ZSM-5 with double 5 membered rings (Madejová, 2003; Yaripour *et al*., 2015; Mohiuddin *et al*., 2017). As the temperature rose from 120 to 180°C, the characteristic wavenumber of 550 cm^{-1} of pentasil extreme structure of 5 membered rings emerged. It was discovered that as the temperature rose, the ZSM-5 zeolite became more crystallined. Physical examination of the FT-IR spectra reveals the lack of peaks at 1224 cm^{-1} in the amorphous band of zeolite synthesized at 120^{o}C. The presence of the 1224 cm^{-1} stretch vibration band is due to TO4 tetrahedral external linkages and is one of the sensitive IR band structures (Dey, Ghosh and Naskar, 2013).

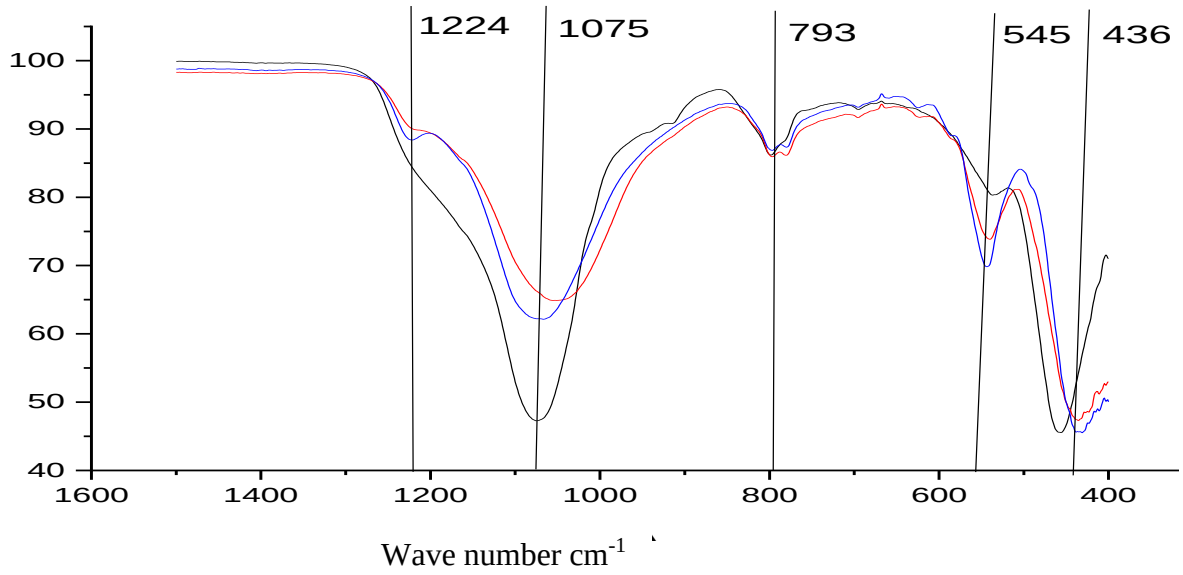

Figure 4-15: FT-IR spectra showing the effect of crystallization temperature on the crystallinity of ZSM-5 zeolite

4.6.7. Hydrothermal Synthesis and characterization of zeolite A from Grahamstown clay

4.6.7.1. Effect of ageing time

The outcome of different ageing times, fixed crystallization time and temperature of 20h and 100℃ respectively depicted in figure 4-16. The XRD pattern confirmed that zeolite A was synthesize for the various ageing times investigated. The XRD pattern was compared with a reference sample and the pattern matched favourably with the reference sample though there is some presence of unreacted impurities of quartz at 20.9 and 26.5° 2 theta.

The relative crystallinity of zeolite A increased with increasing ageing time of synthesis gel and this can be understood from the intensification of the intensity of the core XRD peaks corresponding to the characteristic peaks of zeolite A at 7.2, 10.2 and 12.4 2Θ°. This result is in

agreement with the work of Kovo (2011) and Ayele *et al.* (2016) where zeolite A was formed even without ageing of synthesis precursor. This may be because of the reactive nature of the metakaolin. The formation of zeolite is because of the conversion of metakaolin to zeolite, which occurred in two stages. The metakaolin conversion to aluminosilicate gel and attachment of aluminums into the lattices of the silicate ring for the formation of zeolite framework. Precursor ageing aid in dissolving silica and discharging silica ions into the solution thus increasing crystallization and yield (Kovo, 2011).

The SEM micrograph of zeolite A synthesized and acquired under different ageing times is depicted in figure 4-17. The SEM images indicate a cubic shape that is characteristic of zeolite A even without ageing of the precursor gel. This is in tandem with the XRD result endorsing the formation of zeolite A. The XRD and SEM result confirms that the crystalline phase of zeolite A was produced in almost all the investigated synthesis conditions. Nevertheless, the sample with an ageing time of 12 h, crystallization time of 20 h and crystallization temperature of 100℃ appeared to yield the finest zeolite A crystal that matched well with standard zeolite A.

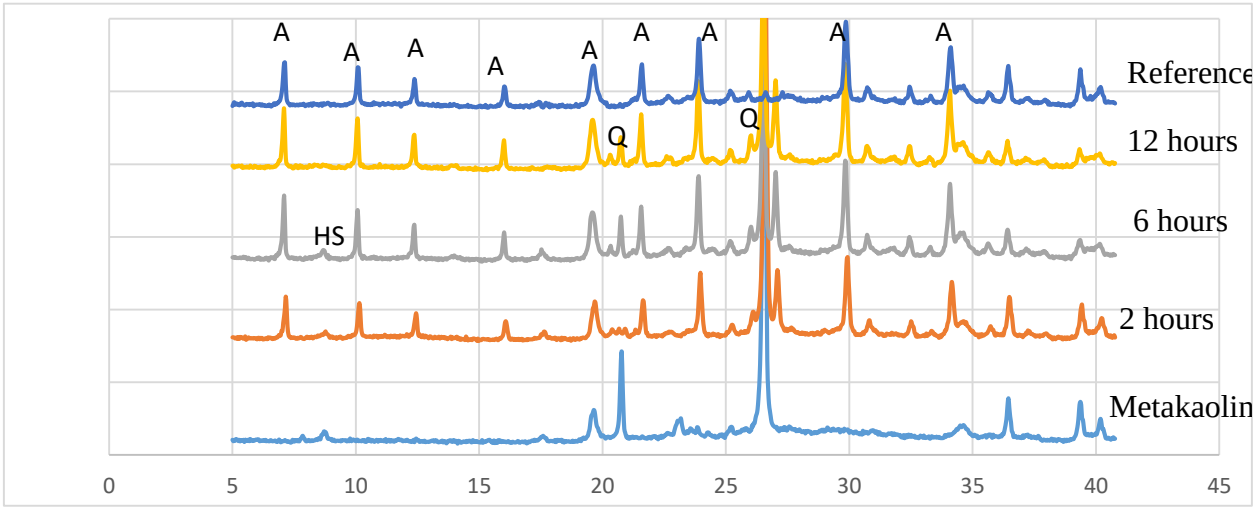

Figure 4-16: XRD pattern of zeolite A showing the effect of ageing time of metakaolin, 2 hours, 6 hours and 12 hours, respectively.

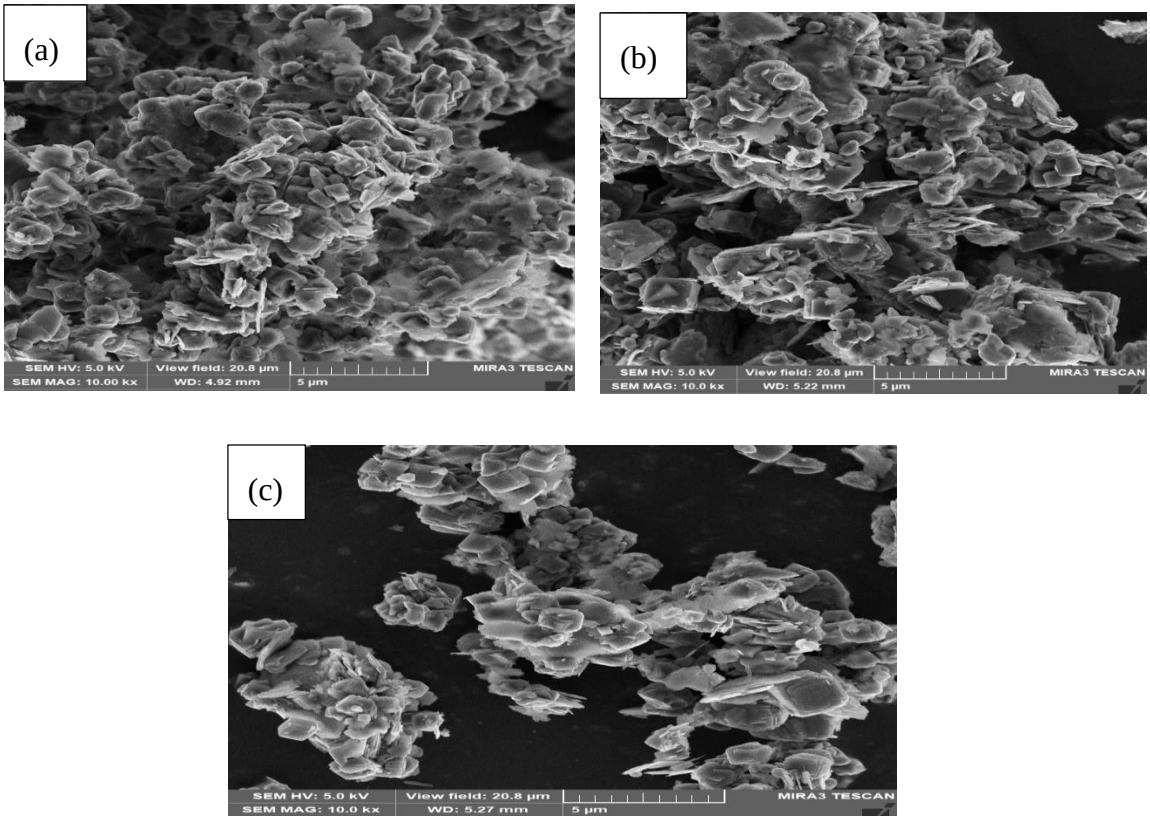

Figure 4-17: The SEM image of zeolite A synthesized at ageing time of (a) 2 hours (b) 6 hours (c) 12 hours at 100℃ and 20 hours crystallization time

4.6.8. Effect of crystallization time

The outcome of the zeolite sample from various crystallization times depicted in figure 4-18. The crystallization time varied 3 times between 3-20h. There was no zeolite phase detected in the first 3h of crystallization. This results from the low time of crystallization. There is a need for the time of dissolution of synthesized gel for NaOH solution and metakaolin dissolution is completed though not yet clear how long it will take for dissolution process to complete before zeoilitization process (Kovo, 2011).

The ageing process was supposed to cause some dissolution and probably affect the rapid formation of zeolite A during crystallization. During the first three (3) hours of crystallization, the gel

produced remained amorphous. The peak due to the impurities in the original refined, mica and quartz, at 2-theta = 9^{o} and 26^{o}, respectively, is still detectable. It is reveal that impurities have no effect on the formation of zeolite A.

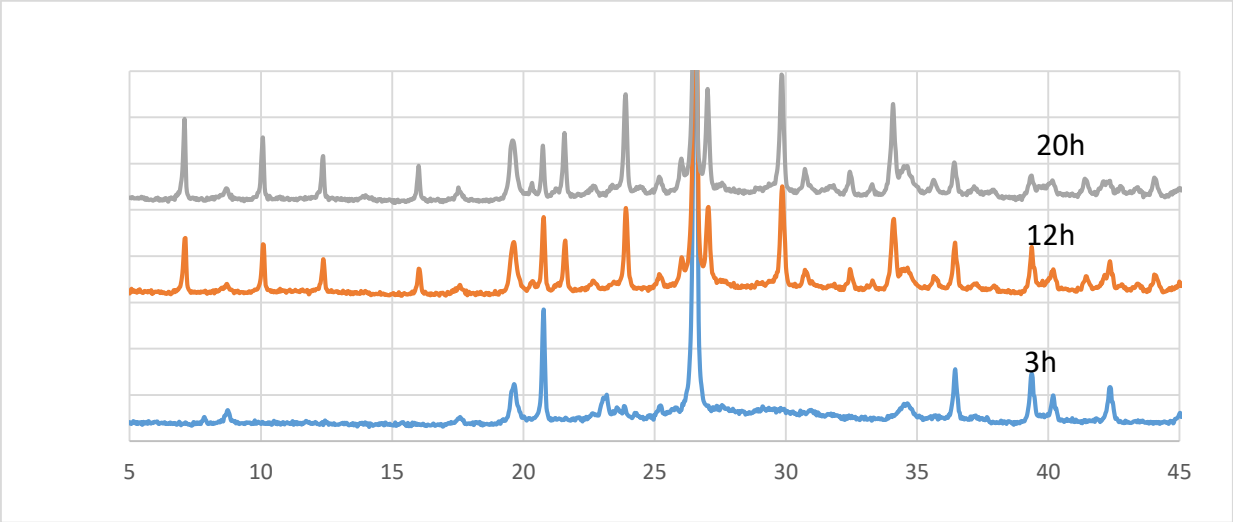

Figure 4-18: Effect of crystallization time (a) 3 hours (b) 12 hours (c) 20 hours

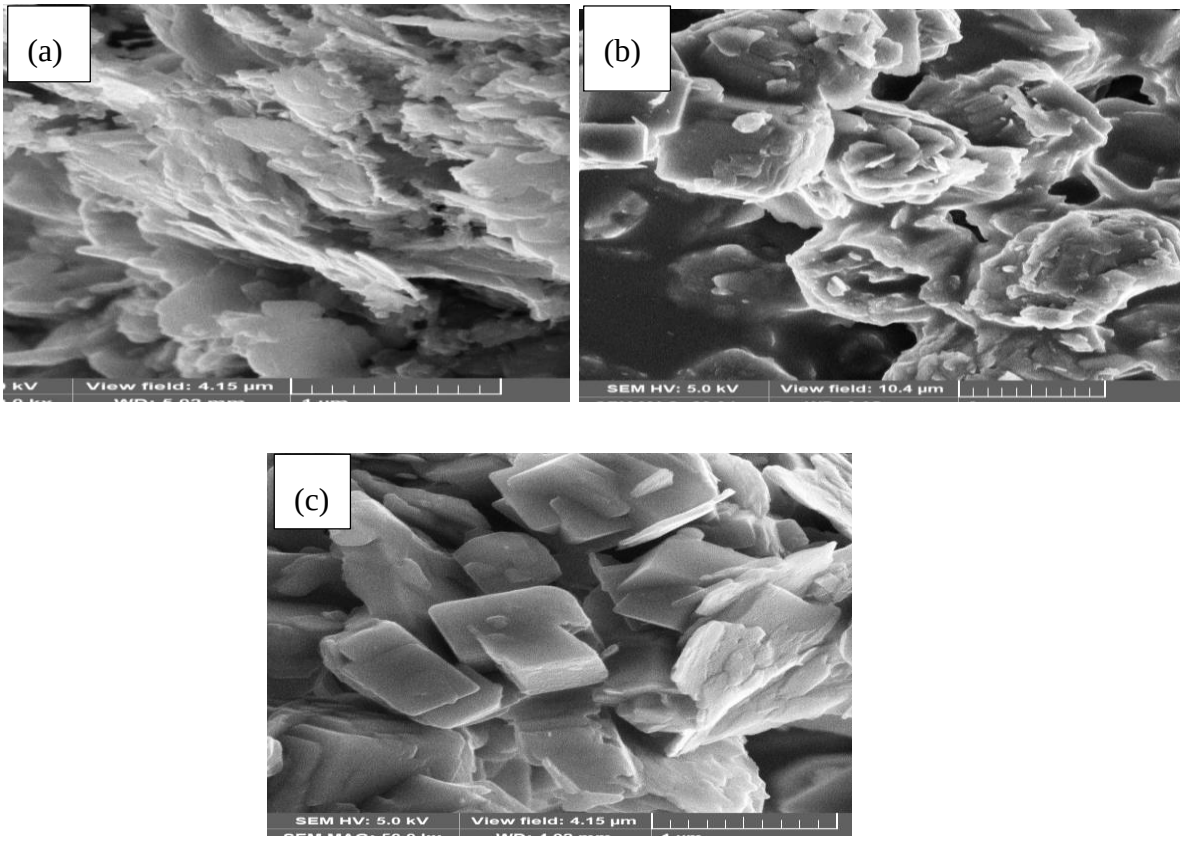

Figure 4-19: SEM micrograph of zeolite A synthesized at crystallization time of (a) 2hours (b) 12 hours (c) 20 hours at the fixed ageing time of 12 hours and 100℃ crystallization temperature

4.6.9. Effect of crystallization temperature

The influence of hydrothermal treatment of synthesized gel from metakaolin to produce zeolite A was investigated by changing the crystallization temperature from 80-120℃, while crystallization and ageing times were kept constant at 20 h and 12 h respectively. From figure 4-20, it was confirmed that when crystallization is at 80℃ for 20 h, small peaks of crystallinity were observed on the XRD pattern, which matched those of standard zeolite A sample. Increasing the crystallization temperature to 100℃ and keeping the crystallization time and ageing times constant at the same value of 20 h and 12 h respectively stimulate the formation of more crystalline zeolite A. At 120°C there was an obvious reduction of the diffraction peaks indicating the crystallinity was

decreased by increasing the temperature of crystallization from 100℃ to 120℃. The decrease of crystallinity confirms that the optimum temperature of crystallization for zeolite A synthesis is 100℃ and this is in agreement with (Gougazeh and Buhl, 2014; Áurea *et al.*, 2015; Pereira *et al.*, 2018).

The morphology of the synthesized zeolite A produced at different crystallization temperatures and fixed crystallization and ageing times was study using SEM images. The crystalline image of the sample crystallized at 80℃ figs. 4-21 presented an obvious crystalline phase with cubic shape. This is in line with the XRD findings, which show weak crystalline zeolite A structure. When the temperature increased to 100°C the morphology revealed a typical zeolite A with pierced crystals and defined cubic shape. This result shows that 100°C is a good crystallization temperature for the synthesis of zeolite-A from South African kaolin. The Si/Al ratio estimated using EDX and the value increased as the temperature of crystallization increased from 80°C to 100°C. The results show that value achieved for 100° is 1.3 which is in agreement to the results obtained by Von-kiti (2012). This result agrees with the value of Si/Al ratio for typical zeolite A.

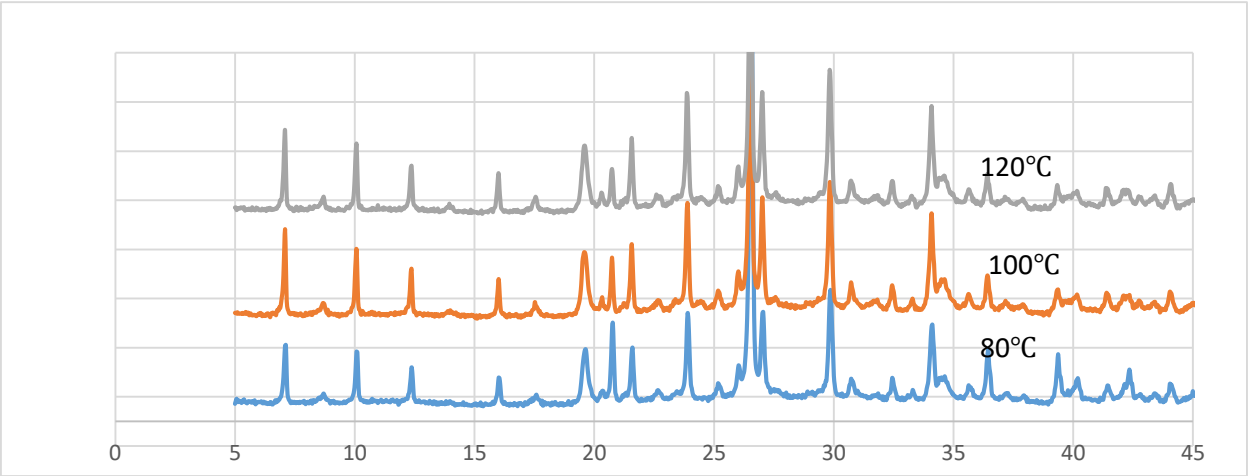

Figure 4-20: XRD pattern of zeolite A synthesized at a temperature of (a) 80℃ (b) 100℃ (c) 120℃ at the fixed ageing time of 12 hours and 20 hours crystallization time

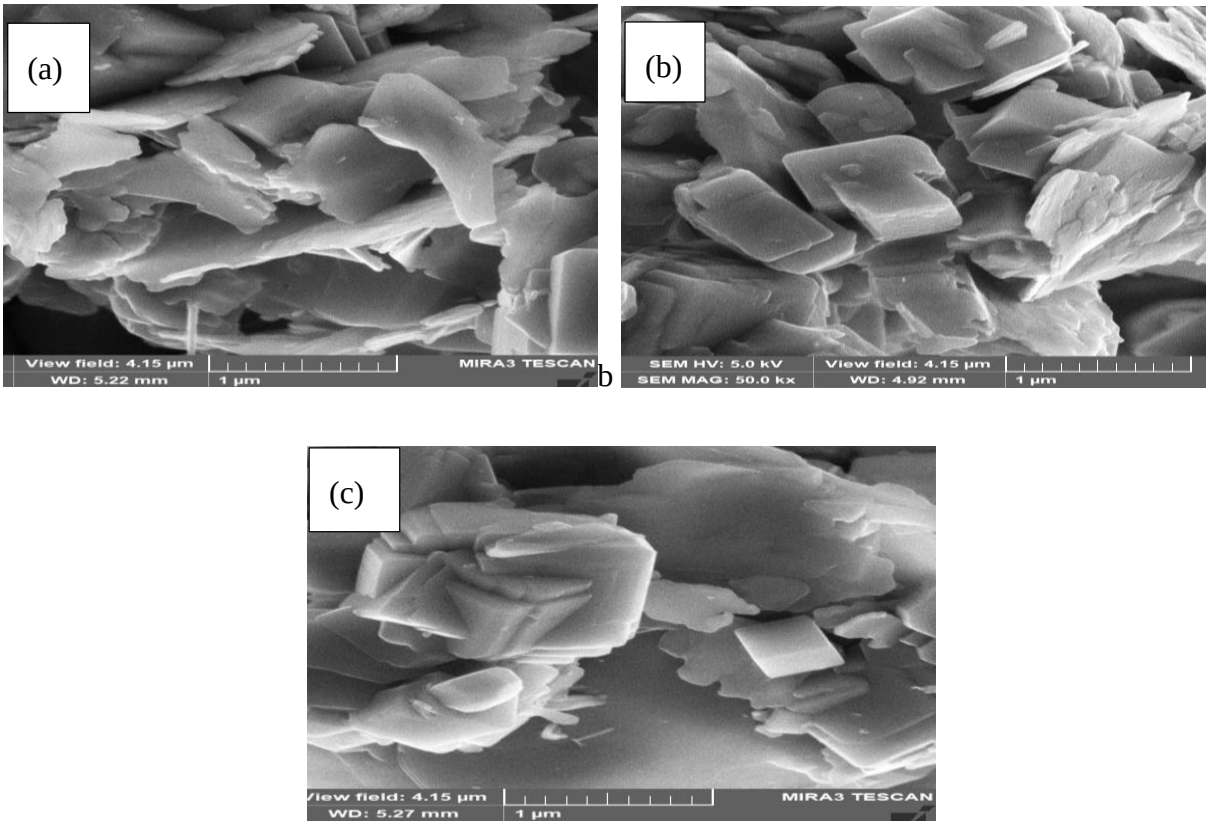

Figure 4-21: SEM micrograph of zeolite A synthesized at a temperature of (a) 80℃ (b) 100℃ (c) 120℃ at the fixed ageing time and 20 hours crystallization time

4.6.11. Prediction of the properties of the synthesized zeolite as a function of the hydrothermal parameters.

4.6.11.1. Prediction of ZSM-5 relative crystallinity and crystalline size

The artificial neural network (ANN) regression plots in Figures 4-22 and 4-23 represent data for training, testing, and validation of an ANN model for the prediction of ZSM-5 relative crystallinity and crystalline size respectively. As shown in Figure 4-22, A coefficient of correlation of 0.9232 was obtained for the data training and When the system was tested with data sets other than those used for training, it produced a strong correlation coefficient (0.9655), confirming the reliability of the developed ANN model. For the case of prediction of ZSM-5 crystalline size as shown in Figure

4-23, the coefficient of correlation of 0.6469 was obtained from data training and When the model was tested with data sets other than those used for training, it generated a strong correlation coefficient (0.9964), confirming the reliability of the developed ANN model. Overall, the plot of ZSM-5 relative crystallinity from expected versus experimental data yielded a higher correlation coefficient (0.8918) when compared to the plot of the ZSM-5 crystalline size with a correlation coefficient of 0.6530. This is an indication that the ANN model for prediction of ZSM-5 relative crystallinity showed superior accuracy when compared to the developed ANN model for prediction of ZSM-5 crystalline size.

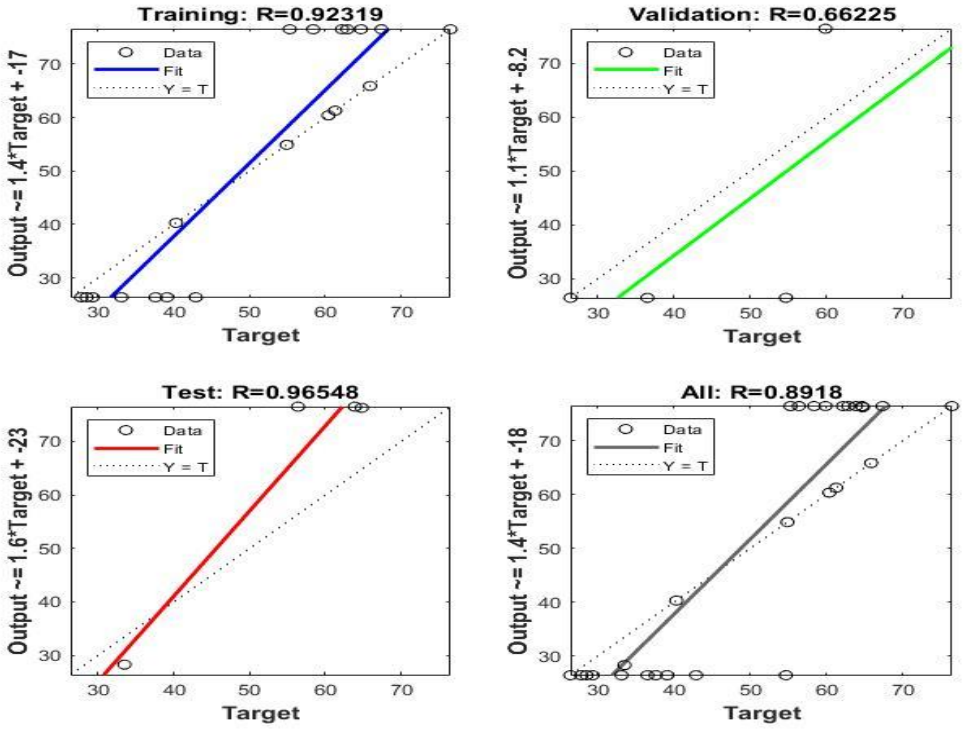

Figure 4-22: Regression plots of predicted versus experimental ZSM-5 relative crystallinity

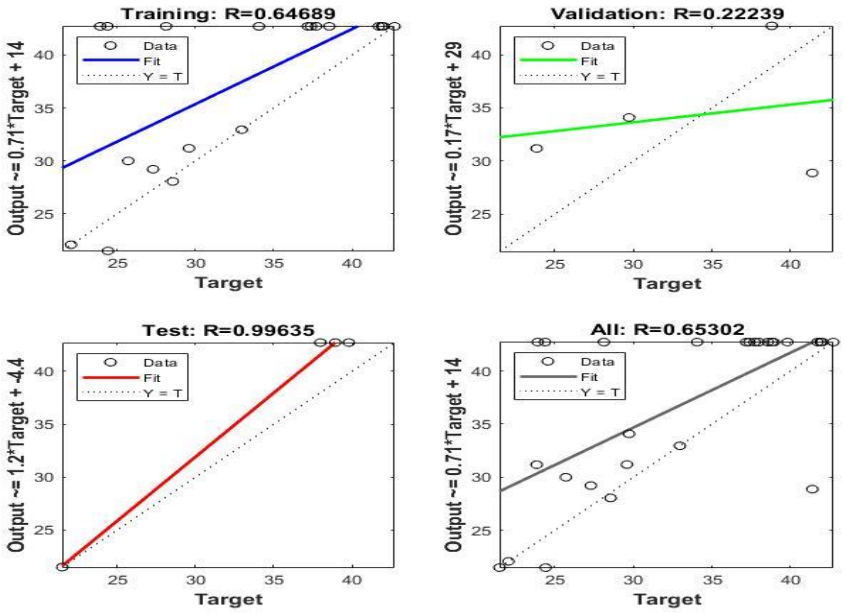

Figure 4-23: Regression plots of predicted versus experimental ZSM-5 crystalline size

4.6.11.2. Prediction of Zeolite A relative crystallinity and crystalline size

The regression plots in Figure 4-24 and 4-25 represent data for training, testing, and validation of the ANN model for the prediction of Zeolite A relative crystallinity and crystalline size. As shown in Figure 4-24, A reasonable coefficient of correlation of 0.9696 and 1.0000 was obtained for training and validation, indicating that the evolved ANN model has high precision and accuracy. When the model validated with data sets other than those used for testing, a strong correlation coefficient (1.0000) obtained, confirming the reliability of the existing ANN model. For the case of zeolite-A crystalline size prediction, as shown in Figure 4-25, a satisfactory correlation coefficient was obtained for validation of the model and when the model was validated with data sets other than those used for testing, it produced a strong correlation coefficient (1.0000), confirming the reliability of the developed ANN model. Overall, the ANN model prediction

accuracy for Zeolite A relative crystallinity was superior when compared to model prediction accuracy for Zeolite A crystalline size.

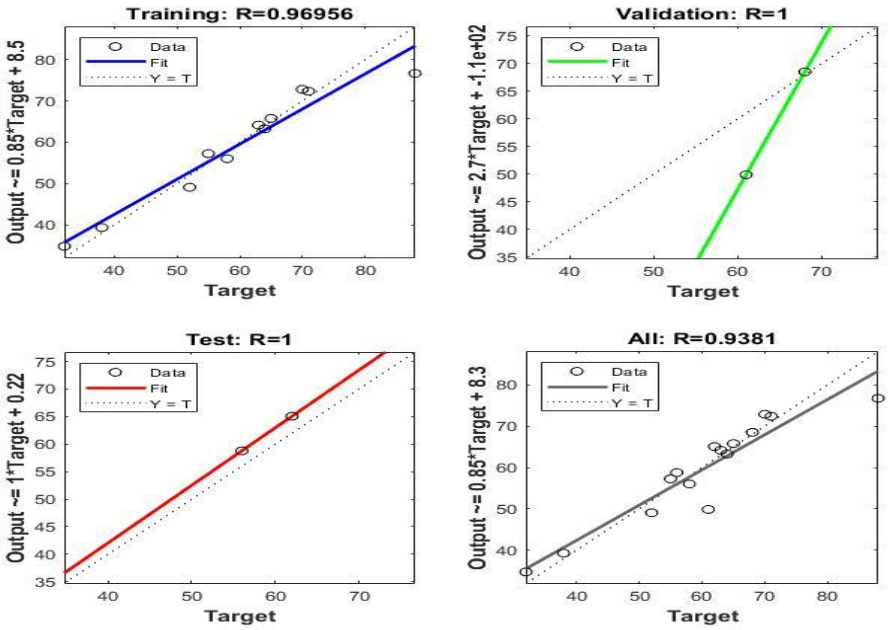

Figure 4-24: Regression plots of predicted versus experimental zeolite A relative crystallinity

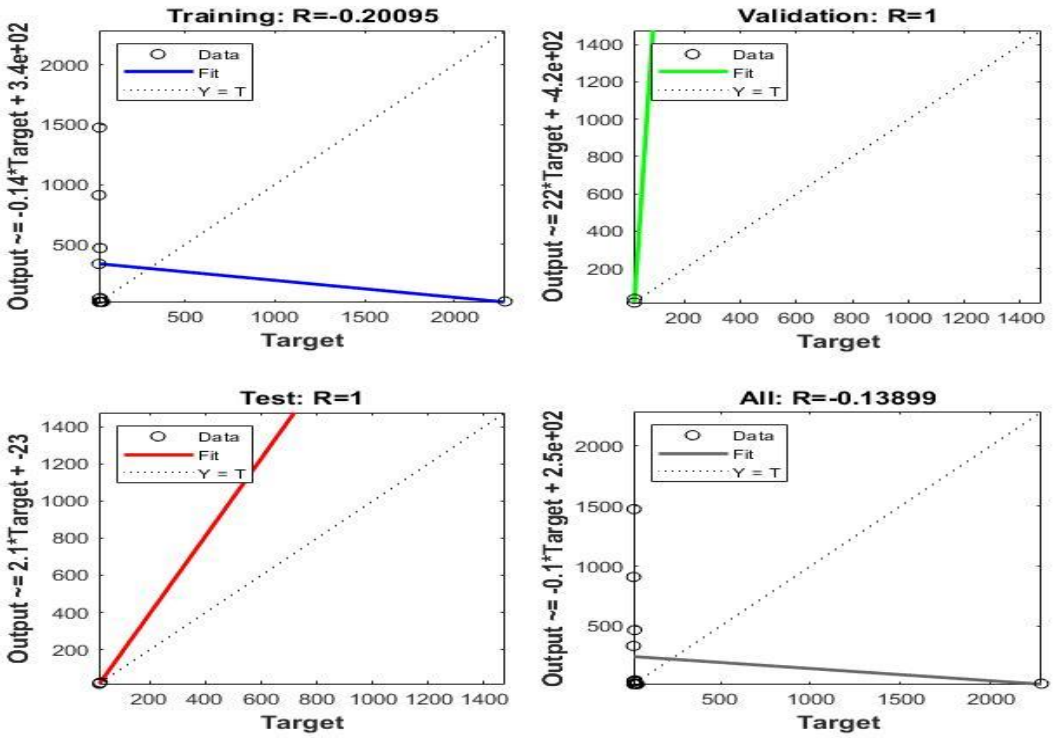

Figure 4-25: Regression plots of predicted versus experimental zeolite A crystalline size

4.6.11.3. Mathematical model for prediction of ZSM-5 properties

Considering the relevance of crystallinity in zeolite properties, two equations were develop with the aid of MATLAB to determine relative crystallinity as a function of crystallization temperature, crystallization time and ageing time. Equations 4-4 and 4-5 have been tested and found to be not less than 95% and 99% accurate respectively.

Relative Crystallinity $= 0.49204 * CRYTSALLIZATION\ TEMPERATURE + 0.10966 * CRYSTALLIZATION\ TIME + 0.047454 * AGEING\ TIME - 30.5444$ (4-4)

Relative Crystallinity $= -0.0033395 * CRYSTALLIZATION\ TEMPERATURE\text{^}2 - 0.0043287 * CRYSTALLIZATION\ TEMPERATURE * CRYSTALLIZATION\ TIME - 0.0056481 * CRYSTALLIZATION\ TEMPERATURE * AGEING\ TIME + 1.8719 * CRYSTALLIZATION\ TEMPERATURE - 0.0047004 * CRYSTALLIZATION\ TIME\text{^}2 + 0.0019759 * CRYSTALLIZATION\ TIME *$

$$AGEING\ TIME\ +\ 1.2917 * CRYSTALLIZATION\ TIME\ +\ 0.0025367 * AGEING\ TIME\text{^}2\ +\ 0.66227 * AGEING\ TIME\ -\ 170.7685 \quad (4\text{-}5)$$

Equations 4-6 and 4-7 were developed using MATLAB for determining crystallite size of ZSM-5 as a function of the synthesis parameters. Both equation had an accuracy of more than 97% for the parameters investigated.

$$\text{Crystallite Size} = 0.18729 * \text{CRYSTALLIZATION TEMPERATURE} + 0.071735 * \text{CRYSTALLIZATION TIME} + 0.13398 * \text{AGEING TIME} - 2.2846 \quad (4\text{-}6)$$

$$\text{Crystallite Size} = -0.00040054 * \text{CRYSTALLIZATION TEMPERATURE}\text{^}2 + 0.00037619 * \text{CRYSTALLIZATION TEMPERATURE} * \text{CRYSTALLIZATION TIME} - 0.0011474 * \text{CRYSTALLIZATION TEMPERATURE} * \text{AGEING TIME} + 0.31392 * \text{CRYSTALLIZATION TEMPERATURE} - 0.0015771 * \text{CRYSTALLIZATION TIME}\text{^}2 + 0.0013607 * \text{CRYSTALLIZATION TIME} * \text{AGEING TIME} + 0.1773 * \text{CRYSTALLIZATION TIME} - 0.0045423 * \text{AGEING TIME}\text{^}2 + 0.44793 * \text{AGEING TIME} - 15.6126 \quad (4\text{-}7)$$

4.6.11.4. Mathematical model for prediction of Zeolite A properties

A number of equations were develop using MATLAB. The equations established a relationship between the investigated synthesis parameters and zeolite-A properties. Equation 4-8 and 4-9 were use to determine the relative crystallinity. The second order equation showed and accuracy of more than 99% while equation 4-8 had an accuracy of more than 94%

$$Relative\ crystallinity\ =\ 0.38221 * CRYSTALLIZATION\ TEMPERATURE\ +\ 1.0165 * CRYSTALLIZATION\ TIME\ +\ 0.3859 * AGEING\ TIME\ -\ 1.7187 \quad (4\text{-}8)$$

$$Relative\ Crystallinity\ =\ -0.02524 * CRYSTALLIZATION\ TEMPERATURE\text{^}2\ +\ 77379454222920.05 * CRYSTALLIZATION\ TEMPERATURE * CRYSTALLIZATION\ TIME\ -\ 0.061958 * CRYSTALLIZATION\ TEMPERATURE * AGEING\ TIME\ -\ 1547589084458397 * CRYSTALLIZATION\ TEMPERATURE\ +\ 0.50082 * CRYSTALLIZATION\ TIME\text{^}2\ -\ 208361911526391.6 * CRYSTALLIZATION\ TIME * AGEING\ TIME\ -\ 7737945422292019 * CRYSTALLIZATION\ TIME\ -\ 0.07113 * AGEING\ TIME\text{^}2\ +\ 4167238230527843 * AGEING\ TIME\ +\ 1.5475890844584e + 17 \quad (4\text{-}9)$$

Another very important property in zeolite synthesis is establishing the relationship between batch Si/Al ratio and that in the synthesized product. Using equation 4-10 and 4-11 a relationship was established for determining the Si/Al of the final zeolite. All tests had an accuracy of more than 97%

$$\text{Si/Al} = -0.0012056 * \text{CRYSTALLIZATION TEMPERATURE} + 0.021496 * \text{CRYSTALLIZATION TIME} - 0.014368 * \text{AGEING TIME} + 1.8222 \quad (4\text{-}10)$$

$$\text{Si/Al} = 0.0020933 * \text{CRYSTALLIZATION TEMPERATURE\^2} + 8610613478227.28 * \text{CRYSTALLIZATION TEMPERATURE} * \text{CRYSTALLIZATION TIME} + 0.0015625 * \text{CRYSTALLIZATION TEMPERATURE} * \text{AGEING TIME} - 172212269564546.2 * \text{CRYSTALLIZATION TEMPERATURE} + 0.02691 * \text{CRYSTALLIZATION TIME\^2} - 2442464436381.106 * \text{CRYSTALLIZATION TIME} * \text{AGEING TIME} - 861061347822728.6 * \text{CRYSTALLIZATION TIME} + 0.0026266 * \text{AGEING TIME\^2} + 48849288727621.88 * \text{AGEING TIME} + 1.72212269564546e+16 \quad (4\text{-}11)$$

Equation 4-11 and 4-12 were develop to establish the relationship between crystallite size and synthesis parameters. Both equations produced results of more than 96% accuracy when tested.

$$\text{Crystallite size} = -2.2544 * \text{CRYSTALLIZATION TEMPERATURE} + 26.6229 * \text{CRYSTALLIZATION TIME} - 15.4825 * \text{AGEING TIME} + 87.6761 \quad (4\text{-}12)$$

$$\text{Crystallite Size} = -2.6485 * \text{CRYSTALLIZATION TEMPERATURE\^2} - 1.077249050143875e+16 * \text{CRYSTALLIZATION TEMPERATURE} * \text{CRYSTALLIZATION TIME} + 4.0314 * \text{CRYSTALLIZATION TEMPERATURE} * \text{AGEING TIME} + 2.154498100287757e+17 * \text{CRYSTALLIZATION TEMPERATURE} - 47.1844 * \text{CRYSTALLIZATION TIME\^2} + 1.745502549118392e+16 * \text{CRYSTALLIZATION TIME} * \text{AGEING TIME} + 1.077249050143876e+18 * \text{CRYSTALLIZATION TIME} + 2.6506 * \text{AGEING TIME\^2} - 3.49100509823679e+17 * \text{AGEING TIME} - 2.154498100287755e+19 \quad (4\text{-}13)$$

4.7. Conclusions

The G&W kaolin from Eastern Cape, Republic of South Africa has been utilize for the production zeolites as an alternative source of silica and alumina. This was effectively beneficiated to reduce

the quartz and mica content by simple sedimentation and decantation of the slurry. The product obtained was calcine at a temperature of 650°C for 3 hours to reactivate it and the obtained metakaolin was used for the synthesis of zeolites A and ZSM-5. Zeolite A and ZSM-5 have been synthesized successfully from South African kaolin. The temperature of crystallization, crystallization time and ageing time influenced the crystallinity of zeolite A and ZSM-5 obtained from kaolin from South African origin. The optimum hydrothermal temperatures, for zeolite A and ZSM-5 were 100 and 180°C respectively, and the ageing times were 12 and 24 hrs respectively. While crystallization time is 20 and 48 hrs respectively. Zeolite A with Si/Al ratio of 1.3, BET surface area 143.88 m^2/g was synthesized from South African Kaolin at an optimum temperature of crystallization of 100°C, the ageing time of 12 hours and a crystallization time of 20 hours. ZSM-5 zeolite with Si/Al ratio 43, BET surface area 282 m^2/g was synthesize from South African Kaolin at an optimum temperature of crystallization of 180°C, the ageing time of 24 hours and a crystallization time of 48 hours. However, a mathematical relationship was establish between synthesis parameters and properties of Zeolite A and ZSM-5.

CHAPTER FIVE

5 Introduction

Investigation of the Efficiency of Different Synthesized Zeolites in the Removal of Salt Ions. In this chapter, the kinetic studies discussed to investigate the performance of adsorbents to understand the desalination mechanisms involved in the investigation of adsorption. The factors affecting the effectiveness of the synthesized zeolites in the removal of salt ions (Na, K, Mg, and Ca) from seawater investigated and presented in detail. Investigating the efficacy of various synthesized zeolites in the absorption of various salt ions.

5.1. Kinetic studies

5.1.1. Preparation of synthetic seawater solution

It is very difficult to synthesize seawater solutions that are identical to seawater. This is because of the inconsistency in the type and quantity of salts and other contaminants. However, the addition of individual salts accurately is very difficult and some of the salts are hygroscopic which is very difficult to weigh accurately. Therefore, in this study, ASTMd1141-98 is use to synthesize seawater base on the assumption that it represents the seawater but not on an accuracy basis.

Synthetic multi-component solutions of Na^+, K^+, Ca^+, and Mg^+ ions were prepared using an analytical grade of sodium chloride (NaCl), Magnesium chloride ($MgCl_2$), Calcium chloride ($CaCl_2$), and Potassium chloride (KCl_2). The required amounts of salts dissolved in 850ml of distilled water and volume brought up to 1000ml with distilled water. The pH adjusted to 7.8 using 0.1M NH_4Cl and 0.1M HCl solutions.

5.1.2. Batch experiment procedure

As result of findings in the previous chapter, the candidate's zeolite identified from the crystallization experiments. Zeolite A and ZSM-5 zeolite synthesized based on the following synthesis parameters were selected for application on batch experiments.

Table 5-1: Show the synthesis parameters of candidate zeolite used for batch experiments

Candidate zeolite	Crystallization temperature (℃)	Crystallization time (h)	Ageing time (h)	BET surface area (m^2/g)	Si/Al ratio
Zeolite A	100	20	12	143	1.3
ZSM-5	180	48	24	282	43

The batch experiments focused on the effectiveness of the synthetic zeolite (ZSM-5 and zeolite A) for removal of Na^+, Ca^{2+}, K^+ and Mg^{2+} ions from the synthetic seawater. The initial concentrations of the elements were 378.40, 198.02, 153.62, and 1348.28 ppm of K, Ca, Mg and Na respectively.

In this study, the mass of zeolites samples of 2.5g, 4.0g, and 6.0g was mixed with 100ml of synthetic seawater solutions containing K^+, Ca^{2+}, Mg^{2+}, and Na^+ ions. The samples were agitated using linear shaker at 100, 140, and 180 rpm at shaking time of 30, 60, 90, 120 150, and 180 minutes' intervals at room temperature. The required amount of water sample filtered and analysed using ICP-OES. The mean value taken after repeating the experiment three times.

5.1.3. Discussions on the ion Removal Efficiency Results for Zeolite A

5.1.3.1. Effect of zeolite A dosage on salt ion removal

The results in figure 5-1 (a) to (d), show that when the mass of the zeolite increased 5-1(a), the removal of the seawater ions increased at the initial stage between 30 to 60 minutes of the

experiment. The removal was then erratic all through to the end of the investigation. 6.0 g zeolite A dosage performed better in Ca^{2+} ion adsorption compared to 2.5 g and 4.0 g through the duration of the experiment. K+ removal from the seawater took place throughout the period though it doesn't have a definite pattern and this fluctuation show that 4.0 g is promising when match to 2.5 g and 6.0 g. Mg^{2+} adsorption is occurred from the beginning to the end and the removal was moderate. 4.0 g and 6.0 g performed well all through the 180 minutes. Na^{+} ion desalination was lowest, and the removal only started after 90 minutes of the experiment and 4.0 g is more promising in the removal of Na^{+} ion. The removal of Ca^{2+}, K^{+}, Mg^{2+} ions mostly occur in the early stage, while Na^{+} removal occurs late. The percentage removal of Ca^{2+}, K^{+}, Mg^{2+} are 89, 57, and 25 respectively while that of Na^{+} is 16% at 180 rpm. This is because as the adsorbent mass provided more adsorption sites increases, which in turn increased the availability of more adsorption sites per unit mass of adsorbent surface and thus increase the total amount of ions removal. This result shows that zeolite mass in seawater solution can affect the adsorption capacity for the removal of salt ions as it controls the availability of adsorption sites.

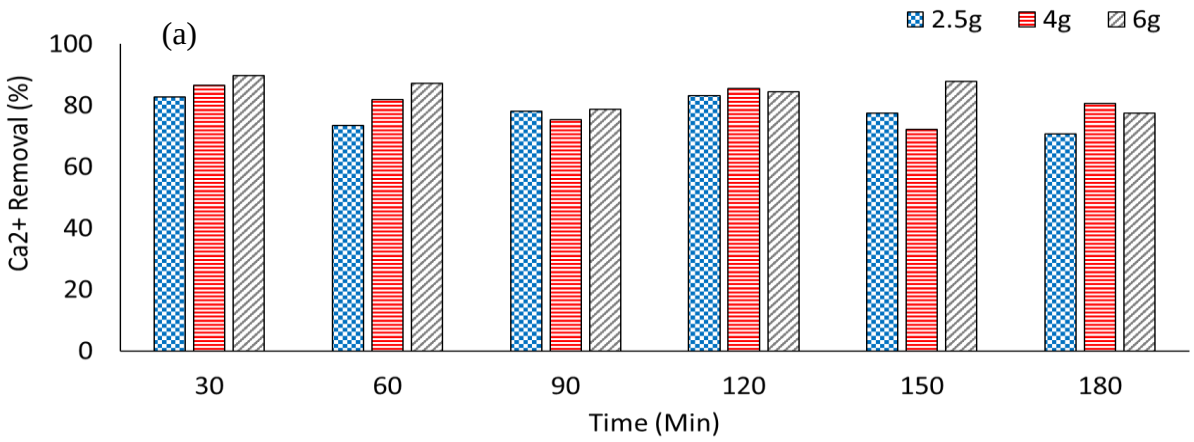

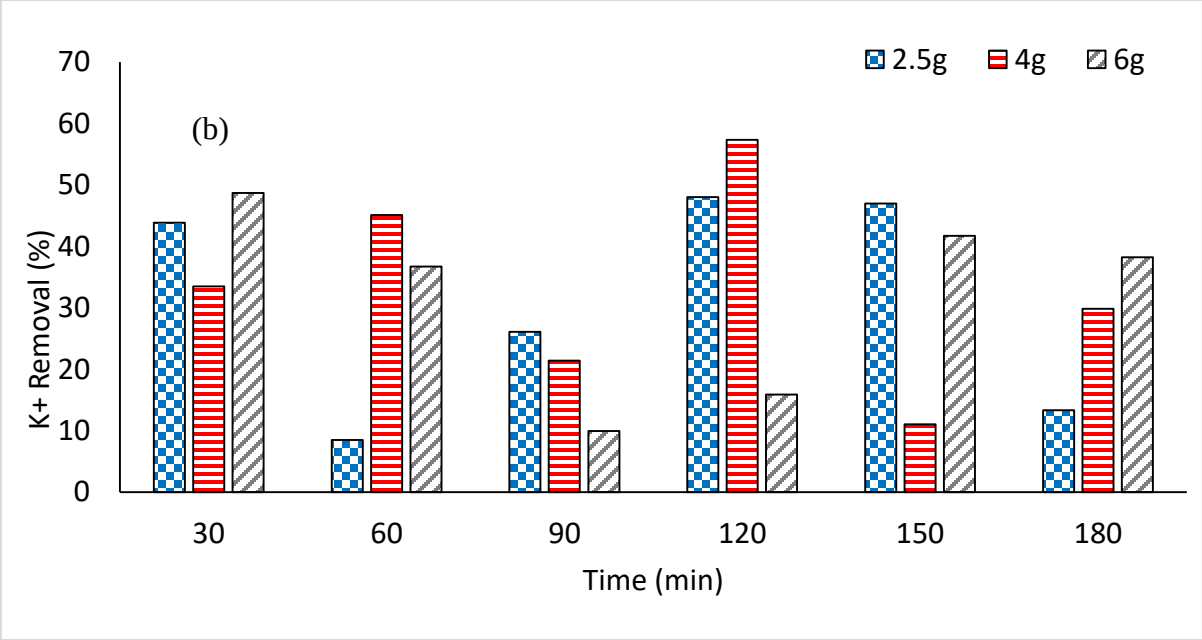
(b)
2.5g
4g
6g
K+ Removal (%)
70
60
50
40
30
20
10
0
30
60
90
120
150
180
Time (min)

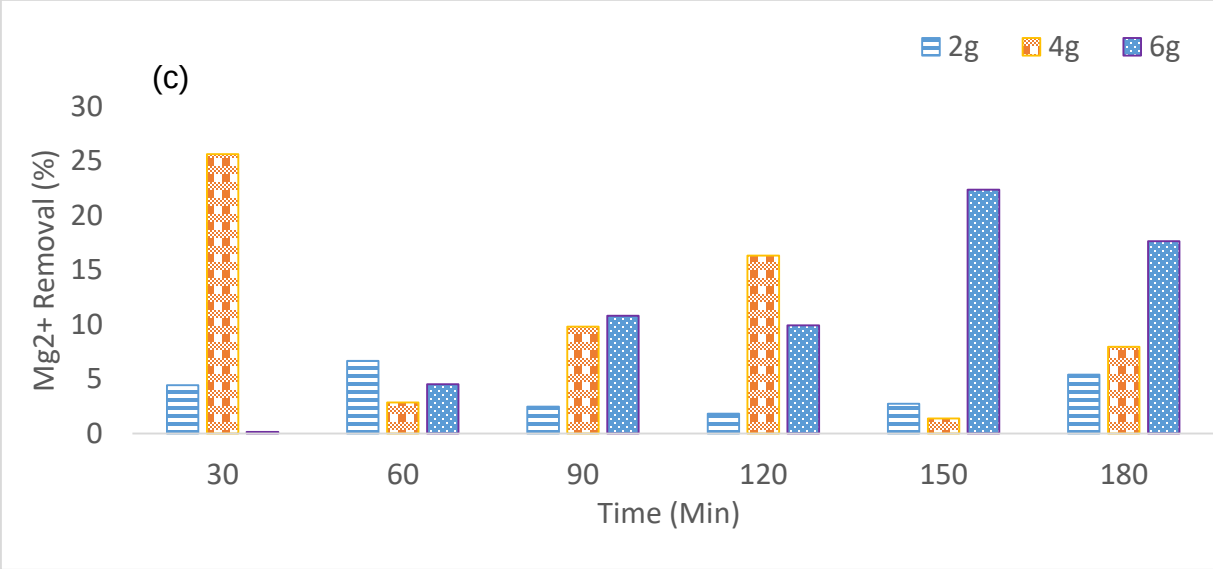
(c)
2g
4g
6g
Mg2+ Removal (%)
30
25
20
15
10
5
0
30
60
90
120
150
180
Time (Min)

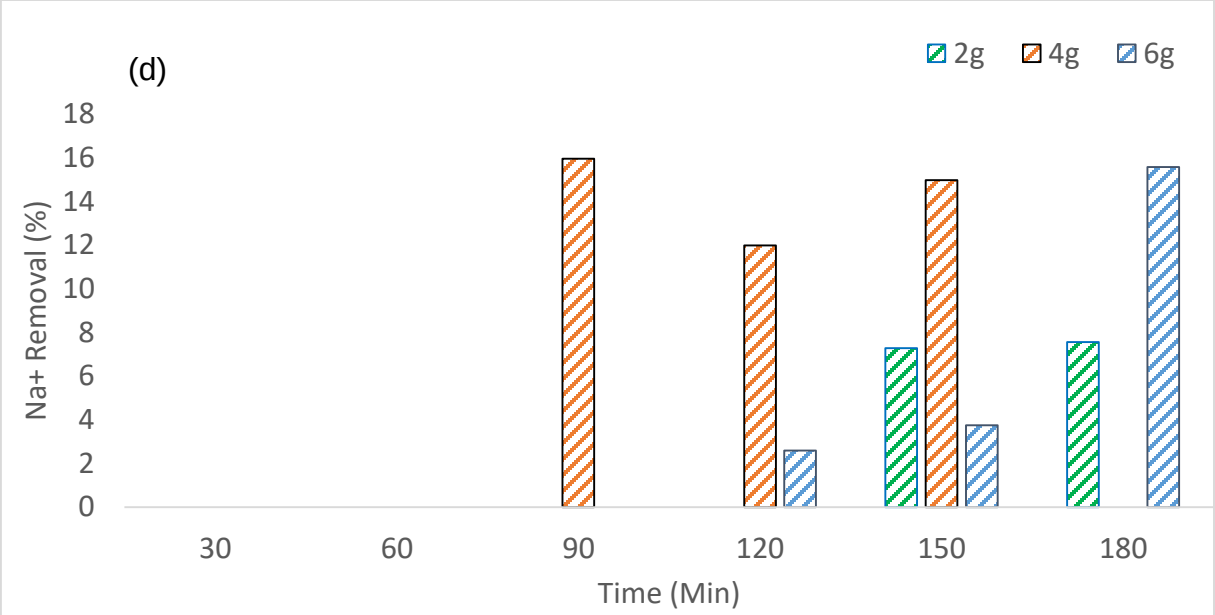

Figure 5-1 Effect of synthesized zeolite A dosage on (a) Ca^{2+} (b) K^{+} (c) Mg^{2+} (d) Na^{+} removal from synthetic seawater at 100 rpm agitation speed

The zeolite dosage of 2.5 g, 4.0 g, and 6.0 g applied in 100ml solutions of seawater. The samples were analysed using ICP-OES. The pH of the water adjusted and maintained at 7.8.

Table 5-2 Represent the effect of zeolite A dosage on the removal of salt ion from synthetic seawater.

Seawater salt ions	Adsorbent dosage (g)	Percentage removal (%)
Ca^{2+}	6.0	89.7
	4.0	86.6
	2.5	82.6
K^{+}	6.0	48.7
	4.0	57.3
	2.5	48
Mg^{2+}	6.0	22.4
	4.0	25.6
	2.5	5.4
Na^{+}	6.0	15.5
	4.0	16
	2.5	7.6

Kinetic studies conducted using different dosage of 25 g, 4.0 g and 6.0 g. The zeolite adsorbent was agitated with 100 ml of synthetic seawater with an agitation speed of 180 rpm for a period of 180 minutes. Samples for analysis taken after every 30 minutes and the results is presented in Table 5-1. The show that when the zeolite A mass was increased from 2.5 to 6.0 g, there was an increase in the removal of Ca^{2+}. At 2.5 g, 4.0 g and 6.0 g the percentage salt ion removal are 82.6%, 86.6% and 89.7% respectively. This result shows that the zeolite mass in the synthetic seawater can affect the removal capacity of the salt ions.

5.1.3.2. Effect of agitation speed

The synthetic seawater was mixed and contacted with 6 g of zeolite A samples for 180 minutes at room temperature while the pH was adjusted to 7.8. The results of the effects of agitation speed depicted in figure 5-2 (a) to (d).

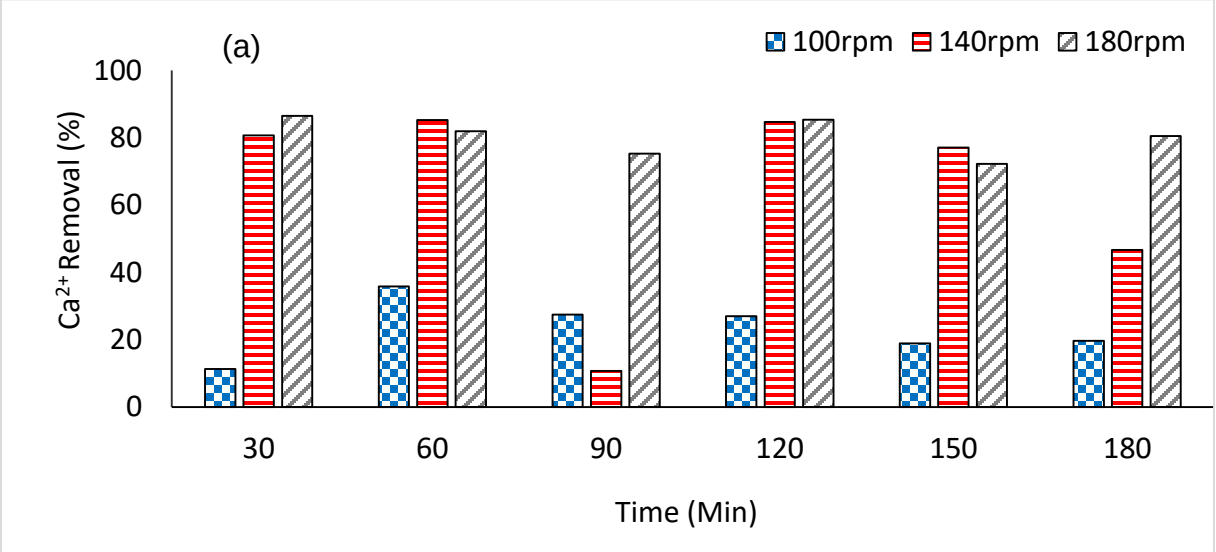

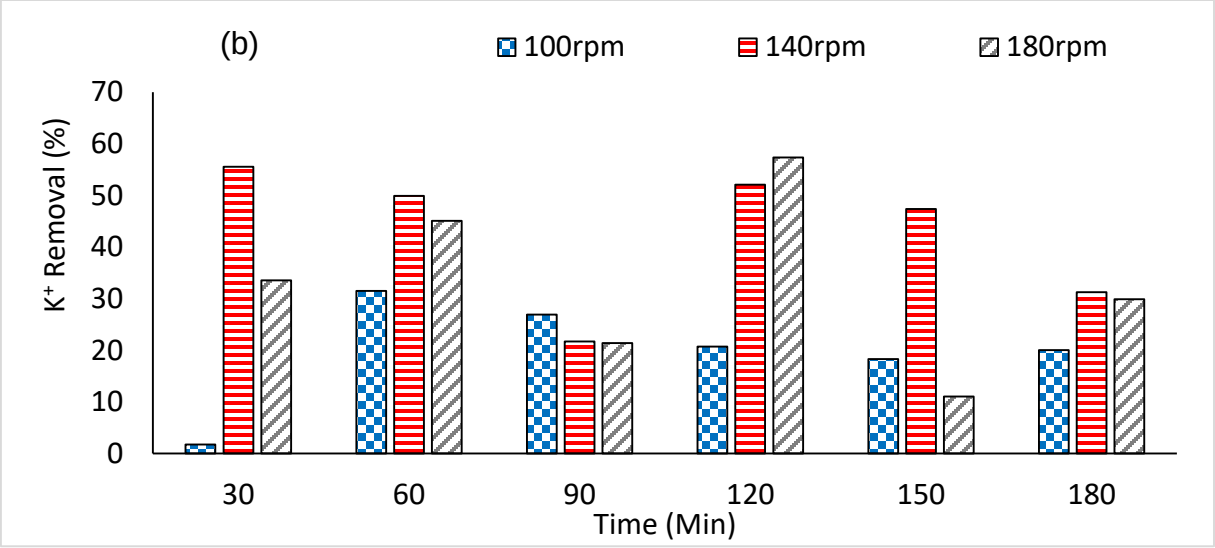

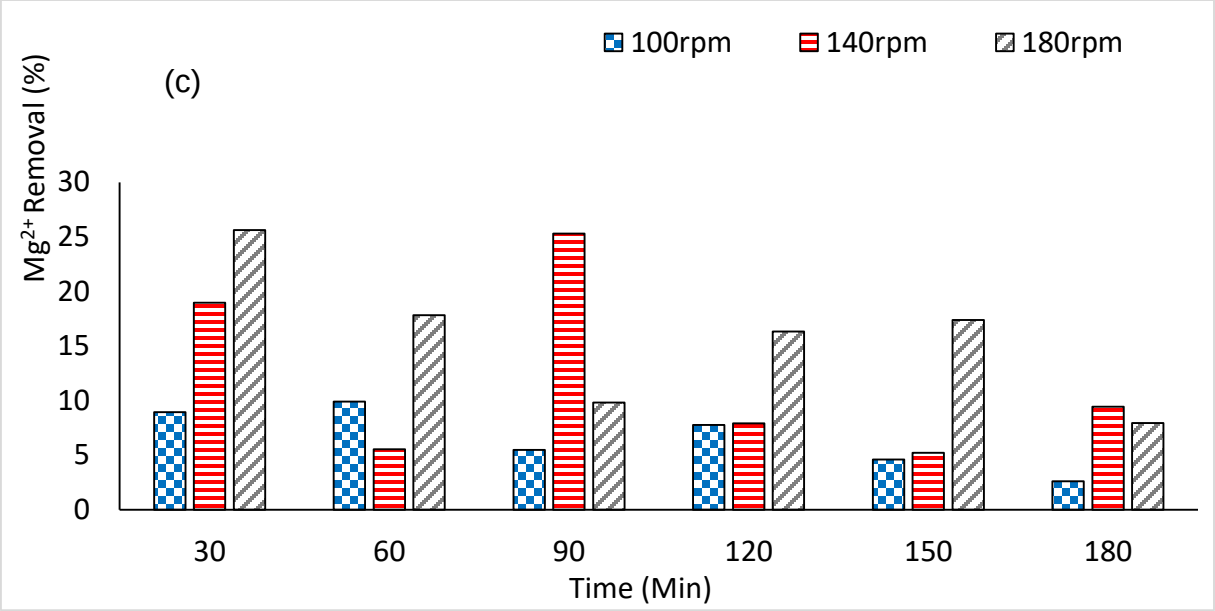

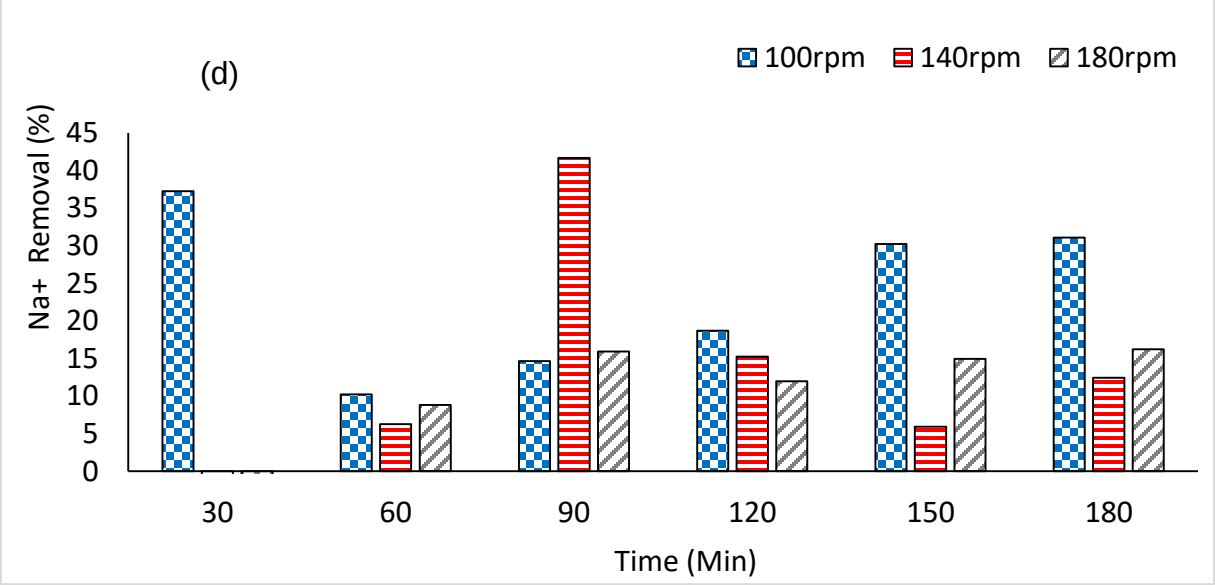

Figure 5-2 Effect of agitation speed on (a) Ca^{2+} (b) K^{+} (c) Mg^{2+} (d) Na^{+} removal from synthetic seawater at 6g dosage of zeolite A

Figure 5-2 (a) to (d) shows the effect of agitation speed on the removal efficiency of seawater salt ions. The removal of the ions (Ca^{2+}, K^{+}, Mg^{2+} and Na^{+}) are erratic and fluctuated across the period

of the experiments. The maximum removal of Ca^{2+}, K^{+} and Mg^{2+} occurred at 140 and 180 rpm and the least reduction is at 100 rpm. Na^{+} removal efficiency is promising at 100rpm as presented in figure 5-2 (d). The results from the experiments show that the salt ions removal efficiency increased with the increase in agitation speed. The outcome of this findings show that an increase in the agitation speed caused a higher adsorption capacity. The agitation aids in incapacitating the external mass transfer resistance that controls the adsorption rate. Therefore, an increase in agitation speed from 100 rpm to 180 rpm aids in an upsurge of salt ions movement in solution and decreases the mass transfer resistance. External diffusion coefficient decreases at high agitation speed and the boundary film turn thinner that mostly increases the solute diffusion rate over the boundary film (Kaplan *et al.*, 2017; Salih and Salih, 2017).

6 g of zeolite mixed in a beaker with 10 ml of synthetic seawater and allowed to be in contact in a linear shaker for the period of the study. The required volume of water sample was taken after 1^{st}, 2^{nd} and 3^{rd} contact speed for analysis using ICP-OES.

The results obtained show that the salt ions rejection efficiency does not follow a particular pattern rather it had a non-uniform format. The results further show the removal of Ca ions of up to 86.6% under 180 rpm at the first 30min of the experiment, which is the optimum removal at all agitation speed and the lowest removal of 11.3% at the first 30min. There was some good removal at all the 3 stirring speeds.

There was removal of about 2% of K^{+} at the first 30 min at 100 rpm. The removal increased significantly to 55.7, 33.6 at 30 min contact time, 140 rpm, and 180 rpm respectively. The best removal 57.3% was achieve at 120 minutes and 180 rpm.

The removal of Mg^{2+} at 30 min increased with a change of agitation speed from 100 to 180 rpm. At 100 rpm the removal was 8.9% whereas at 140 and 180 rpm the removal was 19 and 25.6% respectively. As the time of agitation shifted from 30 to 60 min, there was serious leaching of Mg^{2+} ion from 100 rpm with very considerable removal of 5.5 and 9 % from 140 rpm and 180 rpm respectively. The pattern continues but with a less leaching from 90 and 120 min at both 100 rpm. The Mg^{2+} removal was stable at 120, 150 and 180 rpm.

Adsorption of Na^{+} was very rapid in the first 30min and 100 rpm with the removal of 37.3%. At 140 and 180 rpm, there was a little leaching of 1.0 and 1.1% in the bulk of the water respectively. There was removal of Na^{+} at 60 min with an agitation speed of 100 and 140 rpm while the Na^{+} leached at 180 rpm. From 90 to 180 min there was no Na^{+} removal but the best was desalination noticed at 90 min and 180 rpm.

In this research, the salt ions removal efficiency is not consistent as reported by Kaplan (2017) where it is shown that metal removal increased as the speed of agitation increased. However, an increase in the speed of agitation caused a higher adsorption capacity. The external mass transfer resistance overcome with the help of the agitation that controls the adsorption rate. The salt ions motion is aided by the increase of agitation and hence decrease the mass transfer resistance Salih and Salih, (2017)

5.1.3.3 Effect of contact time

The effect of agitation time on the desalination of salt ions from synthetic seawater investigated to determine the best contact time. The results presented in figure 5-3 to 5-5. From the figure, it can be seen that the fluctuated with an increase of contact time from the first 30minute to the end of 180 minutes of the experiments. It was also shown that the salt ions removal took place fast in the early stage, which can be attributed to the availability of free adsorption sites (Ltaief *et al.*, 2015).

After the rapid adsorption at the initial stage, slow cations uptake may be as a result of slow diffusion rate into the internal pores of the zeolite (Hameed, Din and Ahmad, 2007; Ltaief *et al.*, 2015; Elboughdiri, 2020). The optimal contact times found to be 30 minutes for Ca^{2+}, 90 minutes for K^{+}, 150 minutes for Mg^{2+} and 90 minutes for Na^{+}.

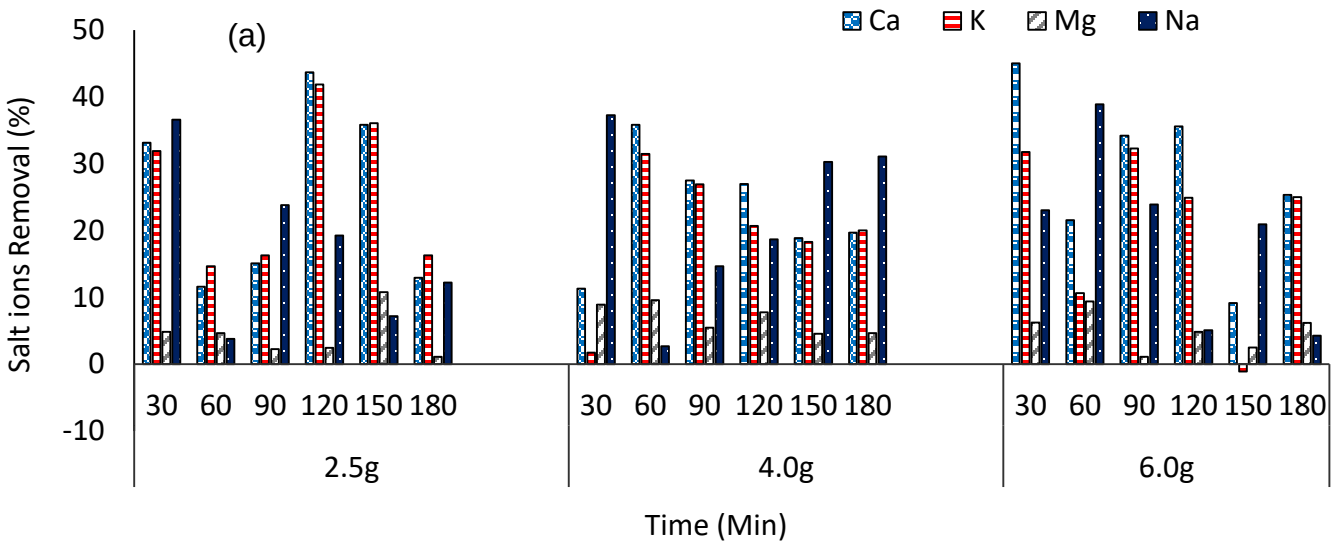

Figure 5-3 Effect of contact time at different zeolite A dosage (agitation speed = 100 rpm)

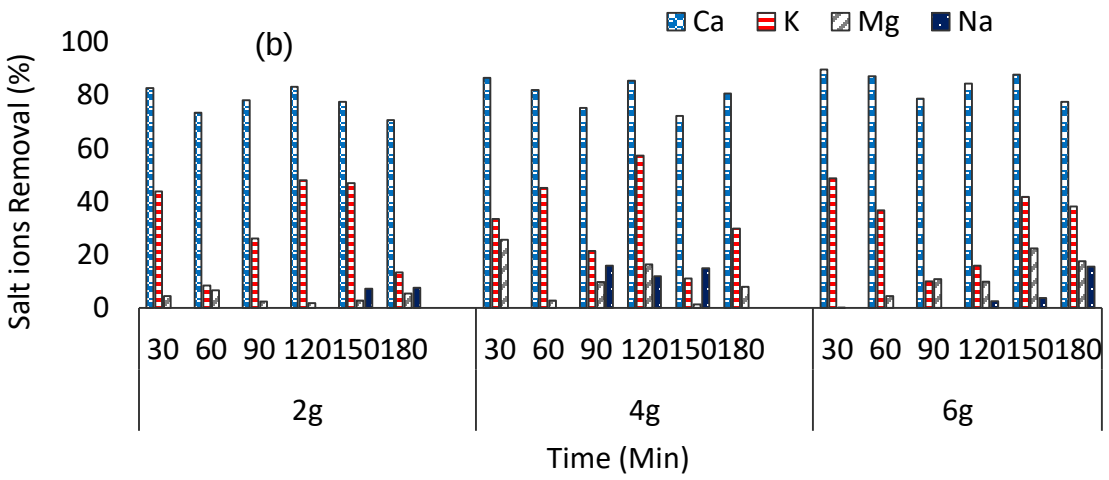

Figure 5-4 Effect of contact time at different zeolite A dosage (Agitation speed = 140 rpm)

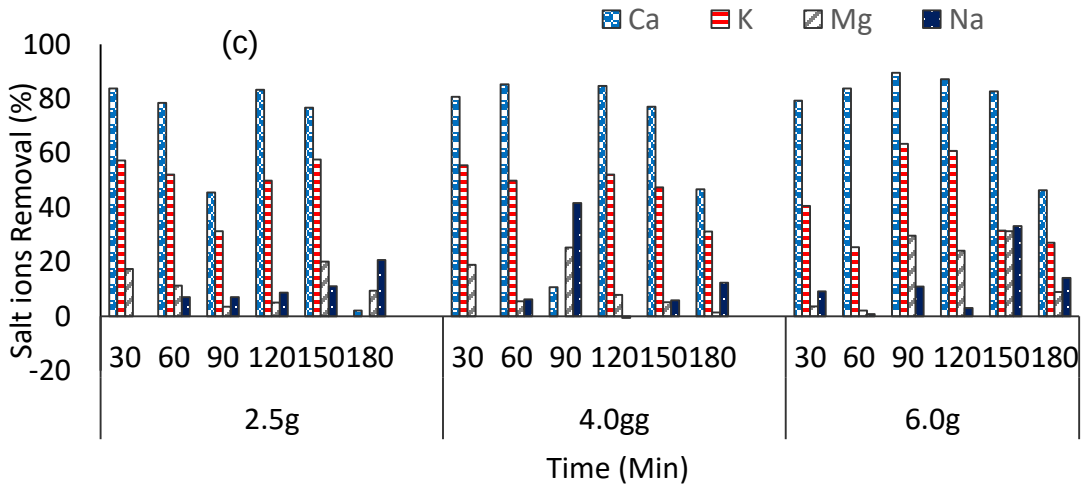

Figure 5-5 Effect of contact time at different zeolite A dosage (Agitation speed = 180 rpm)

Rapid removal of salt ions occurred during the initial 30 minutes of agitation and this is because of the availability of free exchange sites on the zeolite surface, which allowed diffusion, and ions exchange of the salt ions in the solution onto zeolites. Conversely, the degree of metal removal suspends on inherent properties of the types involved (Von-kiti, 2016). The slow removal occurred beyond the time of agitation indicates saturation of most of the active sites of exchange. The fluctuations in the desalination as noticed in all the results are typical because of different exchange

sites within the zeolite frameworks. Subsequently, as the process continued with time at increased agitations speed, the unreacted sites with dissimilar affinities were exposed so that other proton exchanges could occur. The favoured ion is desalinated first by the zeolite which is why Mg^{2+} appears to be least adsorbed with increasing time. The preferential ion removal and selectivity sequence shows that zeolite A demonstrated a better affinity for Ca^{2+} in seawater desalination. However, the relative amount of each salt ions would affect the desalination of each other. The preferential ion desalinated if the exchange capacity of the zeolite is not depleted. This pattern can be observe in the case of zeolite A with Ca^{2+} and Mg^{2+} being the highest and least preferred ions respectively. ($Ca^{2+} > K^{+} > Na^{+} > Mg^{2+}$)

5.1.4. Removal Efficiency Results for ZSM-5 Zeolite

Figure 5-6 (a) to (d) show the effect of synthesized ZSM-5 zeolite dosage on the removal of salt ions from synthetic seawater. Figure 5-6 (a) demonstrate the erratic nature of ZSM-5 zeolite performance in the removal of Ca^{2+}. The removal was poor throughout the period of the experiment. Only 6.0 g is promising and at 60 and 120 minutes only 2.5 g and 4.0 g perform

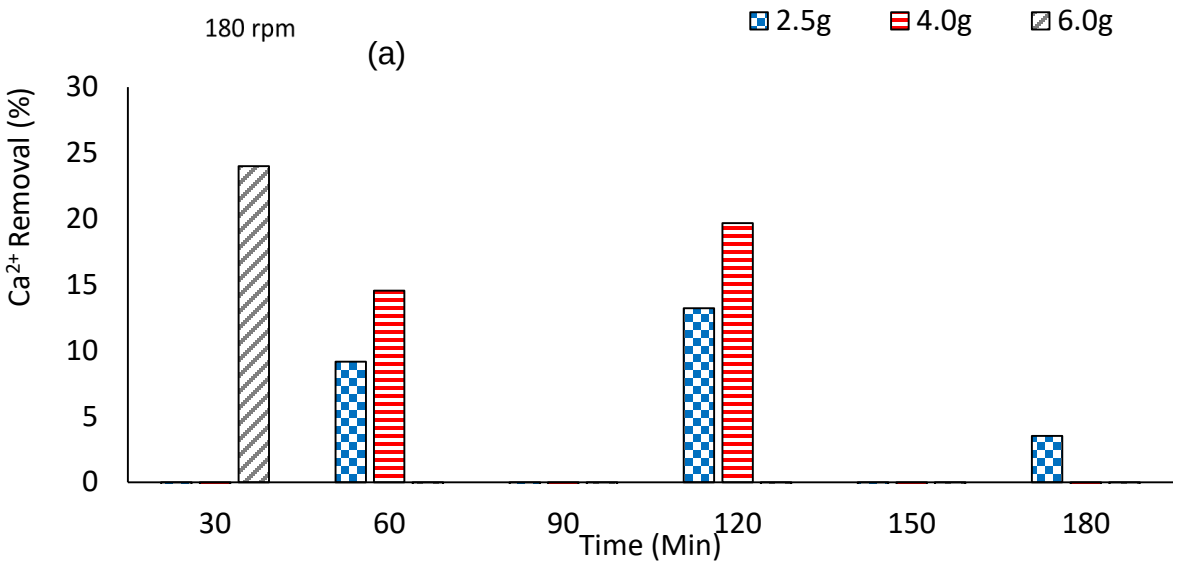

In figure 5-6 (b) all the three dosages show removal ability in the desalination of K^+ but only 2.5 g and 4.0 g favoured the removal efficiencies

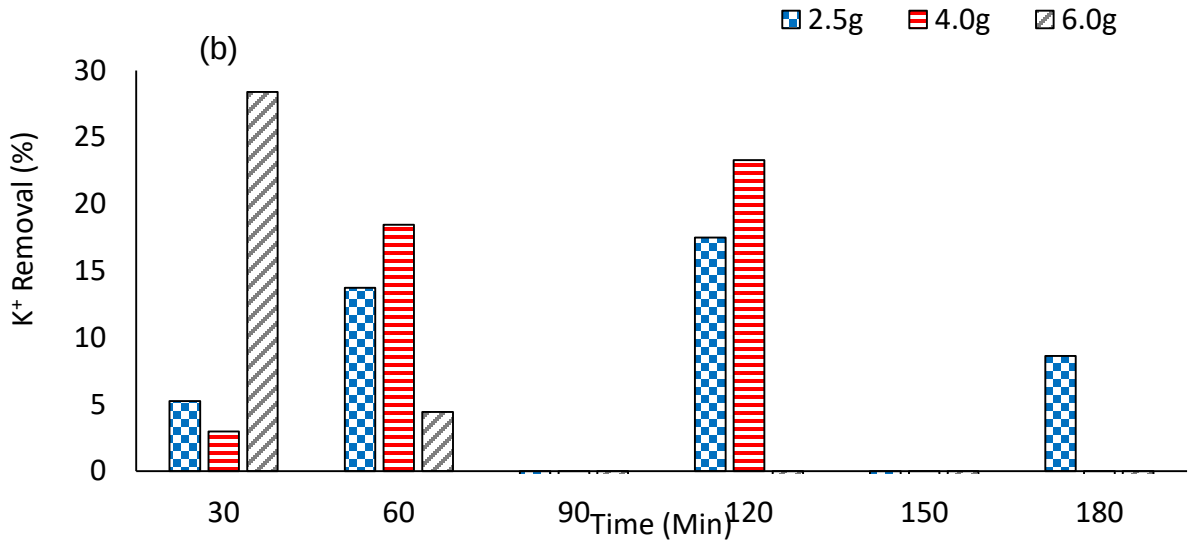

Mg^{2+} removal ability of ZSM-5 zeolite presented in figure 5-6 (c) and the three dosages performed at the initial 30 minutes and continued to be erratic throughout with no removal at 150 and 180 minutes.

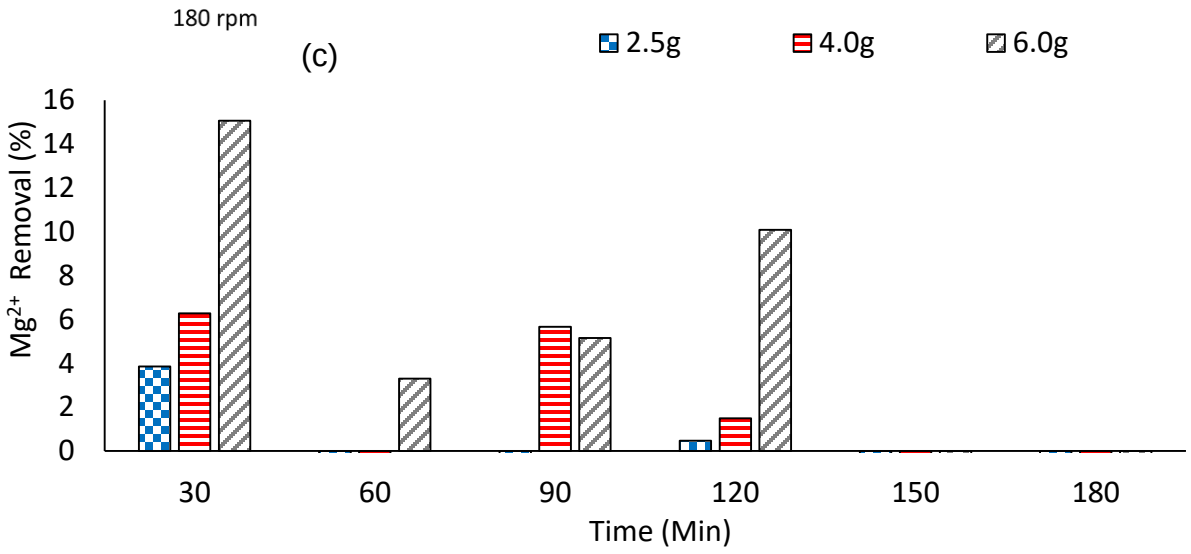

In figure 5-6 (d), the Na^{+} removal result shows a good improvement by the adsorbent compared to the rest and the performance is better at 90 minutes where all the three dosages removed the Na ions very significant**.**

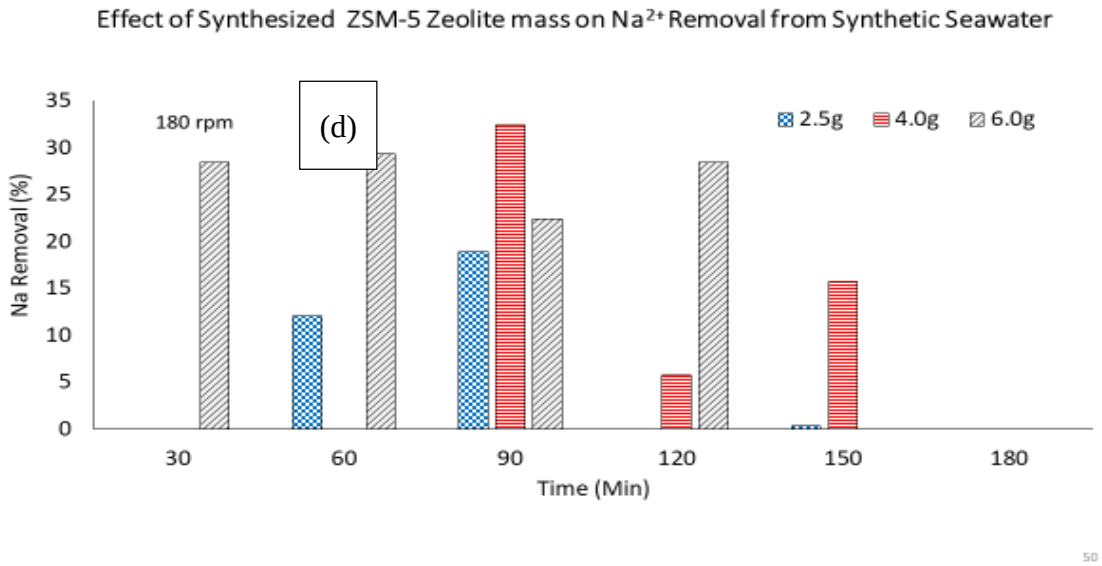

Figure 5-6 effect of synthesized ZSM-5 zeolite mass on (a) Ca^{2+} (b) K^{+} (c) Mg^{2+} (d) Na^{+} removal from synthetic seawater

Figure 5-7 (a) to (d) show the effect of agitation speed on adsorption of (a) Ca^{2+} (b) K^{+} (c) Mg^{2+} (d) Na^{+} using ZSM-5 zeolite and in the removal of Ca^{2+}only 6.0 g dosage performed at 180 rpm figure 5-6 (a)

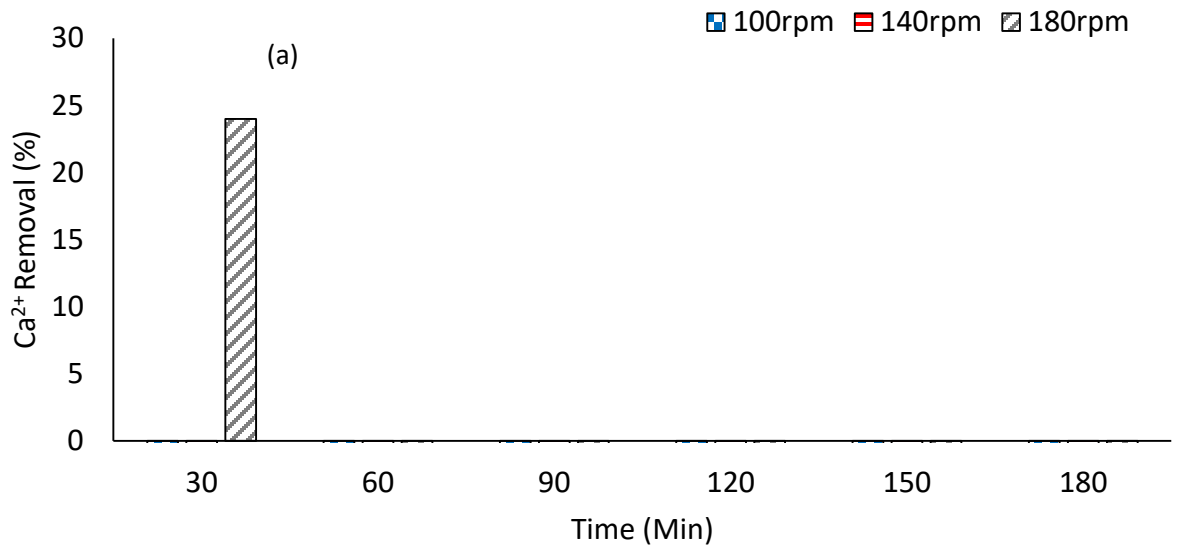

The removal of K^{+} was best at the initial 30 minutes of the experiment where all the dosages performed well and there after the removal was poor and only 4.0 g performed at 90 and 150 rpm

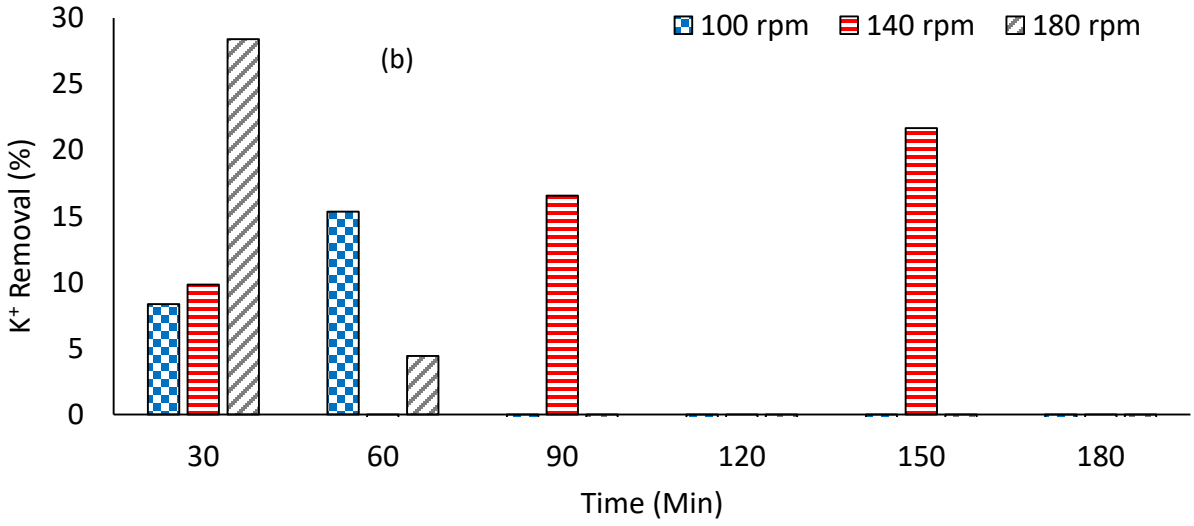

The Mg^{2+} removal only occurred at 180 rpm as presented in figure 5-6 (c) and there was no removal at 100 and 140 rpm

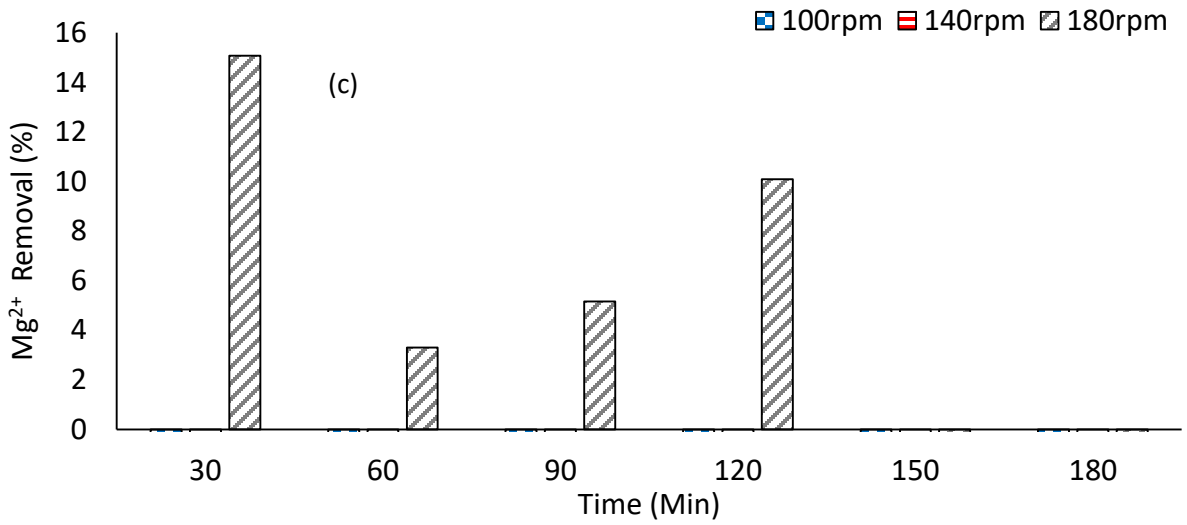

Na^{+} removal was best at 140 and 180 rpm where the zeolite performed well between 30 to 150 minutes and removal at 100 rpm only occurred at 120 minutes.

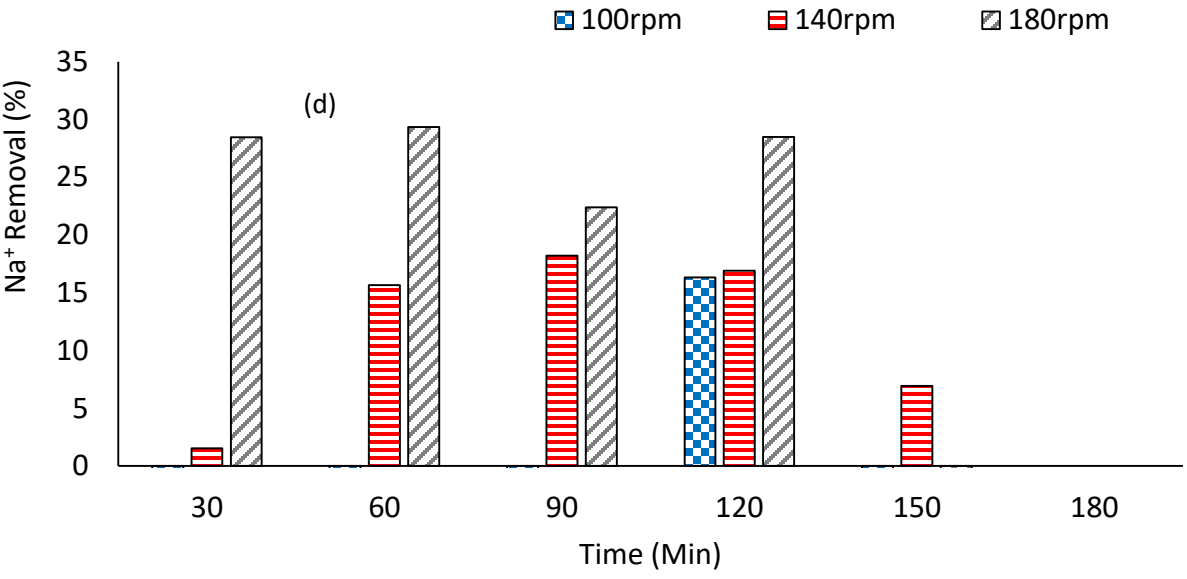

Figure 5-8 Effect of agitation speed on adsorption of (a) Ca^{2+} (b) K^{+} (c) Mg^{2+} (d) Na^{+} using ZSM-5 zeolite

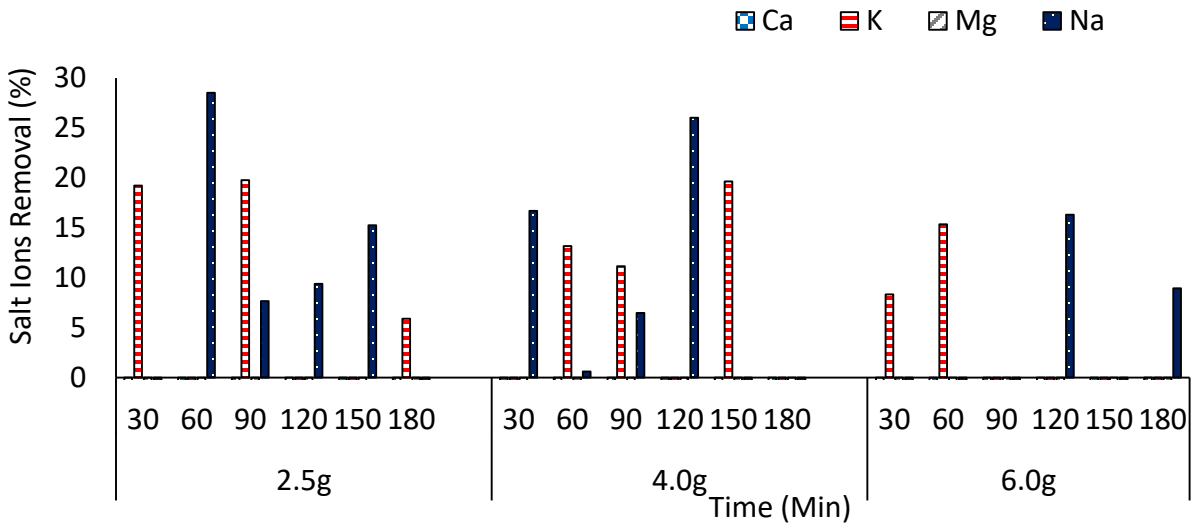

Figure 5-9 Effect of contact time at different ZSM-5 dosage (Agitation speed = 100 rpm)

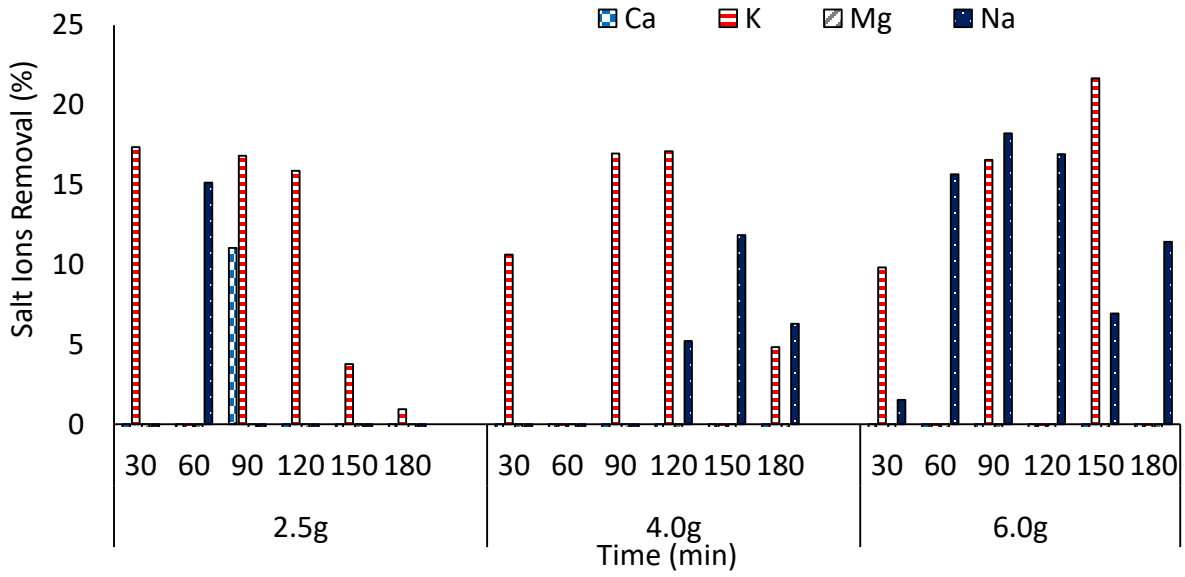

Figure 5-10 Effect of contact time at different ZSM-5 zeolite dosages (Agitation speed = 140 rpm)

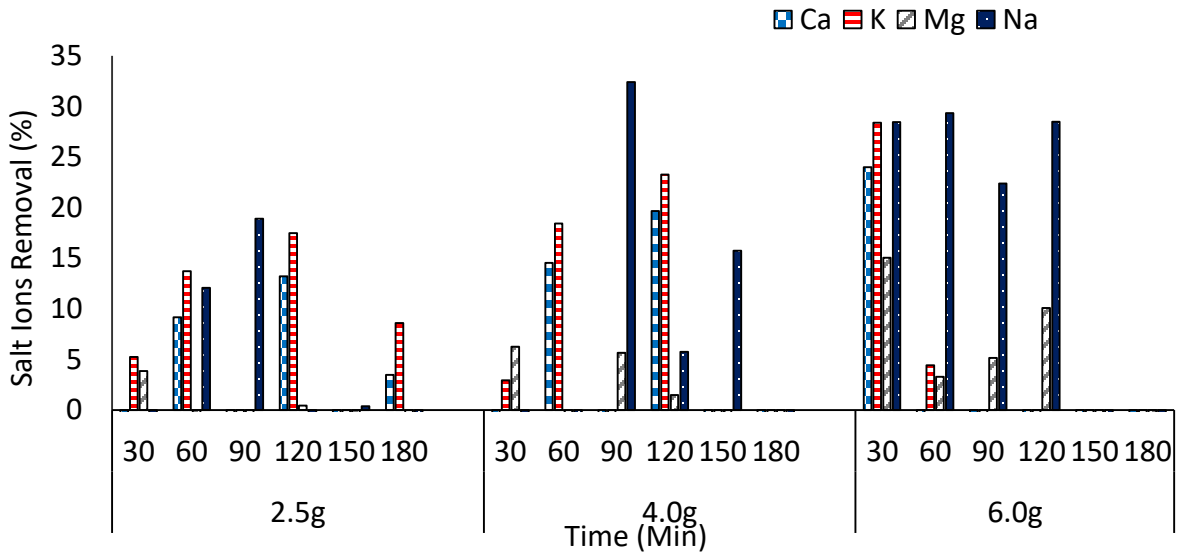

Figure 5-11 Effect of contact time at different ZSM-5 zeolite dosages (Agitation speed = 180 rpm)

Table 5-3: The concentration of seawater elements during adsorption before and after the mixing of ZSM-5

Time (Min)	Ca (mg/l)	K (mg/l)	Mg (mg/l)	Na (mg/l)
Initial	371	743	2150	9964
30	435	600	3230	17175
60	785	1028	2159	7123
90	437	596	2667	9201
120	656	898	2582	9026
150	601	803	2503	8442
180	515	699	3399	15184

The concentration of cations in seawater (Ca^{2+}, K^{+}, Mg^{2+}, and Na^{+}) before the adsorption experiment evaluated before the mixing with ZSM-5 zeolite using ICP OES. Their concentration recorded again after agitation for the period of the experiment. The value of Na^{+}, which was 9964 mg/l and increased to 17175 mg/l after 30 minutes. The table 5-2 show that proportionate activity remarkably occurred after first 30 minutes. The Na^{+} concentration fluctuated from 7123 to 9201

mg/l between 60 and 150 minutes, which is significantly lower than the initial concentration before mixing with ZSM-5 adsorbent. The value of Na^+ ion from 180 minutes is 15184 mg/l, which is higher than the initial concentration when the process commences.

A similar trend observed for Mg^{2+}, with a significant increase that fluctuated between 30 and 120 minutes, and a significant decrease after 150 minutes. The value after 180 minutes was higher than when the experiment started from 2150 mg/l to 3399 mg/l.

The trend was the same for K^+ and Ca^{2+}. The element (K^+) concentration decreased after was ZSM-5 was added to the sample solution for 30 minutes. Potassium concentration level increased substantially after 60 minutes. The desalination of this element concentration levels fluctuated continuously until the end of the experiment. The final value of 459 mg/l is far lower than the initial value concentration of 743 mg/l.

The adsorption of Ca^{2+} was in increase and the increase is across from 30 to 180 minutes. A significant increase of 515 mg/l occurred within the first 180 minutes from the initial concentration of 371 mg/l. A further decrease of the concentration occurs throughout the experiments while the concentration level fluctuated until the end of the experiment.

Table 5-4 Desalination Efficiency of the cation elements

Time/Min	Ca^{2+} (mg/l)	K^+ (mg/l)	Mg^{2+} (mg/l)	Na^+ (mg/l)
Initial	0	0	0	0
30	-17.2507	19.2463	-50.2326	-72.3705
60	-111.59	-38.358	-0.4186	28.51265
90	-17.7898	19.78466	-24.0465	7.657567
120	-76.8194	-20.8614	-20.093	9.41389
150	-61.9946	-8.07537	-16.4186	15.27499
180	-38.814	5.921938	-58.093	-52.3886

The desalination of the cation elements efficiency using ZSM-5 zeolite shown in table 23, Na^+ recorded negative performance values from the beginning of the experiment at 30 minutes and at the end of interaction at 180 minutes and 28.5% removal achieved. This shows that the desalination was not successful and this could be due to the leaching of the sodium from the framework of the zeolite. The amount of all the elements in this type of zeolite was very high and as a result, there is significant leaching from the framework of the zeolite into the seawater.

With high leaching of Ca^{2+} and Mg^{2+} in the treated seawater sample, the concentration of the salinity is significantly high and that means that desalination was not effective. The decrease in Na^+ and K^+ concentration level show that the hardness of the seawater decreased.

Considering the removal efficiency Table 5-3, Na recorded negative values except for the 90 minutes' interaction when a 13.33% removal was achieved. This means that its removal was unsuccessful. The amount of sodium in this type of zeolite was very high causing the sodium in the zeolite framework to leach considerably into the seawater. K^+ recorded negative values all through the test. Potassium also leached due to this same reason. There was, however, no Ca^{2+} or Mg^{2+} in the zeolite framework, thus no leaching occurred for these two elements. The highest effective removal of Ca^{2+} was after 60 minutes when 93.85% recorded and after 15 minutes for Mg^{2+} with a value of 30.96%.

5.2. Conclusion

Based on the application of the candidate zeolite for batch experiment zeolite A performed well in adsorption of salt ions from synthetic seawater whereas ZSM-5 zeolite leached due to excess amount of the elements in within the framework of the zeolite. There was no particular pattern for the removal of the salt ions using both zeolite A and ZSM-5 even though desalination of ions such

as $Ca^{2+}$and K^{+} are promising using zeolite A. Desalination using ZSM-5 was unsuccessful. The presence of Ca^{2+} and Mg^{2+} in the seawater influence the uptake of K^{+} and Na^{+}. The process of cation uptake by zeolites determined by the kinetics of adsorption. The amount of Na+ releases into the seawater by zeolites indicates ions exchange activity. Since there was Na in both seawater and zeolite, the effective removal of all cations hindered. Very often, a zeolite favors the least hydrated ion while the solution phase favors the mostly hydrated ion. The Preference of the overall ion-exchange selectivity of zeolite A is the order $Ca^{+}>K^{+}>Na^{+}>Mg^{2+}$.

CHAPTER SIX

6 To Investigate the Use of the Zeolite as an RO Membrane for Seawater Desalination.

Introduction

In this chapter, we presented the modification of zeolite support and the Zeolite accumulation on the substrate and the utilization of the deposited membrane in a reverse osmosis filtration unit to investigate the membrane performance in desalinating water. The impact of applied pressure studied. The efficiency of the membrane in salt ions removal and the permeation fluxes deduced.

6.1. Synthesis of zeolite membrane from G&W kaolin.

6.1.1. Preamble

A membrane is a thin sheet of natural as well as synthetic material that typically protected by a cellulose network that is impermeable to the contaminant substances (Aliyu *et al*, 2018). The membrane is selective and the selectivity is dependent on variations in physical and chemical properties of the elements of the solution. The mixture to be separated is referred to as feed; whereas the separated portion of the feed through the membrane is permeate. The part of the feed that does not permeate through the membrane is retentate. Flux is the volumetric flow rate of permeate per unit area. Due to their ability to regulate substances that move through the membrane, the membrane is commonly used in different industries for separation processes, thus a high degree of separation is widely achieved, which then makes such processes generally appropriate (Chollom *et al.*, 2015). A membrane has a special role in receiving an enriched content in the permeate and a residue in the retentate (Kovo, 2011).

6.2. Reagents.

Grahamstown clay, sodium silicate solution/water glass (Sigma Aldrich) with SiO2 percent composition of 26.5 and Na_2O 10.6wt percent and NaOH 98 percent purity (Sigma Aldrich) were

used as additional sources of silica and sodium oxide in the synthesis of ZSM-5 and zeolite A. The structure-directing agent (SDA) for ZSM-5 synthesis was tetrapropylammonium bromide (TPABr) from Sigma Aldrich. Ace Enterprises Chemical Association supplied AR grade nitric acid (55 percent) to change the pH. Both reagents were use exactly as obtained, with no post treatment.

6.3. α-Al_2O_3 support and modification.

The natural appearance, texture and surface morphology of the α-Al_2O_3 support is important for zeolite membrane development. Surface modification will lead to finding out the effect of the support morphology on the zeolite membrane from G&W kaolin. In this work, etching surface modification used in the deposition of zeolite. The α-Al_2O_3 support roughened by sandpaper (800-grid size), was washed using detergent water, and sonicated to remove other dirt and impurities from the sandpapering. The substrate rinsed in deionized water and dried at 60℃ overnight. The etched modification was use for the research. The substrate was treated with 2.2 M KOH and then washed with deionized water and thereafter treated with 37% concentrated HCl. It was then washed with 1 M NaOH solution to get rid of all chloride ions and finally washed with deionized water again (Lik *et al.*, 2000; Kovo, 2011). The recovered samples were dried overnight at 60℃ and the substrate characterized by XRD and SEM.

6.4. ZSM-5 and zeolite A membrane synthesis.

ZSM-5 zeolite membranes were synthesized on the surface of the disk-shaped porous alpha-Al_2SiO_3 substrate using a modified in-situ crystallization technique as reported by Kovo, (2011), via traditional hydrothermal treatment. In the preparation of kaolin-based ZSM-5 zeolite membrane, the required amount of G&W metakaolin and sodium hydroxide dissolved in deionized (DI) water and TPABr were mixed separately with the required amount of DI water. The solution

of NaOH/Kaolin and sodium silicate solution added simultaneously to the solution of the TPABr while stirring using a mechanical stirrer. Nitric acid was used to control the pH until the solution mixture was homogenous. The batch composition mixture for this synthesis had the following molar ratio. 50 SiO_2:Al_2O_3:20 Na_2O:2TPABr:2000 H_2O. The synthesized gel was aged for 24 hours. After ageing, the substrate placed at the bottom of the Teflon cup and the gel poured through the side of the Teflon cup gently, then transferred to a stainless steel autoclave, and hydrothermally treated at 180°C for two days. After each crystallization, the autoclave was removed from the oven and the substrate was recovered and wash with deionized water using a vacuum pump filtration unit set up until the pH was less than 8. The samples (substrate and ZSM-5 powder) dried overnight at 80°C and calcined for 5 hours at 550°C at a heating rate of 1℃/min to remove the structural directing agent (SDA).

In the preparation of zeolite A membrane on the surface of the substrate support in which metakaolin function as the growth centre, a small portion of the metakaolin was taken from the amount required to synthesize zeolite. A solution was mix with small amount of deionized water and the etched support dipped into it. This was crystallized to dehydration until a film of metakaolin formed at the surface of the substrate. The synthesis gel of zeolite A was prepared by taking the required amount of 3 molar NaOH solution and mixing with the remaining outstanding amount of metakaolin portion and stirred using the mechanical stirrer at 600 rpm for 45 min. This was then aged for 12 hours under static condition. The support coated with metakaolin film placed at the bottom of the autoclave and the gel poured through the side of the Teflon cup and treated hydrothermally in a preheated oven at 100℃ crystallization temperature and 20 hours crystallization time. The substrate and the zeolite A powder were recovered and washed with deionized water and dried overnight at 60℃.

6.5. Desalination experiment

The desalination performance of the zeolite membrane for seawater solution at different applied pressures evaluated in an RO desalination test unit. The membrane was mounted and sealed in a stainless-steel cell to cover the effective desalination flow area. The feed solution (synthetic seawater) was fed using a high-pressure stainless-steel Fluid-O-Tech magnet drive rotary vane pump, TH series; maximum speed 1725 rpm with an applied gauge pressure ranging between 7 to 15 bars. The total dissolved solids (TDS) and the permeate samples were collect and evaluated using ICP OES. The salt ions (Ca^{2+}, K^{+}, Mg^{2+} and Na^{+}) removal estimated from the TDS values to determine the desalination performance of the membranes.

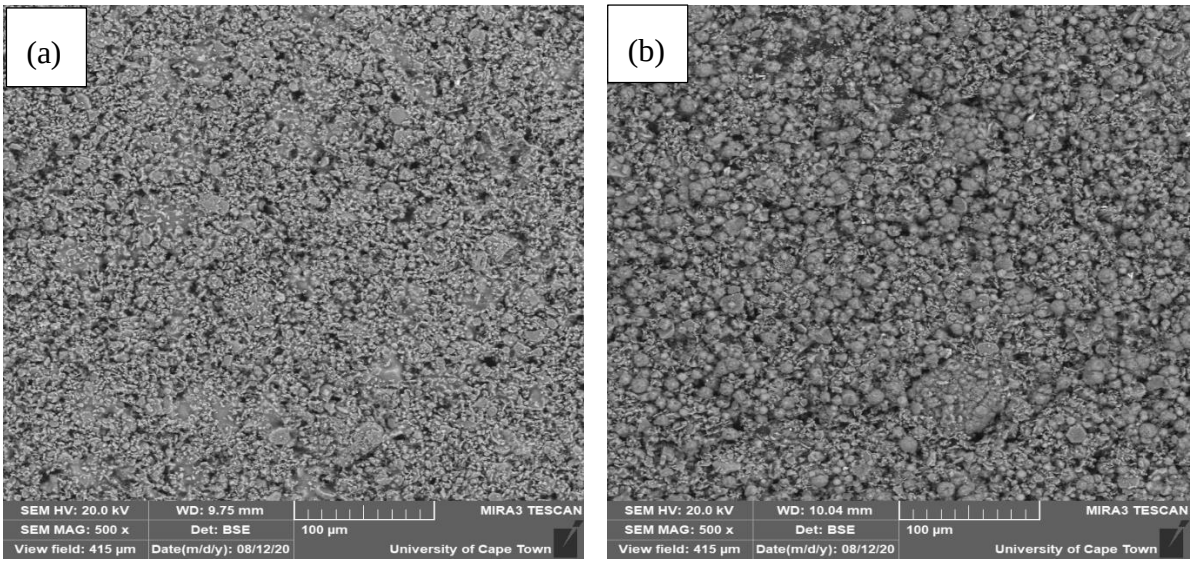

Figure 6-1 SEM micrographs of the surface of a (a) plain and (b) modified alpha-alumina support used in this work

The as-received α-alumina plain support SEM image presented in figure 6-1(a). The SEM micrograph have some impurities, which can possibly restrict the crystallization of zeolites film on the surface, therefore, it is imperative to modify the surface before the zeolite layer deposition. The zeolites modification and the deposition discussed in section 6-4 and 6-5respectively.

The SEM micrograph for the modified α-alumina surface shown in figure 6-1(b) whereas the XRD pattern of the bare and etched support is depicted in figure 6-2.

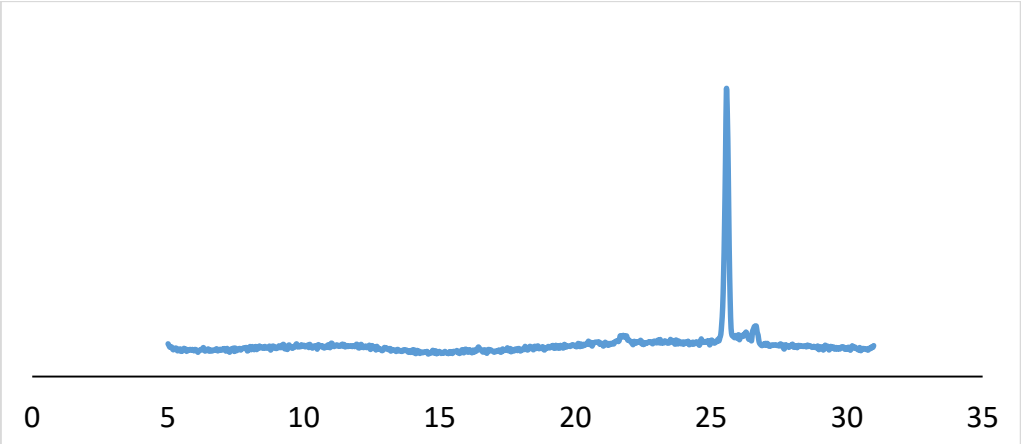

Figure 6-2 XRD pattern of bare alpha-alumina support before deposition of zeolites

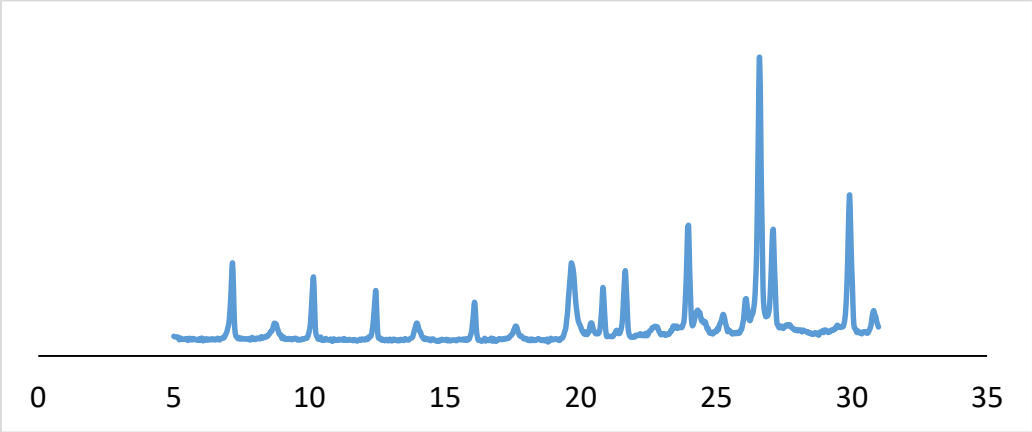

Figure 6-3 XRD pattern of synthesized zeolite A membrane surface morphology of Zeolite A membrane

Figure 6-3 show the XRD film as deposited by crystallization as described in in section 6-5. The XRD peaks intensity at 2-theta 7.15, 10.15, 12.45 and 16.12, 23.90, 27.10 with peak of quartz impurities at 2-theta 26.60. These peaks are assigned to zeolite A characteristic peak. This result indicates that zeolite A successfully deposited on the surface of α-alumina support.

The SEM morphology of zeolite A layer is presented in figure 6-4. The SEM micrograph show no defect on the surface of the support

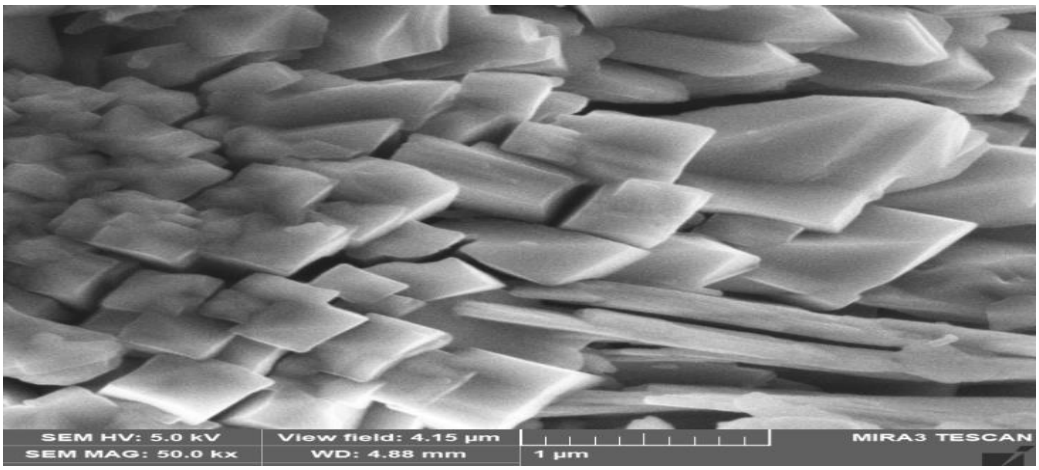

Figure 6-4 Surface morphology of zeolite A membrane

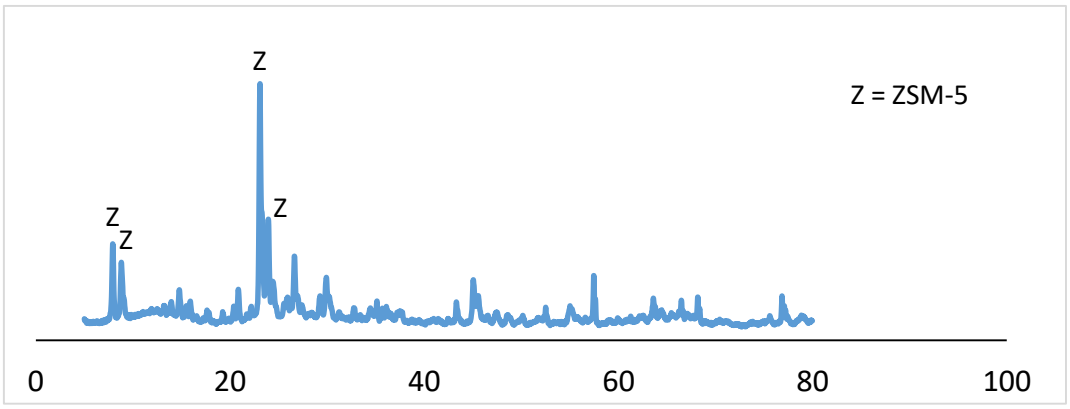

Figure 6-5 XRD pattern of synthesized of ZSM-5 zeolite membrane

ZSM-5 zeolite was crystallize hydrothermally on the etched support of α-alumina and the result of XRD pattern is depicted in figure 6-5 whereas the SEM image of the deposited ZSM-5 zeolite is shown in figure 6-6.

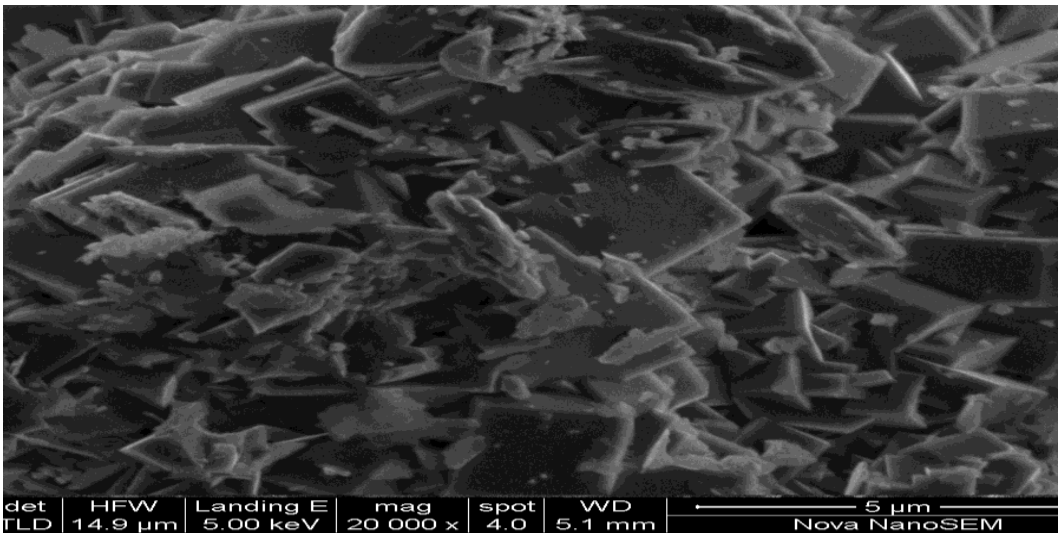

Figure 6-6 Surface morphology of ZSM-5 zeolite membrane

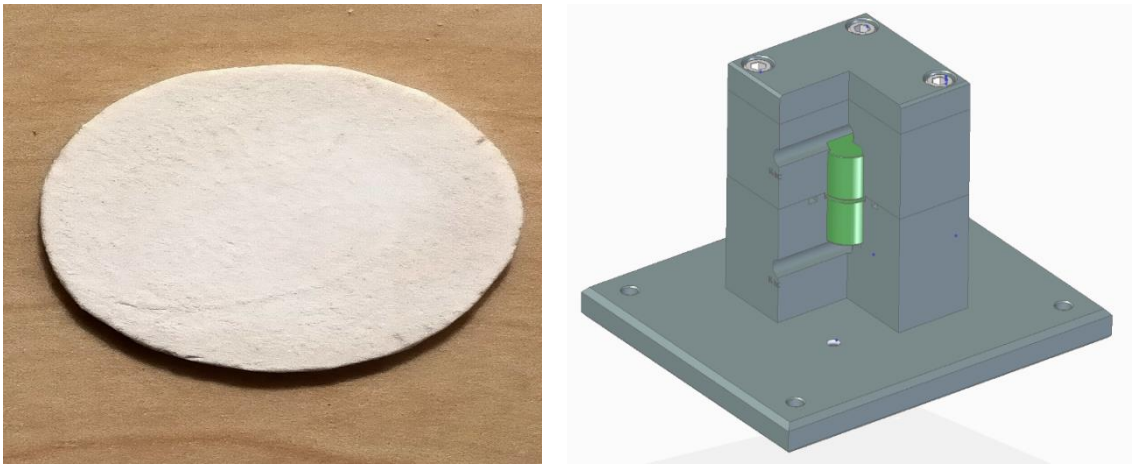

Figure 6-7 Bare alpha-alumina substrate support (20 mm X 1.2 mm) with zeolite deposited and stainless steel cell used in RO desalination unit

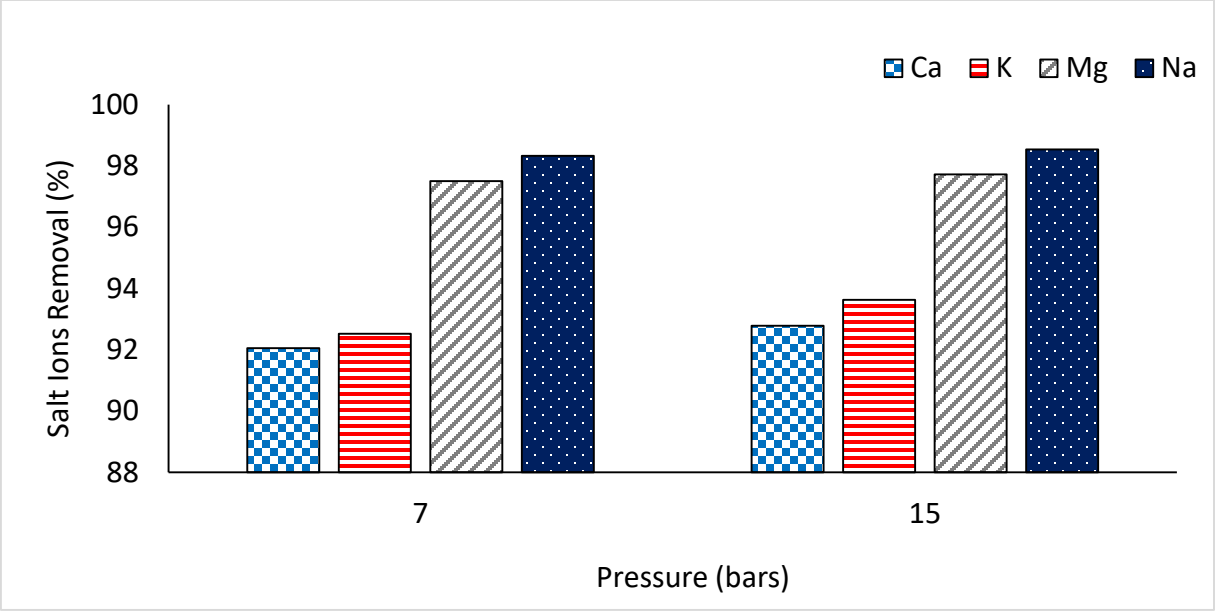

Figure 6-8 Bare alpha-alumina substrate performance at 7 and 15 bars pressures

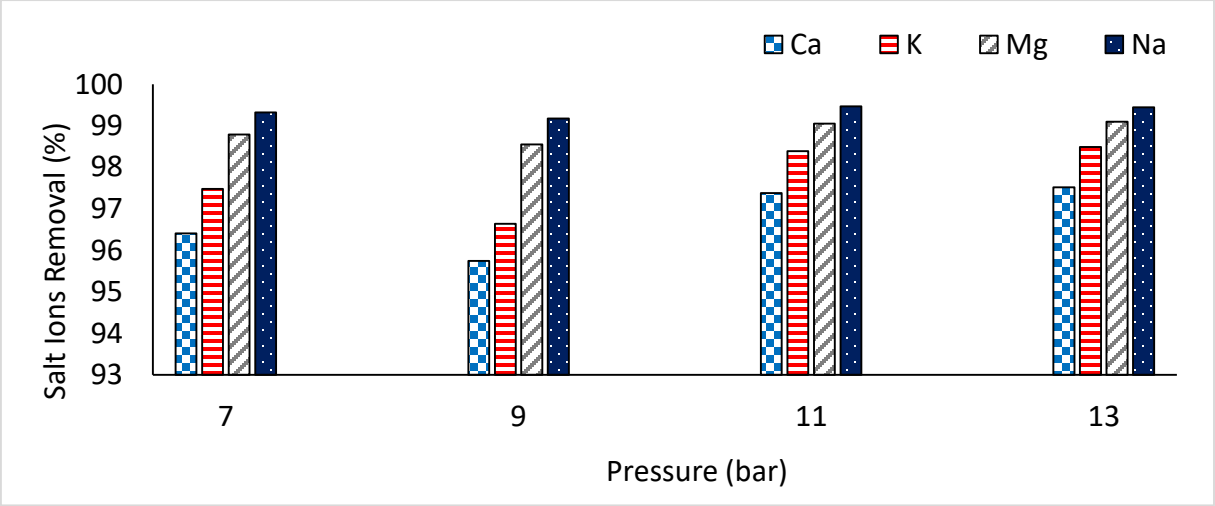

Figure 6-9. The efficiency of ZSM-5 zeolite membrane performance on salt ions removal under different applied pressure

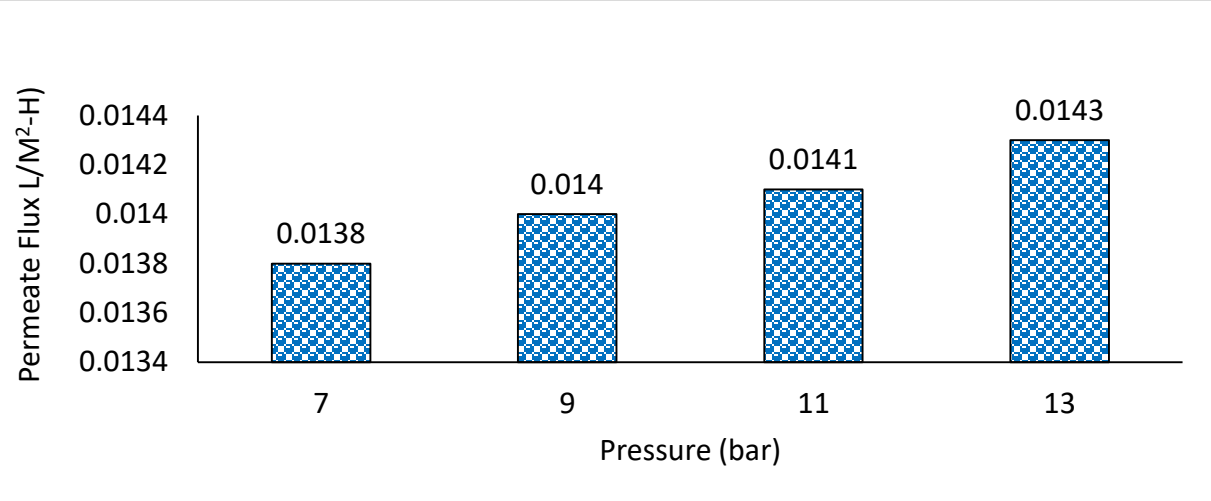

Figure 6-10 Water fluxes at different applied pressures for ZSM-5 zeolite membrane

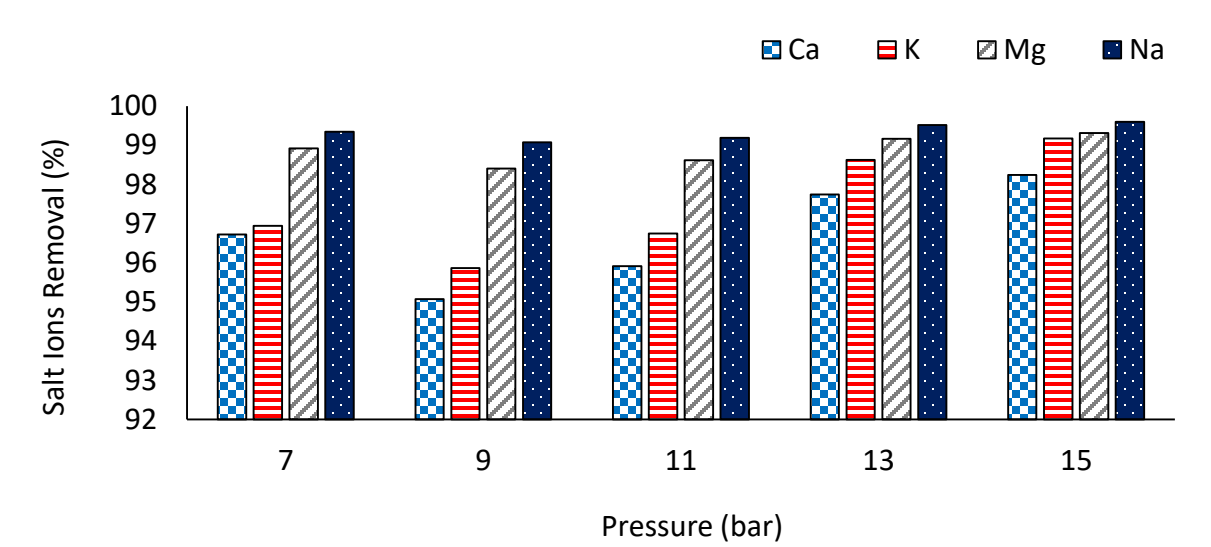

Figure 6-11. The efficiency of zeolite A membrane performance on salt ions removal under different pressures

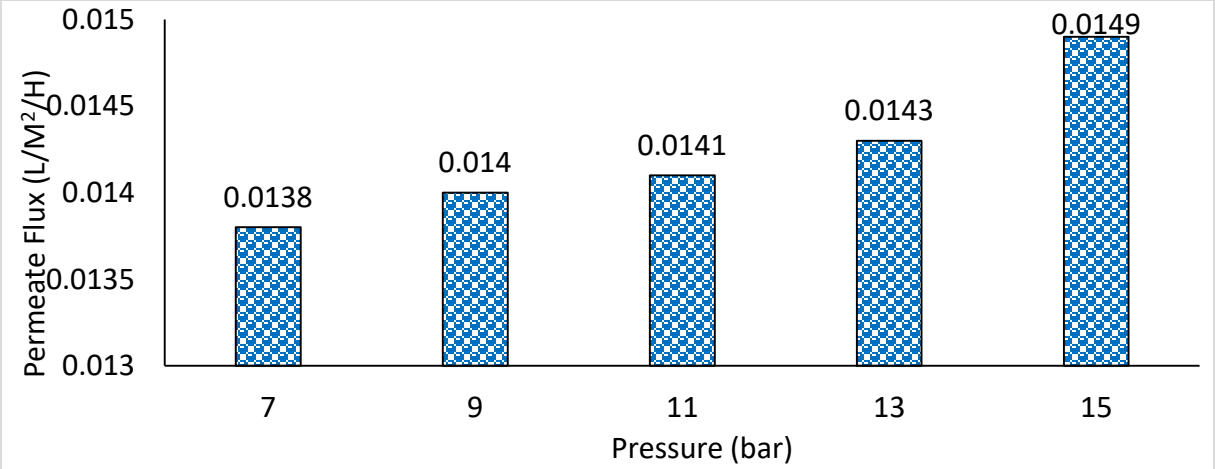

Figure 6-12 Water fluxes at different applied pressure for zeolite A membrane

6.6. Results and Discussion

This section presents the result of the study carried out on the deposition of zeolite film on the surface of the support using South African kaolin as the source of silica and alumina

6.6.1 α-Al_2O_3 Support Characterization better

In this study, the -alumina support is preferred over other supports such as zirconium and stainless steel because it is convenient to deposit zeolite on it and the surface modification aids interaction between the alpha-alumina surface and zeolite crystal growth, nucleation, and film adhesion during membrane formation. The substrate surface modification is important because it promotes the zeolite film formation between the substrate and the zeolite precursor.

The optimum synthesis conditions in chapter four chosen and used for the deposition of the zeolite on the surface the substrate support. The SEM micrograph of the plain and modified alpha-alumina support are shown in Figures 6-1 (a) and 6-1 (b), respectively. The SEM micrograph of both modified and plain support show that both have rough surfaces that are recognized to encourage zeolite growth and nucleation (Lik *et al.*, 2000; Kovo, 2011). Etching of the alpha-alumina support

usually produces a defective surface on the support, which enhances the smooth adhesion between the zeolite and the surface. The XRD pattern of the alpha-alumina support shows that only the quartz phase is present on the surface at 2-theta = 26° (Figure 6-2).

Zeolite A layers with significant XRD peak intensities at 2-theta = 7.16°, 10.15°, 12.40°, 23.95°, and 27.10° were reflected after 20 hours of crystallization at 100℃. The high diffraction peaks of quartz at 2-theta 26.6° show that the quartz impurities dissolved during the hydrothermal synthesis due to its solubility in the gel and this attribute to the attachment on the support used in the development of the zeolite layer. This result reveals that pure zeolite membrane cannot be synthesize from metakaolin with significant quartz impurities. From the figure, it is revealed that zeolite A crystal was developed on the surface of the support with no clear mark of significant flaw or defect.

The cations rejection evaluated from ICP-OES analysis presented in Figures. 6-9 and 6-11, respectively for both zeolites A and ZSM-5 zeolite membrane. The analysis of the results established that the pressure applied ranging from 7 to 15 bar provides high cations rejection. The membrane performance shows a high ions rejection above 99% for Na and Mg and a decent rejection above 95% for Ca and K when the operating pressure was above 11 bar.

The performance and pattern of salt ions desalination using ZSM-5 and zeolite A under different applied pressure presented in figure 6-9 and 6-11 respectively. The pattern shows that the salt ions removal increases as the applied pressure increase from 7 to 15 bars. The water fluxes for ZSM-5 and zeolite A synthesized membrane under different applied pressure are also presented in figure 6-10 and 6-12 respectively. The same trend applied for water fluxes, the flux increases as the applied pressure increase from 7 to 13 bars which show water fluxes of 0.0138, 0.014, 0.0141, 0.0143 L/M^2-H for 7, 9, 11 and 13 bars respectively.

From Figures 6-10 and 6-12, it can be observed that the fluxes were small under an applied pressure range from 7 to 15 bar. It is much smaller than the results reported by Zhu (2014). In their study, they reported that seawater with typical TDS of 35000 mg/l at an operating pressure of 5.5-6.5 MPa achieved water fluxes of 15-17 LMH. In this study, the fluxes obtained is too small for industrial uses, therefore, it was concluding that synthesized zeolite membrane from kaolin using the modified in-situ hydrothermal method are much thicker than the commercial RO membrane (Appendix C) a & b. It has concluded that, membrane resistance to water permeation flux is directly proportional to the thickness of the synthesized membrane. This implies that water permeation on polymeric membrane permeates higher than in zeolite membranes. To reduce the cost of producing water and increase desalination ability with high fluxes, the zeolite membrane need to be improved. Although zeolite membrane thickness attributed as the potential causes of low fluxes, studies have revealed that by altering the hydrophobicity of the membrane, the flux of the zeolite membrane could significantly enhanced.

6.7. Conclusion

The deposition of zeolite membranes on the surface of the alpha-alumina sheet using kaolin as a precursor in the preparation of synthesis gel successfully synthesized using an etched modified in-situ method. XRD and SEM characterization analysis was apply to study the deposition of the zeolite membrane. Two types of zeolite membrane were synthesized specifically ZSM-5 and zeolite A. The two membranes prepared applied for separation performance for desalination of seawater using an RO unit. The results show that the separation performance and the flux obtained presented promising results in term of cations separation performance. The flux for both the zeolite membrane was low compare to the results reported in the literature. This could attributed to the thickness of the membrane synthesized in this research. The synthesized membranes performance

was between 96-99.5% salt ions removal. This study is innovative because kaolin from South Africa was use for the first time as a gel to synthesize zeolites and zeolite membrane for application in water treatment.

CHAPTER SEVEN

7 Techno-economic Analysis of Production of Kaolin-based Zeolite

7.1. Introduction

This report examines the techno-economic viability of the production of ZSM-5 zeolite utilizing the abundance of South African kaolin clay deposits. The kaolin used as an alternative source of silica and alumina to substitute the traditional expensive chemicals used for the production of zeolites. The study of the production of zeolite from kaolin have been reported and still attracting attention because it is inexpensive and offers better revenue in the synthesis of zeolite compares to the application of synthetic chemicals as a source of silica and alumina. The option of synthesizing different categories of zeolite from kaolin has been reported (Lijalem, 2016; Bortolatto *et al.*, 2017). The Physico-chemical characterization of kaolin is symptomatic parameters for its usage as a raw material for the production of zeolite, which fundamentally contains aluminosilicate tetrahedral units. The synthesis of zeolite from kaolin has profitable implications as ZSM-5 offers a profitable and environmentally safe substitute for synthetic chemicals. The production of ZSM-5 technology has an emphasis on the recovery of high value-added materials, thus, offering an edge over other chemical utilization technologies in vogue. This report addresses the application of local contents in commercial production of ZSM-5 as an alternative source of raw materials.

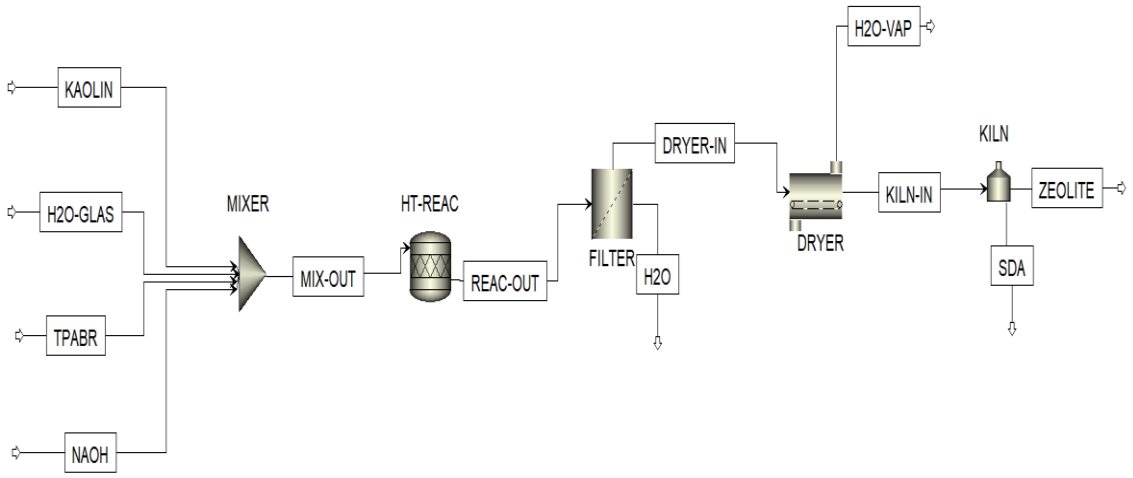

Figure 7-1 Process flow sheet diagram of zeolite synthesis

7.2. Materials and Methods

7.2.1. Economic analysis

The techno-economic feasibility study of ZSM-5 zeolite synthesis derived from kaolin was calculated by an itemized cost estimate method (Biniwale, Rayalu and Hasan, 2000), method of itemized estimation cost was adopted to evaluate the techno-economic analysis for the study of the production of zeolite from a local source of silica and alumina. The process flow diagram is presented in figure. 7.1.

7.2.2. Cost estimation

Itemized cost estimation is the total capital cost and other operating expenses. The fixed capital cost obtained in this study is the total expenses of the equipment cost. was adopted. The chemical engineering plant cost index (CEPCI) concept was applied for the calculation of equipment expenses to consider the current cost data using the following equation

$$C_2 = C_1 * (\frac{CEPCI2}{CEPCI1} \quad (7\text{-}1)$$

Where C_1 is the cost of equipment in a reference year. The CEPCI evaluation for 2001 is 394.3 and that of 2019 is 607.5, therefore, the present fixed capital investment (FCI) is US$ 3.417 x10^5.

The capital cost of the project is related to capacity by the equation

$$C_2 = C_1 * \{\frac{S2}{S1}\}n \quad (7\text{-}2)$$

Where C_2 = capital cost of the project with capacity S_2, C_1 = capital cost of the project with capacity S_1. C_1 = cost of the zeolite US$546800.4 from reference plant while S_1 is 2250 ton/year and S_2 is 500 ton/year and n was taken as 0.6.

The annual total production cost is given as the sum of the annual capital cost and annual operating cost. Then, the ratio of the annual total cost to the annual zeolite production is given as the unit zeolite production cost (equation 7-3).

$$Unit\ zeolite\ production\ cost\ (\$/kg) = \frac{Annual\ total\ costs\ (\$/yr)}{zeolite\ production\ capacity\ (kg/yr)} \quad (7\text{-}3)$$

7.3. Results and Discussion

7.3.1. Economic consideration of kaolin-based ZSM-5 zeolite production

The techno-economic analysis of ZSM-5 zeolite from kaolin was performed for a 500 ton/year production capacity. The material balance of the production process was initially carried out using data obtained from the experimental process. The crystallization of the raw material (Kaolin, water glass, tetra propyl aluminium bromide, sodium hydroxide, and water) was achieved using hydrothermal reactor under the following experimental conditions: crystallization time 48 h, temperature of crystallization 180℃, and ageing time 24 h. Detailed material balance calculation and economic analysis is presented in the appendix section. From the material balance results to achieve the production capacity of 500 ton/year, the required amount of kaolin, water glass, TPABr,

NaOH and water are 20.546 ton/year, 459.194 ton/year, 24.467 ton/year. 9.078 ton/year and 1653.981 ton/year, respectively.

Table 7-1 Estimate of total capital investment cost

Item	Cost (US$)
Direct Cost	
Purchased equipment cost	136,672
Installation cost	61,503
Instrument and control installed	41,002
Piping installation cost	109,338
Electrical installation cost	54,669
The building process and auxiliary	95,671
Service facilities	95,671
Yard improvement	20,501
Land	9,567
Total Direct Cost	624,593
Indirect Cost	
Engineering and supervision	187,378
Construction expenses	187,378
Contractors fee	31,230
Contingency	124,919
Total Indirect Cost	530,904
Fixed Capital Investment	1,155,497
Working Capital Investment	173,325
Total Capital Investment	1,328,821

7.3.2. Cost Estimation

The capital cost investment and operating cost investment of the proposed ZSM-5 zeolite production process using kaolin was derived under direct and indirect costs similar to the reference production plant. The process calculation was designed for 500 ton/year production capacity ZSM-5 zeolite. The total direct cost of the equipment is $ 624,593 which is relatively higher than the indirect cost of $ 530, 904. The fixed capital cost which comprises of direct and indirect cost is $ 1,155,497 and the working capital which is 15% of the fixed capital cost is 173,325. This gives the total investment cost of $ 1,328,821. The details are presented in table 7-2. The total production cost includes total fixed charges (TFC), total product cost (TPC), plant overhead cost (POC) (operating labour, maintenance and operating supplies) and manufacturing cost (TFC+TPC +POC) are US$ 263,453, US$ 1,317,266, US$ 277,435 and US$ 1,858,154, respectively. The manufacturing cost (TFC+TPC+POC), general expenses and total production cost (MC+GE) were estimated as US$ 1,858,154, US$619,115 and US$ 2,477,270 respectively and the detailed calculation is presented in appendix.

Table 7-2: Estimate of total production cost

Item	Cost (US$)
Depreciation	115,550
Local taxes	34,665
Insurances	9,244
Rent	103,995
Total Fixed Charges	263,453
Total Product Cost	1,317,266
Raw material	658,633
Operating labour	263,453
Utilities	263,453
Maintenance	115,550
Operating supplies	17,332
Plant overhead cost (OL+M+OS)	277,435
Manufacturing cost (TFC+TPC +POC)	1,858,154
Administration cost	158,072
Distribution cost	395,180
Research and development cost	65,863
General Expenses	619,115
Total production cost (MC+GE)	2,477,270

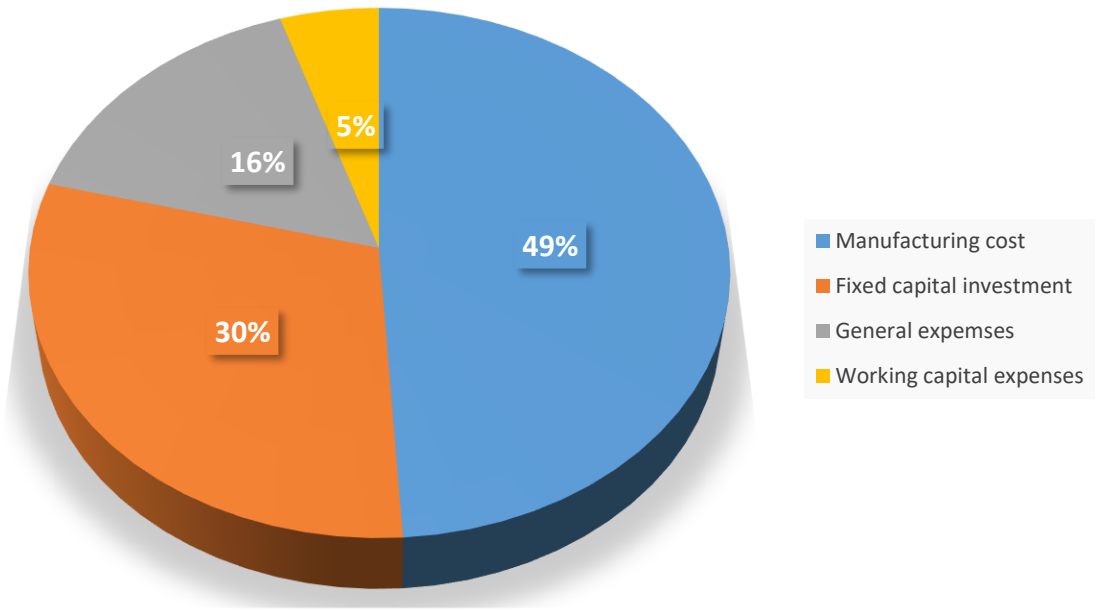

Figure 7-2 Summary of production cost of kaolin-based ZSM-5 zeolite

Table 7-3 Profitability analysis

Summary of Profitability Analysis	
Plant operational year	330 days
Production Capacity	500 tons/yr.
Total production cost	$ 2,477,270
Unit production cost	$ 4.96 /kg
Total Revenue	$ 75,000,000
Gross Income	$ 72,522,730
Taxes	$ 29,009,092
Net Profit	$ 43,513,638
Rate of Return	32.75%
Payback period	3.05 yr.
Break-even production rate	17 tons/yr. (3.5% of production capacity)

7.3.3. The profitability analysis

The profit analysis performed to calculate the techno-economic feasibility of the proposed ZSM-5 zeolite production process. The feasibility study evaluated using economic performance indicators such as payback period, net profit after tax and break-even production rate as presented in table 7-3. In this feasibility study, a 500 ton/year ZSM-5 zeolite production process from kaolin was proposed. The total yearly selling revenue of $75,000,000.00 /year was obtained from the production of 500 ton/year of ZSM-5 zeolite with a selling price of $4.96 $/kg. The gross income from the ZSM-5 zeolite production process evaluated by the difference between the total yearly

selling revenue and the total zeolite production cost. The net profit obtained as the gross income minus tax (40% of gross income). However, the payback period was use to evaluate the economic and financial feasibility of the ZSM-5 zeolite process as presented in table 7-3. The payback period of 3.05 year and the rate of return on investment of 32.75% was established. To improve the profitability of the process, tax exemption could increase the pability of ZSM-5 from the kaolin production process.

7.4. Conclusion

- The plant is economically viable with a payback period of less 4 years

CHAPTER EIGHT

8 General Conclusion

Zeolite A was synthesize from South African Kaolin at an optimum crystallization temperature of 100°C, an ageing time of 12 hours, and a crystallization time of 20 hours. The Si/Al ratio is 1.3, and the BET surface area is 143.88 m^2/g. ZSM-5 zeolite was synthesized from South African Kaolin at an optimum crystallization temperature of 180°C and an ageing time of 24 hours as well as a crystallization time of 48 hours, BET surface area 282m^2/g, Si/Al ratio 43. The synthesis of crystalline zeolite, A, and ZSM-5 zeolite in this work is affected by crystallization temperature, ageing time, and crystallization time. It is concluding that gel ageing influences the relative crystallinity of the zeolite synthesized. However, a mathematical relationship was establish between synthesis parameters and properties of Zeolite A and ZSM-5.

This study is groundbreaking because it is the first time that kaolin from South Africa was use as a gel to synthesize zeolites and zeolite membranes to treat water. Zeolite A performed well in the adsorption of salt ions from synthetic seawater, whereas ZSM-5 zeolite leached due to the abundance of the elements in the zeolite's framework. Desalination with ZSM-5 was unsuccessful.

Using an etched modified in-situ crystallization method, zeolite A and ZSM-5 zeolite were successfully deposited on the surface of the -alumina substrate. Zeolite A and ZSM-5 zeolite successfully deposited on the surface of the α-alumina substrate using etched modified in-situ crystallization method. The synthesized membranes performance was between 96-99.5% salt ions removal. The flux for all the zeolite membranes samples was low compared to reported values in the literature mainly because of the high thickness of the membrane prepared in this work.

Techno-economic analysis conducted with the plant capacity of 500 tons/year and from the analysis, it was proven that the plant is economically viable with a payback period of less 4 years.

8.1 Recommendations

The experiments presented in this thesis have shown that synthetic zeolite have the potential for use in treating seawater. Although, the initial objectives were achieve in this study, some other aspects were not within the scope of this study due to the limitations of time and availability of equipment. Therefore, further research and studies needed, taking into account that modern industrial technologies require the use of zeolitic materials and sorbents with very precisely specified parameters. There are several areas of research, which could give better perspectives in terms of possible applications. Some recommendations for further studies itemize and presented below:

- Although zeolite A and ZSM-5 were successfully synthesized from kaolinite, the method of manufacturing synthetic zeolite should consider a wide variety of experimental parameters and conditions, such as the effect of alkalinity (NaOH), the effect of gel temperature and the gel forming state and, the solid/solution ratio, all of which may influence the final product.
- The adsorbent density, agitation intensity, as well as contact time of the adsorbent in the case of batch experiments analyzed as part of the kinetic analysis, while the effect of temperature on salt ions removal potential and column study was not included. However, for large-scale use, the exact influence of both of these considerations must be consider in future work.
- This research just looked at cation removal and did not look into the impact of anions on the potential and effectiveness of synthetic zeolites from kaolin. More research should be

done to see whether zeolite could extract anions from solution and how anions influences the seawater ions uptake capability and quality of synthetic zeolite in handling industrial wastewaters.

References

Aarts, A., Berends, A., Boeije, G., Calcinai, D., Cerbelaud, E., Certa, H., Egmond, R. van, Elsmore, R., Fox, K., Koch, V., Lopez, I., Masscheleyn, P., Richner, R., Schul, W., Steber, J., Stevens, C., Toy, R. and Wijk, W. van (2004) 'Zeolite A', *Human & Environmental Risk Assessment (HERA) on ingredients of European housedold cleaning product*, 9(1344): p53.

Abu-Zeid, M. A. E. R., Zhang, Y., Dong, H., Zhang, L., Chen, H. L. and Hou, L. (2015) 'A comprehensive review of vacuum membrane distillation technique', *Desalination*, 356: 1–14.

Adeoye, J. B., Omoleye, J. A., Ojewumi, M. E. and Babalola, R. (2017) 'of Zeolite Y from Kaolin Using Novel Method of Dealumination', 12(5): 755–760.

Akther, N., Sodiq, A., Giwa, A., Daer, S., Arafat, H. A. and Hasan, S. W. (2015) 'Recent advancements in forward osmosis desalination: A review', *Chemical Engineering Journal*, 281: 502–522.

Al-Ansari, A., Ettouney, H. and El-Dessouky, H. (2001) 'Water-zeolite adsorption heat pump combined with single effect evaporation desalination process', *Renewable Energy*, 24(1): 91–111.

Aliyu, U. M.; Rathilal, S.; Isa, Y. M. (2018) 'Membrane desalination technologies in water treatment : A review', *IWA Publishing 2018*, 13(4): 738–752.

Aliyu, A., Abdulkareem, A., Kovo, A., Abubakre, O., Tijani, J. and Kariim, I. (2017) 'Synthesize multi-walled carbon nanotubes via catalytic chemical vapour deposition method on Fe-Ni bimetallic catalyst supported on kaolin', *Carbon letters*, 21: 33–50.

Alkhudhiri, A., Darwish, N. and Hilal, N. (2012) 'Membrane distillation: A comprehensive review', *Desalination*, 287: 2–18.

Antony, A., Branch, A., Leslie, G. and Le-Clech, P. (2016) ‘Impact of membrane ageing on reverse osmosis performance Implications on validation protocol’, *Journal of Membrane Science*, 520: 37–44.

Áurea, A., Maia, B., Neves, R. F., Angélica, R. S. and Pöllmann, H. (2015) ‘Applied Clay Science Synthesis , optimisation and characterisation of the zeolite NaA using kaolin waste from the Amazon Region . Production of Zeolites KA , MgA and CaA’, *Applied Clay Science*, 108: 55–60.

Ayele, L., Pérez-Pariente, J., Chebude, Y. and Díaz, I. (2015) ‘Synthesis of zeolite A from Ethiopian kaolin’, *Microporous and Mesoporous Materials*, 215: 29–36.

Ayele, L., Pérez-Pariente, J., Chebude, Y. and Díaz, I. (2016) ‘Conventional versus alkali fusion synthesis of zeolite A from low grade kaolin’, *Applied Clay Science*, 132–133: 485–490.

B. Jha and D.N. Singh (2016) ‘Basics of Zeolites’, *Springer Science+Business Media Singapore*.

Babalola, R., Omoleye, J. A., Plaza, Z. M. and Bello, A. (2015) ‘Comparative Analysis of Zeolite Y From Nigerian Clay and Standard Grade’, : 179–182.

Baker., R. (2012) ‘Membranes and Modules’, *Membrane Technology and Applications*, : 97–178.

Bedard, R. L. (2010) ‘Synthesis of Zeolites and Manufacture of Zeolitic Catalysts and Adsorbents’, *Zeolites in Industrial Separation and Catalysis*, : 61–83.

Belviso, C., Cavalcante, F., Lettino, A. and Fiore, S. (2013) ‘Applied Clay Science A and X-type

zeolites synthesised from kaolinite at low temperature', *Applied Clay Science*, 80–81: 162–168.

Biniwale, R., Rayalu, S. and Hasan, M. Z. (2000) 'Cost Estimates for Production of Flyash Based Zeolllte -A', 60: 574–579.

Bortolatto, L. B., Boca Santa, R. A. A., Moreira, J. C., Machado, D. B., Martins, M. A. P. M., Fiori, M. A., Kuhnen, N. C. and Riella, H. G. (2017) 'Synthesis and characterization of Y zeolites from alternative silicon and aluminium sources', *Microporous and Mesoporous Materials*, 248: 214–221.

Burn, S., Hoang, M., Zarzo, D., Olewniak, F., Campos, E., Bolto, B. and Barron, O. (2015) 'Desalination techniques - A review of the opportunities for desalination in agriculture', *Desalination*, 364: 2–16.

Busch, M., Chu, R. and Rosenberg, S. (2010) 'Novel Trends in Dual Membrane Systems for Seawater Desalination: Minimum Primary Pretreatment and Low Environmental Impact Treatment Schemes', *IDA Journal of Desalination and Water Reuse*, 2(1): 56–71.

Bush, J. A., Vanneste, J. and Cath, T. Y. (2016) 'Membrane distillation for concentration of hypersaline brines from the Great Salt Lake : Effects of scaling and fouling on performance , efficiency , and salt rejection', *Separation and Purification Technology*.

Cath, T. Y., Childress, A. E. and Elimelech, M. (2006) 'Forward osmosis: Principles, applications, and recent developments', *Journal of Membrane Science*, 281(1–2): 70–87.

Chareonpanich, M., Namto, T., Kongkachuichay, P. and Limtrakul, J. (2004) 'Synthesis of ZSM-5 zeolite from lignite fly ash and rice husk ash', *Fuel Processing Technology*, 85(15): 1623–

1634.

Chekli, L., Phuntsho, S., Kim, J. E., Kim, J., Choi, J. S., Kim, S., Kim, J. H., Hong, S. and Shon, H. K. (2015) ‘A comprehensive review of hybrid forward osmosis systems: performance, applications and future prospects’, *Journal of Membrane Science*.

Chollom, M. N., Rathilal, S., Pillay, V. L. and Alfa, D. (2015) ‘The applicability of nanofiltration for the treatment and reuse of textile reactive dye effluent’, *Water SA*, 41(3): 398–405.

Colella, C. (2012) ‘The Fascinating Story of Porous Materials’, : 126–135.

Czarnecki, J. and Šesták, J. (2000) ‘PRACTICAL THERMOGRAVIMETRY’, 60: 759–778.

Demirbas, A. (2008) ‘Heavy metal adsorption onto agro-based waste materials: A review’, *Journal of Hazardous Materials*, 157(2–3): 220–229.

Elboughdiri, N. (2020) ‘The use of natural zeolite to remove heavy metals Cu (II), Pb (II) and Cd (II), from industrial wastewater’, *Cogent Engineering*, 7(1).

Flanigen, E. M., Broach, R. W. and Wilson, S. T. (2010) ‘Zeolites in Industrial Separations and Catalysis’, *Zeolites in Industrial Separation and Catalysis*, : 1–26.

Goh, P. S., Matsuura, T., Ismail, A. F. and Hilal, N. (2016) ‘Recent trends in membranes and membrane processes for desalination’, *Desalination*, 391: 43–60.

Gougazeh, M. and Buhl, J. C. (2014) ‘Synthesis and characterization of zeolite A by hydrothermal transformation of natural Jordanian kaolin’, *Journal of the Association of Arab Universities for Basic and Applied Sciences*, 15(1): 35–42.

Granizo M. L., M. T. Blanco-Varela, A. P. (2000) ‘Influence of the starting kaolin on alkali-activated materials based on metakaolin . Study of the reaction parameters by isothermal conduction calorimetry’, 5: 6309–6315.

Greenlee, L. F., Lawler, D. F., Freeman, B. D., Marrot, B. and Moulin, P. (2009) ‘Reverse osmosis desalination: Water sources, technology, and today’s challenges’, *Water Research*, 43(9): 2317–2348.

Greń, W., Parker, S. C., Slater, B. and Lewis, D. W. (2010) ‘Structure of zeolite A (LTA) surfaces and the zeolite A/water interface’, *Journal of Physical Chemistry C*, 114(21): 9739–9747.

Hameed, B. H., Din, A. T. M. and Ahmad, A. L. (2007) ‘Adsorption of methylene blue onto bamboo-based activated carbon: Kinetics and equilibrium studies’, *Journal of Hazardous Materials*, 141(3): 819–825.

Hartanto, D., Sin, L., Mutia, S., Sugiarso, D., Kris, I., Ersam, T., Prasetyoko, D. and Nur, H. (2016) ‘Can kaolin function as source of alumina in the synthesis of ZSM-5 without an organic template using a seeding technique ?’, 12(2): 85–90.

Holmes, S. M., Alomair, A. A. and Kovo, A. S. (2012) ‘The direct synthesis of pure zeolite-A using “virgin” Kaolin’, *RSC Advances*, 2(30): 11491.

Iwakai, K., Tago, T., Konno, H., Nakasaka, Y. and Masuda, T. (2011) ‘Preparation of nano-crystalline MFI zeolite via hydrothermal synthesis in water/surfactant/organic solvent using fumed silica as the Si source’, *Microporous and Mesoporous Materials*, 141(1–3): 167–174.

Jacob, R. E., Mitha, V. R. and Macpherson, D. (2004) ‘The kaolinitic clay deposits on Beaconsfield , north of Grahamstown’, : 1–5.

Jiang, S., Li, Y. and Ladewig, B. P. (2017) ‘A review of reverse osmosis membrane fouling and control strategies’, *Science of The Total Environment*, 595: 567–583.

Kahraman, S. (2005) ‘Characterization of silica polymorphs in kaolins by X-ray diffraction before and after phosphoric acid digestion and thermal treatment us’, 552: 201–206.

Kaplan, R., Mamrosh, D., Salih, H. and Dastgheib, S. A. (2017) ‘Assessment of desalination technologies for treatment of a highly saline brine from a potential CO 2 storage site’, 404: 87–101.

Khawaji, A. D., Kutubkhanah, I. K. and Wie, J. M. (2008) ‘Advances in seawater desalination technologies’, *Desalination*, 221(1–3): 47–69.

Kiricsi, A. (1999) ‘POROUS MATERIALS IN ENVIRONMENTALLY FRIENDLY PROCESSES’.

Kovo, A. S. and Holmes, S. M. (2010) ‘Effect of aging on the synthesis of kaolin-based zeolite Y from Ahoko Nigeria using a novel metakaolinization technique’, *Journal of Dispersion Science and Technology*, 31(4): 442–448.

Kovo, S. A. (2011) ‘Development of zeolites and zeolite membranes from Ahoko Nigerian Kaolin’, *Doctoral thesis. The University of Manchester, England*.

Lawson, K. W. and Lloyd, D. R. (1997) ‘Membrane distillation’, *Journal of Membrane Science*, 124(1): 1–25.

Lee, K. L., Baker, R. W. and Lonsdale, H. K. (1981) ‘Membranes for power generation by pressure-retarded osmosis’, *Journal of Membrane Science*, 8(2): 141–171.

Lee, N. H. (2008) ‘Water Treatment by Microfiltration and Ultrafiltration’.

Lijalem Ayele Regassa (2016) ‘Synthesis and Characterization of Zeolite A from Kaolin of Ethiopia : Studies of its application as detergent builder and in tannery wastewater treatment Lijalem Ayele Regassa A Thesis Submitted to Department of Chemistry Presented in Fulfillment of the R’.

Lik, J., Chau, H., Tellez, C., Lun, K. and Ho, K. (2000) ‘The role of surface chemistry in zeolite membrane formation’, 164: 257–275.

Ltaief, O. O., Siffert, S., Fourmentin, S. and Benzina, M. (2015) ‘Synthesis of Faujasite type zeolite from low grade Tunisian clay for the removal of heavy metals from aqueous waste by batch process: Kinetic and equilibrium study’, *Comptes Rendus Chimie*, 18(10): 1123–1133.

Maab, H., Al Saadi, A., Francis, L., Livazovic, S., Ghafour, N., Amy, G. L. and Nunes, S. P. (2013) ‘Polyazole Hollow Fiber Membranes for Direct Contact Membrane Distillation’, *Industrial & Engineering Chemistry Research*, 52(31): 10425–10429.

Majeed, T., Phuntsho, S., Jeong, S., Zhao, Y., Gao, B. and Shon, H. K. (2016) 'Understanding the risk of scaling and fouling in hollow fiber forward osmosis membrane application', *Process Safety and Environmental Protection*, 104: 452–464.

Makarfi, Y. I., Yakimova, M. S., Lermontov, A. S., Erofeev, V. I., Koval, L. M. and Tretiyakov, V. F. (2009) 'Conversion of bioethanol over zeolites', *Chemical Engineering Journal*, 154(1–3): 396–400.

Mayere, A. (2011) 'Solar powered desalination . PhD thesis , University of Nottingham .', *Book*, 1(1).

Micromeritics (2007) *TriStar 3000 Manual*.

Mineralogy, C. (1976) 'Clay Mineralogy and Geology of Minnesota's Kaolin Clays'.

Mohiuddin, E., Isa, Y. M., Mdleleni, M. M., Sincadu, N., Key, D. and Tshabalala, T. (2016) 'Synthesis of ZSM-5 from impure and beneficiated Grahamstown kaolin: Effect of kaolinite content, crystallisation temperatures and time', *Applied Clay Science*, 119(November): 213–221.

Morsy, F. A., El-Sherbiny, S., Hassan, M. S. and Mohammed, H. F. (2014) 'Modification and evaluation of Egyptian kaolinite as pigment for paper coating', *Powder Technology*, 264: 430–438.

Mota, C. J. A. and Rosenbach, N. (2011) 'Carbocations on zeolites. Quo vadis?', *Journal of the Brazilian Chemical Society*, : 1197–1205.

Nair, M. and Kumar, D. (2013) ‘Water desalination and challenges: The Middle East perspective: A review’, *Desalination and Water Treatment*, 51(10–12): 2030–2040.

Noghabi, M. S., Razavi, S. M. A., Mousavi, S. M., Elahi, M. and Niazmand, R. (2011) ‘Effect of operating parameters on performance of nanofiltration of sugar beet press water’, *Procedia Food Science*, 1: 160–164.

Parnham, E. R. and Morris, R. E. (2007) ‘Ionothermal Synthesis of Zeolites , Metal – Organic Frameworks , and Inorganic – Organic Hybrids’, *Acc. Chem. Res.*, 40(10): 1005–1013.

Pereira, P. M., Ferreira, B. F., Oliveira, N. P., Nassar, E. J., Ciuffi, K. J., Vicente, M. A., Trujillano, R., Rives, V., Gil, A., Korili, S. and de Faria, E. H. (2018) ‘Synthesis of zeolite A from metakaolin and its application in the adsorption of cationic dyes’, *Applied Sciences (Switzerland)*, 8(4).

Pérez-González, A., Urtiaga, A. M., Ibáñez, R. and Ortiz, I. (2012) ‘State of the art and review on the treatment technologies of water reverse osmosis concentrates’, *Water Research*, 46(2): 267–283.

Petrov, I. and Michalev, T. (2012) ‘Synthesis of Zeolite A : A Review’, (2): 30–35.

Publishers, K. A. (2000) ‘Influence of the starting kaolin on alkali-activated materials based on metakaolin . Study of the reaction parameters by isothermal conduction calorimetry’, 5: 6309–6315.

Radetié, T. (2011) ‘Fundamentals of Scanning Electron Microscopy and Energy Dispersive X-ray Analysis in SEM and TEM’, (April): 1–26. Available at:

http://www.nanotechftm.tmf.bg.ac.rs/images/stories/dokumenti/lecture_book_em_school/tamara radetic.pdf.

Riittonen, T., Toukoniitty, E., Madnani, D. K., Leino, A. and Mikkola, J. (2012) 'One-Pot Liquid-Phase Catalytic Conversion of Ethanol to 1-Butanol over Aluminium Oxide—The Effect of the Active Metal on the Selectivity', (13): 68–84.

Sahebi, S., Phuntsho, S., Kim, J. E., Hong, S. and Shon, H. K. (2015) 'Author ' s Accepted Manuscript', *Journal of Membrane Science*.

Saikia, N. J., Bharali, D. J., Sengupta, P., Bordoloi, D., Goswamee, R. L., Saikia, P. C. and Borthakur, P. C. (2003) 'Characterization, beneficiation and utilization of a kaolinite clay from Assam, India', *Applied Clay Science*, 24(1–2): 93–103.

Salih, A. M. and Salih, A. M. (2017) 'Doctoral Thesis The purification of industrial wastewater to remove heavy metals and investigation into the use of zeolite as a remediation tool'.

Salou, M., Kooli, F., Kiyozumi, Y. and Mikamizu, F. (2001) 'Effect of aluminium source and content on the synthesis of zeolite ZSM-5 from kanemite solid-state transformation', *Journal of Materials Chemistry*, 11(5): 1476–1481.

Sánchez, a. G. and García-Sánchez, A. (2011) *Computational Study of Adsorption and Diffusion in Zeolites with Cations*, *Upo.Es*. Available at: http://www.upo.es/raspa/media/archives/Thesis_AlmudenaGarcia_13Jan2012.pdf

.

Sari, M. A. and Chellam, S. (2016) 'Reverse osmosis fouling during pilot-scale municipal water reuse: Evidence for aluminum coagulant carryover', *Journal of Membrane Science*, 520: 231–

239.

Shabani, J. M. (2016) ‘Synthesis of clay-based catalysts for bioethanol conversion Masters of Engineering : Chemical Engineering’, (September).

Shannon, M. A., Bohn, P. W., Elimelech, M., Georgiadis, J. G., Marinas, B. J. and Mayes, A. M. (2008) ‘Science and technology for water purification in the coming decades’, *Nature (London, U. K.)*, 452(March): 301–310.

Sirkar, K. K. and Qin, Y. (2001) ‘Novel Membrane and Device for Direct Contact Membrane Distillation Based Desalination Process’, : 5300–5309.

Sun, C., Xie, L., Li, X., Sun, L. and Dai, H. (2015) ‘Study on different ultrafiltration-based hybrid pretreatment systems for reverse osmosis desalination’, *Desalination*, 371: 18–25.

Swenson, P., Tanchuk, B., Gupta, A., An, W. and Kuznicki, S. M. (2012) ‘Pervaporative desalination of water using natural zeolite membranes’, *DES*, 285: 68–72.

Tang, Q., He, Y., Wang, Y. pin, Wang, K. tuo and Cui, X. min (2016) ‘Study on synthesis and characterization of ZSM-20 zeolites from metakaolin-based geopolymers’, *Applied Clay Science*, 129: 102–107.

Tijing, L. D., Woo, Y. C., Choi, J. S., Lee, S., Kim, S. H. and Shon, H. K. (2015) ‘Fouling and its control in membrane distillation-A review’, *Journal of Membrane Science*, 475: 215–244.

Von-kiti, E. (2012) *SYNTHESIS OF ZEOLITES AND THEIR APPLICATION TO THE,*

Msc.thesis Knust.

Von-kiti, E. (2016) *AND KAOLIN : APPLICATION TO THE REMOVAL OF HEAVY METALS*. Knust.

Voutchkov, N. (2010) 'Considerations for selection of seawater filtration pretreatment system', *Desalination*, 261(3): 354–364.

Wang, P. and Chung, T. S. (2015) 'Recent advances in membrane distillation processes: Membrane development, configuration design and application exploring', *Journal of Membrane Science*, 474: 39–56.

Wang, W., Zhang, Y., Esparra-Alvarado, M., Wang, X., Yang, H. and Xie, Y. (2014) 'Effects of pH and temperature on forward osmosis membrane flux using rainwater as the makeup for cooling water dilution', *Desalination*, 351: 70–76.

Wang, Wendong, Feng, P., Yang, Q., Wang, Wen and Wang, X. (2016) 'Effects of sodium, magnesium, and calcium salts on the coagulation performance of cucurbit [8]uril for humic acid removal from synthetic seawater', *Desalination*, 386(13): 77–83.

Wenten, I. G. and Khoiruddin (2016) 'Reverse osmosis applications: Prospect and challenges', *Desalination*, 391: 112–125.

Wibowo, E., Sutisna, Rokhmat, M., Murniati, R., Khairurrijal and Abdullah, M. (2017) 'Utilization of Natural Zeolite as Sorbent Material for Seawater Desalination', *Procedia Engineering*, 170: 8–13.

Worch, P. D. E., Technology, D. U. of, Chemistry, I. of W., Dresden, 01062 and Germany (2012) *Adsorption Technology in Water Treatment*. first edit. Germany: Hubert & Co. GmbH & Co. KG, Go ¨ttingen.

Zegeye, A., Yahaya, S., Fialips, C. I., White, M. L., Gray, N. D. and Manning, D. A. C. (2013) 'Refinement of industrial kaolin by microbial removal of iron-bearing impurities', *Applied Clay Science*, 86: 47–53.

Zhao, L., Chang, P. C. Y. and Ho, W. S. W. (2013) 'High-flux reverse osmosis membranes incorporated with hydrophilic additives for brackish water desalination', *Desalination*, 308: 225–232.

Zhao, L. and Ho, W. S. W. (2014) 'Novel reverse osmosis membranes incorporated with a hydrophilic additive for seawater desalination', *Journal of Membrane Science*, 455: 44–54.

Zhu, B., Doherty, C. M., Hu, X., Hill, A. J., Zou, L., Lin, Y. S. and Duke, M. (2013) 'Designing hierarchical porous features of ZSM-5 zeolites via Si/Al ratio and their dynamic behavior in seawater ion complexes', *Microporous and Mesoporous Materials*, 173: 78–85.

Zhu, B., Hong, Z., Milne, N., Doherty, C. M., Zou, L., Lin, Y. S., Hill, A. J., Gu, X. and Duke, M. (2014) 'Desalination of seawater ion complexes by MFI-type zeolite membranes : Temperature and long term stability', *Journal of Membrane Science*, 453: 126–135.

Zhu, Y., Gupta, K. M., Liu, Q., Jiang, J., Caro, J. and Huang, A. (2016) 'Synthesis and seawater desalination of molecular sieving zeolitic imidazolate framework membranes', *Desalination*, 385: 75–82.

Appendices

Appendix A

Table A-1: Optimized experimental conditions for ZSM-5 zeolite synthesized zeolite from G&W kaolin

S/NO	Experimental run	Crystallization temperature (°C)	Crystallization time (Hour)	Ageing time (Hour)
1.	R1	120	24	0
2.	R2	120	48	0
3.	R3	120	96	0
4.	R4	150	24	0
5.	R5	150	48	0
6.	R6	150	96	0
7.	R7	180	24	0
8.	R8	180	48	0
9.	R9	180	96	0
10.	R10	120	24	24
11.	R11	120	48	24
12	R12	120	96	24
13	R13	150	24	24
14	R14	150	48	24
15	R15	150	96	24
16	R16	180	24	24
17	R17	180	48	24
18	R18	180	96	24
19	R19	120	24	48
20	R20	120	48	48
21	R21	120	96	48
22	R22	150	24	48
23	R23	150	48	48
24	R24	150	96	48
25	R25	180	24	48
26	R26	180	48	48

27	R27	180	96	48

Table A-2: Optimized experimental conditions for zeolite A synthesized zeolite from G&W kaolin

S/NO	Experimental run	Crystallization temperature (°C)	Crystallization time (Hour)	Ageing time (Hour)
1.	A1	80	20	0
2.	A2	80	20	24
3.	A3	90	20	0
4.	A4	90	20	24
5.	A5	100	20	0
6.	A6	100	20	3
7.	A7	100	20	6
8.	A8	100	20	12

Appendix B

Table B - 3 : Material Balance around the Mixer (Unit 1)

	INPUT STREAMS	OUTPUT STREAMS
Components	Stream 1 (tonne/yr)	Stream 2 (tonne/yr)
Kaolin	20.546	20.546
Water glass	469.194	469.194
TPABR	24.467	24.467
NaOH	9.078	9.078
Water	1653.981	1653.981
	Total Input Stream 1 (tonne/yr)	Total Output Stream 2 (tonne/yr)
Overall Total	2177.265	2177.265

Table B-4: Material Balance around the Reactor (Unit 2)

	INPUT STREAMS	OUTPUT STREAMS
Components	Stream 2 (tonne/yr)	Stream 3 (tonne/yr)
Kaolin	20.546	0.00
Water glass	469.194	0.00
TPABR	24.467	0.00
NaOH	9.078	0.00
Water	1653.981	1653.981
Zeolite	0.00	523.284
	Total Input Stream 2 (tonne/yr)	Total Output Stream 3 (tonne/yr)
Overall Total	2177.265	2177.265

Table B-5: Material Balance around the Filtration (Unit 3)

	INPUT STREAMS	OUTPUT STREAMS	
Components	Stream 3 (tonne/yr)	Stream 4 (tonne/yr)	Stream 5 (tonne/yr)
Kaolin	0.00	0.00	0.00
Water glass	0.00	0.00	0.00
TPABR	0.00	0.00	0.00
NaOH	0.00	0.00	0.00
Water	1653.981	1604.362	49.619
Zeolite	523.284	15.699	507.586
	Total Input Stream 3 (tonne/yr)	Total Output Stream 4 + Stream 5 (tonne/yr)	
Overall Total	2177.265	2177.265	

Table B-6: Material Balance around the Dryer (Unit 4)

Components	INPUT STREAMS Stream 5 (tonne/yr)	OUTPUT STREAMS Stream 6 (tonne/yr)	 Stream 7 (tonne/yr)
Kaolin	0.00	0.00	0.00
Water glass	0.00	0.00	0.00
TPABR	0.00	0.00	0.00
NaOH	0.00	0.00	0.00
Water	49.619	49.123	0.496
Zeolite	507.586	5.076	502.51
	Total Input Stream 5 (tonne/yr)	Total Output Stream 6 + Stream 7 (tonne/yr)	
Overall Total	557.205	557.205	

Table B-7: Material Balance around the Kiln (Unit 5)

	INPUT STREAMS	OUTPUT STREAMS	
Components	Stream 7 (tonne/yr)	Stream 8 (tonne/yr)	Stream 9 (tonne/yr)
Kaolin	0.00	0.00	0.00
Water glass	0.00	0.00	0.00
TPABR	0.00	0.00	0.00
NaOH	0.00	0.00	0.00
Water	0.496	0.494	0.002
Zeolite	502.51	3.006	499.997
	Total Input Stream 7 (tonne/yr)	Total Output Stream 8 + Stream 9 (tonne/yr)	
Overall Total	503.006	503.006	

Table B-8: Material Balance around the Zeolite Storage Tank (Unit 6)

	INPUT STREAMS	OUTPUT STREAMS
Components	Stream 9 (tonne/yr)	Stream 10 (tonne/yr)
Kaolin	0.00	0.00
Water glass	0.00	0.00
TPABR	0.00	0.00
NaOH	0.00	0.00
Water	0.002	0.002
Zeolite	499.997	499.997
	Total Input Stream 9 (tonne/yr)	Total Output Stream 10 (tonne/yr)
Overall Total	500.000	500.000

Appendix C

(a) Zeolite A thickness after deposition on the sufrface of the α-alumina support.

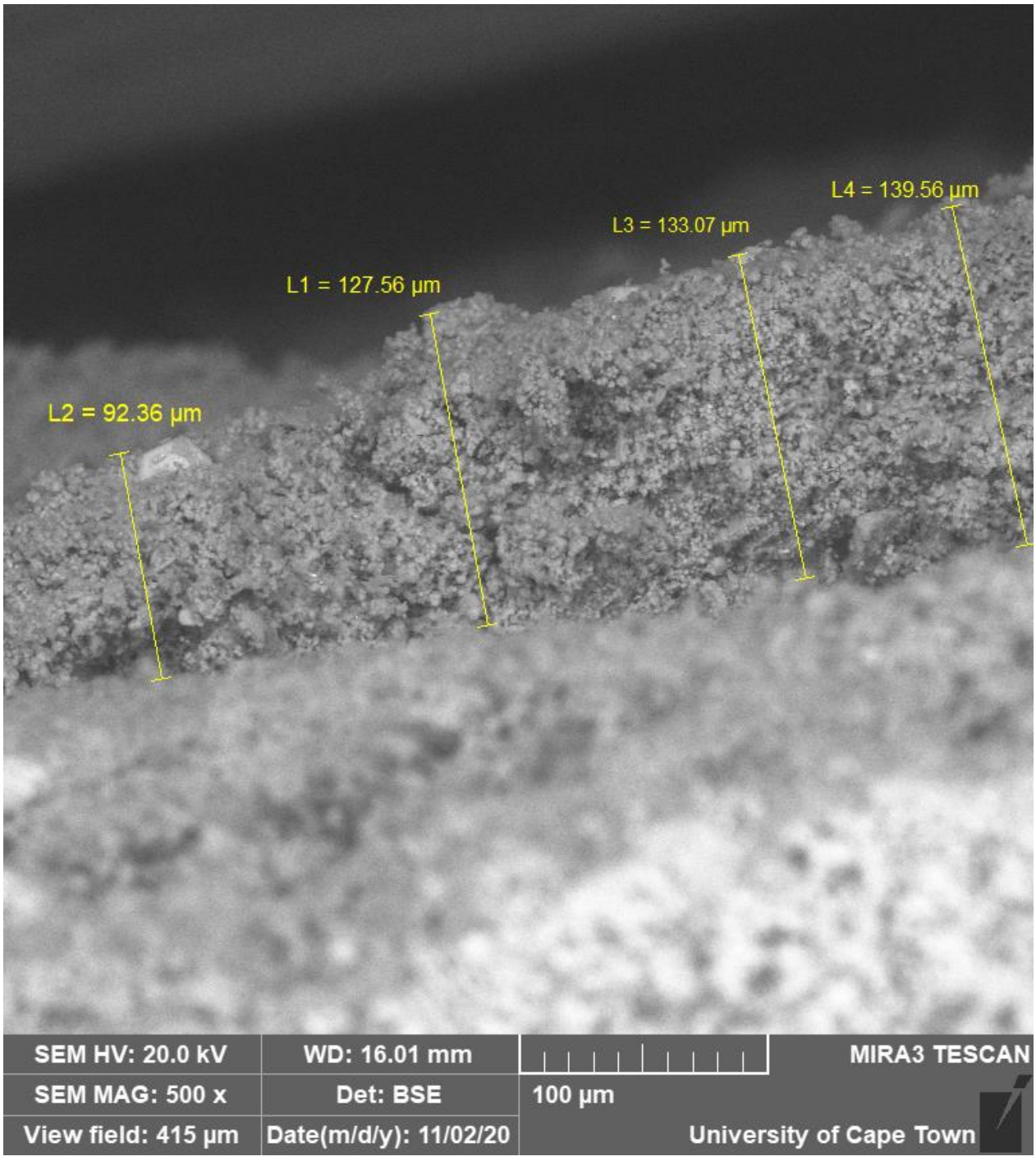

(b) ZSM-5 zeolite thickness after deposition on the surface of the α-alumina support